# Ultracold Dilute Boson-Fermion Mixtures

Diplomarbeit von

Steffen Röthel

Hauptgutachter: Prof. Dr. Hagen Kleinert


vorgelegt dem
Fachbereich Physik der
Freien Universität Berlin
im August 2006

# Contents

# Chapter 1

# Introduction

## 1.1 History and Motivation

The phenomenon of Bose-Einstein condensation (BEC) was first predicted by A. Einstein in 1924 [1,2] when he reviewed a work of S.N. Bose [3] about the statistics of photons and applied it to massive bosonic particles. He found out that, when a gas of indistinguishable bosonic atoms is cooled below a critical temperature $T_c$, a macroscopic fraction of the bosons condenses into the quantum mechanical ground state. Einstein interpreted this condensation as a phase transition since the condensed particles no longer contribute to the entropy. Similar to the optical field of a laser with many photons in a single mode the matter wave of $N_0$ condensed bosons, called the condensate wave function, is the superposition of $N_0$ single-particle ground-state wave functions which can serve as a source of a coherent matter beam, i.e. an atom laser. The macroscopic occupation of the ground state with massive bosons is possible due to the particle number conservation. Contrary to that a nonequilibrium process in the laser is necessary to achieve a macroscopic photon population in a single mode of the electromagnetic field. As photons have no mass, their number in a black-body cavity is not conserved. Thus, photons do not condense into the lowest mode, but are absorbed by the walls of the black-body cavity, when the latter is cooled. It took until 1995 when BEC was observed experimentally in $^4$He by momentum distribution measurements [4], in semiconductors, where paraexcitons were found to condense [5], and in dilute alkali gases, namely in $^{87}$Rb [6], in $^7$Li [7], and in $^{23}$Na [8]. The BEC in the alkali gases were only possible due to trapping and cooling techniques, which had been developed the decade before, and can be created in an almost pure form. BEC's have been realized with all alkali gases, except francium, and with hydrogen and chromium [9] as well. The latter interacts in addition to the isotropic short-range atomic interaction by an anisotropic long-range magnetic dipole-dipole interaction due to six unpaired electrons inducing a strong magnetic moment. In the case of $^{41}$K the difficulties in direct forced evaporative cooling, due to limitations in the temperature and density ranges achievable by laser cooling, were overcome by thermalization through evaporatively cooled $^{87}$Rb [10]. Thus, the bosons are used as a coolant being in thermal equilibrium with the fermions through interspecies interaction to bring them into the quantum degenerate regime. This method is called sympathetic cooling.

Six years after the first experimental achievement of BEC of trapped atomic gases in 1995 fermionic atomic gases were brought together with bosonic atoms to quantum degeneracy in a $^7$Li–$^6$Li mixture [11,12], $^{23}$Na–$^6$Li mixture [13], and $^{87}$Rb–$^{40}$K mixture [14], as shown in Figure 1.1. In contrast to

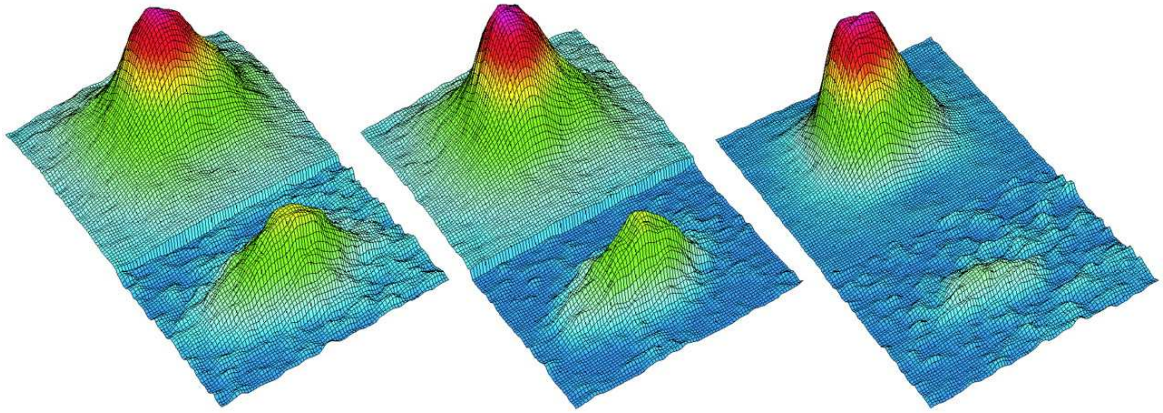

**Figure 1.1:** False-color reconstruction of the density distributions of a gas with fermionic $^{40}$K (front) and bosonic $^{87}$Rb (back) during the evaporative cooling process, as detected after a ballistic expansion of the mixture [19]. The left picture shows how the BEC starts to form out of the thermal cloud while coexisting with the fermion gas. In the middle picture the BEC grows whereas the fermion gas is slightly depleted by inelastic collisions. When an almost pure condensate of $10^5$ atoms has formed, the fermion gas has practically collapsed, as shown in the right picture.

the BEC in a Bose system, quantum degeneracy in a Fermi system with only one spin component means that all energy states below the Fermi energy $E_F$ are occupied with one fermion each, whereas all states above $E_F$ remain empty, which happens when $T \ll T_F = E_F/k_B$. The main problem to achieve quantum degeneracy in a Fermi gas is the inability of fermions to be directly evaporatively cooled. This is because fermions obey the Pauli exclusion principle, which forbids fermions in the same spin polarized hyperfine state to be close together, so that they can not collide via short range $\delta$-interaction to rethermalize the gas during the evaporative cooling. This handicap was circumvented before in the experiment of DeMarco and Jin [15], where a mixture with two different spin states of $^{40}$K was simultaneously evaporated by mutual cooling. It turned out there as a disadvantage that rethermalizing collisions were suppressed by the decreasing fraction of available unoccupied states when the gas became sufficiently quantum degenerate. This process is known as Pauli blocking. In combination with a Bose gas the fermions are sympathetically cooled by elastic interactions with the bosons in the overlapping region whereby the Pauli blocking effects are minimized [14,16].

Beside the exploration of quantum degeneracy, one is also interested in studying how the two-particle interaction influences the system properties. This opens a huge range of experimental regimes to be explored from noninteracting to strongly scattered. In the first case, pure quantum statistical effects, such as the consequences of the Pauli exclusion principle on the scattering properties of the system, can be investigated. The other extreme, with the prominent example of $^4$He–$^3$He liquid [17,18], leads to new phenomena like phase separation or BEC-induced interactions between fermions. Depending on the nature of the interspecies interaction, a repulsion between bosons and fermions tends to a demixing in order to minimize the overlapping region, whereas in the case of an attraction the mixture can collapse, as shown in Figure 1.1, as long as the particle numbers are sufficiently large [16,19]. The possibility of superfluidity in a Fermi gas, especially the predicted BEC-BCS crossover between BCS-type superfluidity of Cooper pairs of fermionic atoms

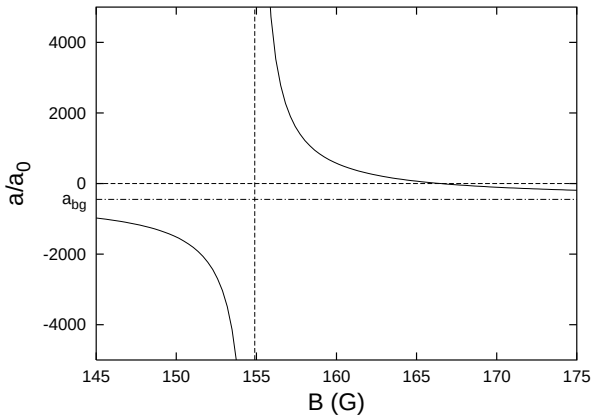


**Figure 1.2:** Example of a Feshbach resonance for $^{85}$Rb in the state $|F = 2, m_F = -2\rangle$, taken from [22], shows the scattering length $a$ in units of the Bohr radius $a_0$ as a function of the magnetic field $B$. The position of the resonance is marked by the vertical dashed line. A repulsive (attractive) interaction of arbitrary strength can be adjusted by a slight detuning from the resonance to stronger (weaker) magnetic fields.

and BEC of molecules was probed recently [20,21]. A magnetic-field Feshbach resonance was used to tune the interaction strength between fermionic atoms of two different spin states, characterized by the s-wave scattering length $a$, from effectively repulsive ($a > 0$) to attractive ($a < 0$), see Figure 1.2. On the $a > 0$, or BEC, side of the magnetic field, there exists a weakly bound molecular state whose binding energy and life time depends strongly on the detuning from the Feshbach resonance. Fermionic atoms are bound into bosonic molecules which can condense at sufficient low temperatures. On the other $a < 0$, or BCS, side of the resonance two fermions each of different spin states form a loosely bounded Cooper pair. The condensate of Cooper pairs, where the underlying role of Fermi statistics of the paired particles plays an essential role, is distinct from that of molecules where no fermionic degree of freedom remains. In the experiments [20,21] condensation of fermionic atom pairs was observed on both the BEC and BCS side of the Feshbach resonance. Furthermore, the system was observed to vary smoothly in the BEC-BCS crossover regime. An alternative and complementary access to Fermi superfluidity is expected from quantum degenerate Bose-Fermi mixtures where an effective interaction between fermions is mediated by the bosons [23,24], similarly to the role of phonons in a solid state superconductor.

Another recent and fast growing field is the investigation of ultracold boson-fermion mixtures trapped in an optical lattice which is created by standing waves of the electric field of counterpropagating laser beams. When atoms or molecules are loaded into an optical lattice with a total filling factor less than unity, the undesirable inelastic collisions, which usually occur in experiments with optical or magnetic traps, are reduced whereby the lifetime of the particles is significantly enhanced [25]. With the periodicity of the optical lattice the conditions in a solid body with crystalline structure can be simulated where the lattice constant and the potential-well depth can be varied with great precision by the wavelength and the intensity of the laser light, respectively. This opens the way to simulate complex quantum systems, traditionally associated with condensed matter physics, by means of atomic systems with perfectly controllable parameters. The atoms can be confined to different lattice sites and, by varying the laser intensity, the tunneling of them to neighbouring sites as well as the strength of their on-site repulsive interactions can be controlled. In the case of

a pure ultracold Bose-Einstein condensate with repulsive interaction, held in a three-dimensional optical lattice potential, a quantum phase transition from a superfluid to a Mott insulator phase was observed as the depth of the lattice is increased leading to a suppression of the tunneling between neighbouring lattice sites [26]. Within the Bose-Hubbard model [27] superfluidity means that each atom is spread out over the entire lattice with long-range phase coherence, whereas in the insulating phase a certain number of atoms is localized at each individual lattice site with no phase coherence across the lattice. The presence of fermionic atoms together with the Bose-Einstein condensate makes the system more complex and richer in its behavior at low temperatures. It has been predicted that novel quantum phases in the strong coupling regime occur which involve the pairing of fermions with one or more bosons or bosonic holes respectively, when the boson-fermion interaction is attractive or repulsive [28]. Depending on the physical parameters of the system these composite fermions may appear as a normal Fermi liquid, a density wave, a superfluid, or an insulator with fermionic domains. In the limit of very large lattice potential strength the mixture in an one-dimensional lattice passes through a disordered phase which possess many degenerate or quasidegenerate ground states separated by very high potential energy barriers [27]. Such a disordered phase is related to a breaking of the mirror symmetry in the lattice. Instead of varying the lattice potential depth the transition from a superfluid to a Mott insulator in bosonic $^{87}$Rb can be shifted towards larger lattice depth by adding of fermionic $^{40}$K which interacts attractively with rubidium and therefore increases the effective lattice depth [29]. On the way from the single superfluid phase without fermions in the three-dimensional optical lattice to the single Mott insulator phase with uniform distributed fermions one observes also localized bosonic ensembles or domains in superfluid "islands" due to percolation by a random fermion distribution, where the fermions act as impurities.

## 1.2 Experiment

Atoms are composite particles and consist of protons, neutrons, and electrons which all are fermions. An isotope of an element is a boson (fermion) if its spin is integer (half-integer), or equivalently, if the number of neutrons it contains is even (odd) since, roughly spoken, each proton is paired with an electron to form a boson. The question whether these composite particles can be regarded as pointlike depends on the occurrence of internal excitations within the atoms. If the energy needed for an internal excitation is much larger than $k_BT$, then all internal degrees of freedom are frozen out and have no consequences for the thermodynamics at temperature $T$ [30]. The energy of the first electronic excitation state of an atom of size $a$ is not larger than $\hbar^2/m_e a^2$ due to the uncertainty principle, where $m_e$ is the electron mass. As the thermal de Broglie wavelength

$$\lambda_T = \sqrt{\frac{2\pi\hbar^2}{mk_BT}}, \tag{1.1}$$

which is comparable with the mean interatomic separation in a quantum degenerate gas, is much larger than the size $a$ of an atom, it is obviously that

$$\frac{\hbar^2}{m_e a^2} \gg k_BT = \frac{2\pi\hbar^2}{m\lambda_T^2}. \tag{1.2}$$

The choice of elements for bosons and for fermions to be trapped and cooled to quantum degeneracy is mainly determined by the trapping and cooling techniques. Magnetic traps require atoms

with strong magnetic fields. The alkali gases with an unpaired electron are suitable candidates. Atoms with strong transition in the spectrum of the applied laser are useful for laser cooling. The sympathetic cooling of fermions by evaporatively cooled bosons requires a large ratio between "good" elastic collisions leading to a quick thermalization and "bad" inelastic collisions resulting in a loss of particles mainly by three-body recombination. A large intraspecies scattering length is therefore essential. Furthermore, a short thermalization time during the cooling, enabling the cooling process to be shorter than the formation time for molecules and clusters, is also necessary in order to prevent that the ultracold gas makes a transition into the more stable solid or liquid phase which is natural at these low temperatures. A first step towards the transition into the solid state is the recombination of two atoms to a molecule. This process is forbidden for two particles due to energy and momentum conservation and requires a third atom to take the surplus energy away. It is now clear that the gas must be dilute to maintain the metastable gaseous phase by reducing the three-body recombination rate.

The necessary temperature $T$ for achieving quantum degeneracy in dilute bosonic and fermionic gases depends in homogeneous gases on the respective particle densities $n_B$, $n_F$ and in trapped gases on the particle numbers $N_B$, $N_F$ and on the trap frequencies. Here we assume that the trap potential is described by a three-dimensional harmonic oscillator with the frequencies $\omega_x$, $\omega_y$, and $\omega_z$. The critical temperature $T_c$ for the onset of the BEC is given for a homogeneous boson gas by

$$T_{c,\mathrm{homog}} = \frac{2\pi\hbar^2}{m_B k_B}\left[\frac{n_B}{\zeta(3/2)}\right]^{2/3} \approx 3.312\,\frac{\hbar^2 n_B^{2/3}}{m_B k_B}, \tag{1.3}$$

and for a trapped boson gas by [31]

$$T_{c,\mathrm{trap}} = \frac{\hbar\tilde{\omega}_B}{k_B}\left[\frac{N_B}{\zeta(3)}\right]^{1/3} \approx 0.9405\,\frac{\hbar\tilde{\omega}_B N_B^{1/3}}{k_B}, \tag{1.4}$$

where $\zeta(3/2) \approx 2.612$ and $\zeta(3) \approx 1.202$ as defined in Eq. (D.19). Furthermore $m_B$ is the mass of a bosonic atom and $\tilde{\omega} = (\omega_x\omega_y\omega_z)^{1/3}$ denotes the geometrical average of the trap frequencies. On the other hand, the Fermi temperature $T_F$ of a homogeneous spin polarized fermion gas reads

$$T_{F,\mathrm{homog}} = \frac{6^{2/3}\pi^{4/3}\hbar^2 n_F^{2/3}}{2m_F k_B} \approx 7.596\,\frac{\hbar^2 n_F^{2/3}}{m_F k_B}, \tag{1.5}$$

and for a trapped spin polarized fermion gas [32]

$$T_{F,\mathrm{trap}} = \frac{6^{1/3}\hbar\tilde{\omega}_F N_F^{1/3}}{k_B} \approx 1.817\,\frac{\hbar\tilde{\omega}_F N_F^{1/3}}{k_B}, \tag{1.6}$$

where $m_F$ denotes the mass of a fermionic atom. A high density or a large number of fermions is needed to attain proper quantum degeneracy in the fermion gas with $T < 0.2\,T_F$, where only a few states above the Fermi energy $E_F$ are occupied.

In the following we briefly describe the experiments with a $^{87}$Rb–$^{40}$K boson-fermion mixture which were performed by the Sengstock group in Hamburg [16] and by the Inguscio group in Florence [14,19] as the theoretical investigation of this thesis is based on these experiments. The vapor of both $^{87}$Rb and $^{40}$K is generated by an oven or a dispenser and confined in a two-species magneto-optical trap (MOT). Because of the requirement of simultaneous trapping of two different atomic species, these traps are more complex compared to traps for a single boson gas. There, the vapor

is precooled by resonant laser beams to about 100 $\mu$K within 10 s. Precooling is necessary as the energy depth of the following magnetic trap is much less than 1 K if we assume that the magnetic moments $\mu$ of the atoms due to their unpaired electron are of the order of the Bohr magneton $\mu_B = e\hbar/2m_e$ and the magnetic fields $B$ in the laboratory are far below 1 T resulting in a Zeeman energy $\mu B \approx 0.67\,K/T$ [33]. The mixture consisting of $10^{10}$ ($5{\cdot}10^8$) $^{87}$Rb and $2{\cdot}10^8$ ($10^5$) $^{40}$K atoms in the Hamburg (Florence) experiment is prepared in the doubly polarized state $|F = 2,\, m_F = 2\rangle$ for $^{87}$Rb and the state $|F = 9/2,\, m_F = 9/2\rangle$ for $^{40}$K and loaded in a Ioffe-Pritchard-type magnetic trap for the evaporative cooling. In a doubly polarized state the nuclear spin $I = 3/2$ for $^{87}$Rb and $I = 4$ for $^{40}$K and the electron spin $J = 1/2$ for both have the largest possible projection on the axis of the magnetic field $\mathbf{B}$ and point to the same direction maximizing the total atomic spin $\mathbf{F} = \mathbf{I} + \mathbf{J}$ and its magnetic quantum number $m_F$ being the projection of $\mathbf{F}$ on the axis of $\mathbf{B}$. If an atom in the hyperfine state $m_F$ with a magnetic moment $\boldsymbol{\mu}_m$ experiences an external magnetic field $\mathbf{B}$, its energy $E_m$ is shifted by

$$\Delta E_m = -\boldsymbol{\mu}_m \cdot \mathbf{B} = g\mu_B m_F B, \tag{1.7}$$

where $g$ is the Landé g factor of the atom. Thus, atoms in a state with $gm_F > 0$ ($gm_F < 0$) experience in an inhomogeneous field a spatially varying potential and are driven towards the minimum (maximum) of the magnetic field to minimize the energy and are therefore called low-field seekers (high-field seekers). The latter possibility is ruled out since a local maximum of the magnitude $B = |\mathbf{B}|$ is impossible due to Maxwell's equations in regions of magnetic fields where no electrical currents occur. So atom traps have to generate magnetic fields with a local minimum and may be realized by a pair of Helmholtz coils with identical currents in the coils in opposite directions producing a quadrupolar field. The trap can confine atoms without losses only if the atoms remain in the same quantum state $m$ relative to the instantaneous direction of the magnetic field and hence follow the variation of the magnetic field adiabatically [33]. This is ensured if the magnetic field experienced by an atom changes slower than the precession frequency $\omega_{\text{Larmor}}$ of the magnetic moment around the axis of $\mathbf{B}$

$$\frac{d\theta}{dt} < \frac{g\mu_B m_F B}{\hbar} = \omega_{\text{Larmor}}, \qquad \theta = \sphericalangle(\mathbf{B}, \boldsymbol{\mu}_m), \tag{1.8}$$

which is equal to the transition frequency between magnetic sublevels $m_F$.

The magnetic field of the trap is rotationally symmetric and can be well approximated in the vicinity of the trap center by

$$B(\mathbf{x}) = B_0 + B_r r^2 + B_z z^2, \tag{1.9}$$

using cylindrical coordinates $\{r,\, \phi,\, z\}$. Due to Eq. (1.7) both atom species experience an external potential in the form of an anisotropic harmonic oscillator

$$V_i(\mathbf{x}) = V_0 + \frac{m_i}{2}\left(\omega_{i,r}^2 r^2 + \omega_{i,z}^2 z^2\right), \qquad i = B, F. \tag{1.10}$$

As a boson and a fermion at the same position within the trap feel forces of equal size, the trap frequencies for bosons and fermions are related by their masses

$$\omega_{F,k} = \sqrt{\frac{m_B}{m_F}}\,\omega_{B,k}, \qquad k = r, z, \tag{1.11}$$

and are listed in Table 1.1. The main tasks of the magnetic trap are to confine and compress the

| | Hamburg Experiment | Florence Experiment |
|---|---|---|
| mass of $^{87}$Rb atom | $m_B = 14.43 \cdot 10^{-26}$ kg | |
| mass of $^{40}$K atom | $m_F = 6.636 \cdot 10^{-26}$ kg | |
| s-wave scattering length (bosons $\leftrightarrow$ bosons) | $a_{BB} = (5.238 \pm 0.002)$ nm | |
| s-wave scattering length (bosons $\leftrightarrow$ fermions) | $a_{BF} = -15.0$ nm | $a_{BF} = (-20.9 \pm 0.8)$ nm |
| radial trap frequency (bosons) | $\omega_{B,r} = 2\pi \cdot 257$ Hz | $\omega_{B,r} = 2\pi \cdot 215$ Hz |
| axial trap frequency (bosons) | $\omega_{B,z} = 2\pi \cdot 11.3$ Hz | $\omega_{B,z} = 2\pi \cdot 16.3$ Hz |
| radial trap frequency (fermions) | $\omega_{F,r} = 2\pi \cdot 379$ Hz | $\omega_{F,r} = 2\pi \cdot 317$ Hz |
| axial trap frequency (fermions) | $\omega_{F,z} = 2\pi \cdot 16.7$ Hz | $\omega_{F,z} = 2\pi \cdot 24.0$ Hz |
| number of bosons | $N_B = 10^6$ | $N_B = 2 \cdot 10^5$ |
| number of fermions | $N_F = 7.5 \cdot 10^5$ | $N_F = 3 \cdot 10^4$ |

**Table 1.1:** List of parameters of the experiments with a $^{87}$Rb–$^{40}$K boson-fermion mixture. The values are taken from the experiments of the Sengstock group in Hamburg [16] and of the Inguscio group in Florence [14,19,35].

mixture to particle densities around $10^{14}$ cm$^{-3}$ whereby the collision rate is increased to make the evaporative cooling more efficient. Radio-frequency evaporative cooling is performed selectively on the Rb sample where the most energetic atoms can escape from the trap and carry more than the average energy per atom away, leading to a decrease of the temperature in the mixture. This process is very similar to a steaming cup of hot coffee where the cooling can be speed up by blowing over the coffee. Thermal equilibrium in the sample is kept by thermalization through elastic collision between the atoms. The K atoms are sympathetically cooled by the Rb atoms with high efficiency due to the large intraspecies scattering length and large ratio between elastic and inelastic collisions. At the final stage after 25 s of evaporative cooling below 1 $\mu$K a condensate of $10^6$ ($2 \cdot 10^5$) $^{87}$Rb atoms coexisting with $7.5 \cdot 10^5$ ($3 \cdot 10^4$) $^{40}$K atoms with a quantum degeneracy of $T/T_F = 0.1$ ($T/T_F = 0.3$) is achieved in the Hamburg (Florence) experiment. One uses a false-color coding of the optical density of both components, which are taken after a ballistic expansion for 4 ms time of flight (TOF) for $^{40}$K and 19 ms TOF for $^{87}$Rb by using two short, delayed light pulses, after the trap potential is suddenly switched off. This false-color coding makes the density distribution visible and allows to draw conclusions from the momentum distribution of the gas in the trap. The density distribution of the BEC sample and of the thermal boson cloud can be fitted by expected theoretical curves, which allow to estimate the condensed fraction $n_0 = N_0/N_B$ and the temperature $T$, where $N_0$ denotes the number of condensed bosons.

| $a_{BF}/a_{\text{Bohr}}$ | Method of determination | Reference (year) |
|---|---|---|
| $-261^{+170}_{-159}$ | measurement of the elastic cross section for collisions between $^{41}$K and $^{87}$Rb in different temperature regimes and following mass scaling to the fermionic $^{40}$K isotope | [34] (2002) |
| $-330^{+160}_{-100}$ | measurement of the rethermalization time in the mixture in [14,19] after a selectively heating of $^{87}$Rb | [14] (2002) |
| $-410^{+81}_{-91}$ | measurement of the damping of the relative oscillations of $^{40}$K and $^{87}$Rb in a magnetic trap | [19] (2002) |
| $-395 \pm 15$ | mean-field analysis of the stability of the mixture in [14,19] | [35] (2003) |
| $-281 \pm 15$ | magnetic Feshbach spectroscopy of an ultracold mixture of $^{40}$K and $^{87}$Rb atoms | [36] (2004) |
| $250 \pm 30$ | cross dimensional thermal relaxation in a mixture of $^{40}$K and $^{87}$Rb atoms after a increase of the radial confinement of the magnetic trap, here only $\lvert a_{BF}/a_0 \rvert$ | [37] (2004) |
| $-284$ | mean-field analysis of the stability, based on [38], of the mixture in [16] | [16] (2006) |
| $-205 \pm 5$ | extensive magnetic Feshbach spectroscopy of an ultracold mixture of $^{40}$K and $^{87}$Rb atoms | [39] (2006) |

**Table 1.2:** List of several published values of the s-wave scattering length between $^{87}$Rb and $^{40}$K including their determination method and their references.

The experimental parameters of both experiments are summarized in Table 1.1. The distinct values for the interspecies s-wave scattering length $a_{BF}$ for each experiment are worth a detailed explanation since this parameter is of great importance for the system, especially for the stability of the mixture against collapsing. An overview of different values for $a_{BF}$ and their determination method along with a reference are shown in Table 1.2. A comparison of the incompatible values for $a_{BF}$ shows the need of further investigation in this field.

## 1.3 Outline of this Thesis

After this overview over the fascinating field of boson-fermion mixtures we sketch what we investigate in the present thesis.

The aim of Chapter 2 is to derive the Gross-Pitaevskii equation for an ultracold dilute boson-fermion

mixture in $D$ dimensions. For that purpose we describe a dilute gaseous boson-fermion mixture in a grand-canonical ensemble within the functional integral representation. For more generality we include the time dependence in the formulas, so that also the dynamics of the mixture could be described at a later date beyond this thesis. By splitting the Bose fields into background fields and fluctuation fields and integrating out the Fermi fields, we derive an effective action of the Bose subsystem within the semiclassical Thomas-Fermi approximation. Its extremization at zero temperature yields the Gross-Pitaevskii equation for the condensate wave function where besides the conventional form for a BEC an additional nonlinear term occurs due to the interaction with the fermions. A modified effective action without integrating out the fermionic degrees of freedom is used to get two coupled equations of motion, one for the condensate wave function and another one for the Green function of the fermions.

In Chapter 3 we apply the Thomas-Fermi approximation again by neglecting the kinetic energy of the bosons and obtain an algebraic Gross-Pitaevskii equation, which can be easily solved. With the help of this solution we determine the density profiles of both components in a $^{87}$Rb–$^{40}$K mixture where the $\delta$-interaction is repulsive between the bosons and attractive between both components. Furthermore, we investigate the stability of the Bose-Fermi mixture with respect to collapse by evaluating numerically the effective action for a trial Gaussian density profile of the condensate. We compare our results, which strongly depend on the value of the Bose-Fermi s-wave scattering length, with the experiments on $^{87}$Rb–$^{40}$K mixtures in Hamburg and Florence.

Finally, in Chapter 4 we present our conclusions and give suggestions for further investigations.

# Chapter 2

# Derivation of Gross-Pitaevskii Equation

A many-body system is described within the grand-canonical ensemble by assuming that it is connected with its environment so that an exchange of both energy and particles is allowed. Furthermore, the system is in thermodynamic equilibrium with its environment sharing with it a temperature $T$ and a chemical potential $\mu$. The environment as a heat and particle reservoir is assumed to be much larger than the system, so that the exchange of energy and particles with the system does not alter its energy and particle number significantly.

## 2.1 Grand-Canonical Partition Function

We consider a dilute gaseous mixture of ultracold bosonic and fermionic atoms. In order to obtain statistical quantities for such a Bose-Fermi mixture, we use the grand-canonical partition function in the functional integral formalism. Thus, we integrate over all possible Bose fields $\psi_B^*(\mathbf{x},\tau)$, $\psi_B(\mathbf{x},\tau)$ and Fermi fields $\psi_F^*(\mathbf{x},\tau)$, $\psi_F(\mathbf{x},\tau)$, which are weighted by a Boltzmann factor with the euclidean action $\mathcal{A}$:

$$\mathcal{Z} = \oint \mathcal{D}\psi_B^* \oint \mathcal{D}\psi_B \oint \mathcal{D}\psi_F^* \oint \mathcal{D}\psi_F \, e^{-\mathcal{A}[\psi_B^*,\psi_B,\psi_F^*,\psi_F]/\hbar}. \tag{2.1}$$

The complex fields $\psi_B^*(\mathbf{x},\tau)$, $\psi_B(\mathbf{x},\tau)$ represent the bosons and are periodic on the imaginary time interval $[0,\hbar\beta]$, whereas the fermions are described by Grassmann fields $\psi_F^*(\mathbf{x},\tau)$, $\psi_F(\mathbf{x},\tau)$, explained briefly in Appendix A, which are antiperiodic on this interval:

$$\psi^*(\mathbf{x},\hbar\beta) = \epsilon\,\psi^*(\mathbf{x},0), \qquad \psi(\mathbf{x},\hbar\beta) = \epsilon\,\psi(\mathbf{x},0). \tag{2.2}$$

Here $\epsilon = \pm 1$ holds for bosons and fermions, respectively. These fields are nonrelativistic Schrödinger fields and are not second quantized in accordance with the classical field theory of the nonrelativistic quantum mechanics. In this thesis the second quantization is taken into account by using the functional integral (2.1). The euclidean action $\mathcal{A}$ in Eq. (2.1) follows from the quantum-mechanical action $\mathcal{A}_{\mathrm{QM}}$ via a Wick rotation $t = -i\tau$. The quantum-mechanical action $\mathcal{A}_{\mathrm{QM}}$ is the space-time integral

$$\mathcal{A}_{\mathrm{QM}}[\psi_B^*,\psi_B,\psi_F^*,\psi_F] = \int dt \int d^D x \, \mathcal{L}(\psi_B^*,\psi_B,\psi_F^*,\psi_F), \tag{2.3}$$

where the Lagrange density consists of three terms

$$\mathcal{L}(\psi_B^*, \psi_B, \psi_F^*, \psi_F) = \mathcal{L}_B(\psi_B^*, \psi_B) + \mathcal{L}_F(\psi_F^*, \psi_F) + \mathcal{L}_{BF}(\psi_B^*, \psi_B, \psi_F^*, \psi_F). \tag{2.4}$$

The first term describes the bosonic component of the mixture:

$$\mathcal{L}_B(\psi_B^*, \psi_B) = i\hbar\psi_B^*(\mathbf{x},t)\,\frac{\partial\psi_B(\mathbf{x},t)}{\partial t} - \frac{\hbar^2}{2m_B}\,|\boldsymbol{\nabla}\psi_B(\mathbf{x},t)|^2 \\ - \left\{V_B(\mathbf{x}) + \frac{1}{2}\int d^Dx'\,V_{BB}^{(\mathrm{int})}(\mathbf{x},\mathbf{x}')\,|\psi_B(\mathbf{x}',t)|^2\right\}\,|\psi_B(\mathbf{x},t)|^2. \tag{2.5}$$

It contains the Legendre transform, the kinetic energy, the external trap potential $V_B(\mathbf{x})$, and the two-particle interaction potential $V_{BB}^{(\mathrm{int})}(\mathbf{x},\mathbf{x}')$ between two bosons. As we deal with a dilute gas, collisions of three and more particles at the same time occur very rarely compared to two-particle collisions, so that an interaction between more than two particles is negligible. Since the Pauli principle forbids fermions in the same hyperfine state to be close together and therefore to collide via $\delta$-interaction, we can write the action term for the fermionic component of the mixture as

$$\mathcal{L}_F(\psi_F^*, \psi_F) = i\hbar\psi_F^*(\mathbf{x},t)\,\frac{\partial\psi_F(\mathbf{x},t)}{\partial t} - \frac{\hbar^2}{2m_F}\,|\boldsymbol{\nabla}\psi_F(\mathbf{x},t)|^2 - V_F(\mathbf{x})\,|\psi_F(\mathbf{x},t)|^2, \tag{2.6}$$

where $V_F(\mathbf{x})$ represents an external trap potential for fermions. The last term in Eq. (2.4)

$$\mathcal{L}_{BF}(\psi_B^*, \psi_B, \psi_F^*, \psi_F) = -\int d^Dx'\,V_{BF}^{(\mathrm{int})}(\mathbf{x},\mathbf{x}')\,|\psi_B(\mathbf{x}',t)|^2\,|\psi_F(\mathbf{x},t)|^2 \tag{2.7}$$

describes the interaction between bosons and fermions. Since the energy in a grand-canonical ensemble is reduced by a contribution describing the exchange of a particle with the environment, we must subtract the respective chemical potentials $\mu_B$ and $\mu_F$ multiplied with the corresponding particle density. As we assume a situation, where the bosonic and fermionic atoms cannot be transformed into each other, each of both species has its own chemical potential. Furthermore, we have to transform Eqs. (2.3) and (2.4) from the real time $t$ to the imaginary time $\tau$ via Wick rotation $t = -i\tau$. Thus, the total euclidean action of a Bose-Fermi mixture has the form

$$\mathcal{A}[\psi_B^*, \psi_B, \psi_F^*, \psi_F] = \mathcal{A}_B[\psi_B^*, \psi_B] + \mathcal{A}_F[\psi_F^*, \psi_F] + \mathcal{A}_{BF}[\psi_B^*, \psi_B, \psi_F^*, \psi_F], \tag{2.8}$$

where all three terms correspond to the Lagrange densities (2.5)–(2.7). The bosonic action reads

$$\mathcal{A}_B[\psi_B^*, \psi_B] = \int_0^{\hbar\beta} d\tau \int d^Dx\,\psi_B^*(\mathbf{x},\tau)\left[\hbar\frac{\partial}{\partial\tau} - \frac{\hbar^2}{2m_B}\Delta + V_B(\mathbf{x}) - \mu_B \right. \\ \left. + \frac{1}{2}\int d^Dx'\,V_{BB}^{(\mathrm{int})}(\mathbf{x},\mathbf{x}')\,|\psi_B(\mathbf{x}',\tau)|^2\right]\psi_B(\mathbf{x},\tau), \tag{2.9}$$

the fermionic action is given by

$$\mathcal{A}_F[\psi_F^*, \psi_F] = \int_0^{\hbar\beta} d\tau \int d^Dx\,\psi_F^*(\mathbf{x},\tau)\left[\hbar\frac{\partial}{\partial\tau} - \frac{\hbar^2}{2m_F}\Delta + V_F(\mathbf{x}) - \mu_F\right]\psi_F(\mathbf{x},\tau), \tag{2.10}$$

and the interspecies interaction is described by

$$\mathcal{A}_{BF}[\psi_B^*, \psi_B, \psi_F^*, \psi_F] = \int_0^{\hbar\beta} d\tau \int d^Dx \int d^Dx'\,V_{BF}^{(\mathrm{int})}(\mathbf{x},\mathbf{x}')\,|\psi_B(\mathbf{x}',\tau)|^2\,|\psi_F(\mathbf{x},\tau)|^2. \tag{2.11}$$

## 2.2 Background Method

In order to account for the fact that the bosons in the mixture can condense, we apply the background method of field theory [40–43] and split the bosonic Schrödinger fields $\psi_B^*(\mathbf{x},\tau)$, $\psi_B(\mathbf{x},\tau)$ into two parts

$$\psi_B^*(\mathbf{x},\tau) = \Psi_B^*(\mathbf{x},\tau) + \delta\psi_B^*(\mathbf{x},\tau), \qquad \psi_B(\mathbf{x},\tau) = \Psi_B(\mathbf{x},\tau) + \delta\psi_B(\mathbf{x},\tau). \tag{2.12}$$

The first part represents the background fields $\Psi_B^*(\mathbf{x},\tau)$, $\Psi_B(\mathbf{x},\tau)$. Their absolute square is identified with the density of the condensed bosons. The second part are the fluctuation fields $\delta\psi_B^*(\mathbf{x},\tau)$, $\delta\psi_B(\mathbf{x},\tau)$ of the Bose gas describing the excited bosons, which are not in the ground state. Note that the background field is equipped with a time dependence in order to maintain the possibility for a later description of the dynamics in the mixture. Expanding the euclidean action (2.8) in a functional Taylor series with respect to the Bose fields $\psi_B^*(\mathbf{x},\tau)$, $\psi_B(\mathbf{x},\tau)$ around the background fields $\Psi_B^*(\mathbf{x},\tau)$, $\Psi_B(\mathbf{x},\tau)$ up to the second order yields

$$\begin{aligned}
\mathcal{A}[\Psi_B^* + \delta\psi_B^*, \Psi_B + \delta\psi_B, \psi_F^*, \psi_F] &= \mathcal{A}[\Psi_B^*, \Psi_B, \psi_F^*, \psi_F] \\
&+ \int_0^{\hbar\beta} d\tau \int d^D x \left\{ \frac{\delta\mathcal{A}[\psi_B^*, \psi_B, \psi_F^*, \psi_F]}{\delta\psi_B^*(\mathbf{x},\tau)} \Big|_{\psi_B(\mathbf{x},\tau)=\Psi_B(\mathbf{x},\tau)}^{\psi_B^*(\mathbf{x},\tau)=\Psi_B^*(\mathbf{x},\tau)} \delta\psi_B^*(\mathbf{x},\tau) + c.c. \right\} \\
&+ \frac{1}{2} \int_0^{\hbar\beta} d\tau \int_0^{\hbar\beta} d\tau' \int d^D x \int d^D x' \\
&\times \left\{ \frac{\delta^2\mathcal{A}[\psi_B^*, \psi_B, \psi_F^*, \psi_F]}{\delta\psi_B^*(\mathbf{x},\tau)\,\delta\psi_B^*(\mathbf{x}',\tau')} \Big|_{\psi_B(\mathbf{x},\tau)=\Psi_B(\mathbf{x},\tau)}^{\psi_B^*(\mathbf{x},\tau)=\Psi_B^*(\mathbf{x},\tau)} \delta\psi_B^*(\mathbf{x}',\tau')\,\delta\psi_B^*(\mathbf{x},\tau) + c.c. \right. \\
&+ \left. \frac{\delta^2\mathcal{A}[\psi_B^*, \psi_B, \psi_F^*, \psi_F]}{\delta\psi_B(\mathbf{x},\tau)\,\delta\psi_B^*(\mathbf{x}',\tau')} \Big|_{\psi_B(\mathbf{x},\tau)=\Psi_B(\mathbf{x},\tau)}^{\psi_B^*(\mathbf{x},\tau)=\Psi_B^*(\mathbf{x},\tau)} \delta\psi_B^*(\mathbf{x}',\tau')\,\delta\psi_B(\mathbf{x},\tau) + c.c. \right\}.
\end{aligned} \tag{2.13}$$

Eq. (2.13) can be written in terms with respect to the order in the fluctuation fields $\delta\psi_B^*(\mathbf{x},\tau)$, $\delta\psi_B(\mathbf{x},\tau)$:

$$\mathcal{A}[\Psi_B^* + \delta\psi_B^*, \Psi_B + \delta\psi_B, \psi_F^*, \psi_F] = \mathcal{A}^{(0)}(\delta\psi_B^*, \delta\psi_B) + \mathcal{A}^{(1)}(\delta\psi_B^*, \delta\psi_B) + \mathcal{A}^{(2)}(\delta\psi_B^*, \delta\psi_B). \tag{2.14}$$

The zeroth order term does not contain the fluctuation fields $\delta\psi_B^*(\mathbf{x},\tau)$, $\delta\psi_B(\mathbf{x},\tau)$ and is equivalent to the euclidean action (2.8) evaluated at the background fields $\Psi_B^*(\mathbf{x},\tau)$, $\Psi_B(\mathbf{x},\tau)$:

$$\begin{aligned}
\mathcal{A}^{(0)}(\delta\psi_B^*, \delta\psi_B) = \mathcal{A}[\Psi_B^*, \Psi_B, \psi_F^*, \psi_F] = \int_0^{\hbar\beta} d\tau \int d^D x \left\{ \Psi_B^*(\mathbf{x},\tau) \left[ \hbar\frac{\partial}{\partial\tau} - \frac{\hbar^2}{2m_B}\Delta + V_B(\mathbf{x}) - \mu_B \right.\right. \\
\left. + \frac{1}{2}\int d^D x'\, V_{BB}^{(\mathrm{int})}(\mathbf{x},\mathbf{x}')\,|\Psi_B(\mathbf{x}',\tau)|^2 \right] \Psi_B(\mathbf{x},\tau) + \psi_F^*(\mathbf{x},\tau) \left[ \hbar\frac{\partial}{\partial\tau} - \frac{\hbar^2}{2m_F}\Delta + V_F(\mathbf{x}) - \mu_F \right. \\
\left.\left. + \int d^D x'\, V_{BF}^{(\mathrm{int})}(\mathbf{x},\mathbf{x}')\,|\Psi_B(\mathbf{x}',\tau)|^2 \right] \psi_F(\mathbf{x},\tau) \right\}.
\end{aligned} \tag{2.15}$$

The first order term being linear with respect to $\delta\psi_B^*(\mathbf{x},\tau)$, $\delta\psi_B(\mathbf{x},\tau)$ vanishes as we require the background fields $\Psi_B^*(\mathbf{x},\tau)$, $\Psi_B(\mathbf{x},\tau)$ to extremize the euclidean action (2.8) within the background method:

$$\mathcal{A}^{(1)}(\delta\psi_B^*, \delta\psi_B) = 0. \tag{2.16}$$

The second order term is quadratically in $\delta\psi_B^*(\mathbf{x},\tau)$, $\delta\psi_B(\mathbf{x},\tau)$ and would lead to the Bogoliubov theory:

$$\begin{aligned}\mathcal{A}^{(2)}(\delta\psi_B^*,\delta\psi_B) = \int_0^{\hbar\beta} d\tau \int d^D x \Bigg\{ \delta\psi_B^*(\mathbf{x},\tau) \Bigg[ \hbar\frac{\partial}{\partial\tau} - \frac{\hbar^2}{2m_B}\Delta + V_B(\mathbf{x}) - \mu_B \\ + \int d^D x'\, V_{BF}^{(\mathrm{int})}(\mathbf{x},\mathbf{x}')\,|\psi_F(\mathbf{x}',\tau)|^2 \Bigg] \delta\psi_B(\mathbf{x},\tau) + \frac{1}{2}\int d^D x'\, V_{BB}^{(\mathrm{int})}(\mathbf{x},\mathbf{x}') \\ \times \Big[ \Psi_B(\mathbf{x},\tau)\,\Psi_B(\mathbf{x}',\tau)\,\delta\psi_B^*(\mathbf{x}',\tau)\,\delta\psi_B^*(\mathbf{x},\tau) + \Psi_B^*(\mathbf{x},\tau)\,\Psi_B^*(\mathbf{x}',\tau)\,\delta\psi_B(\mathbf{x}',\tau)\,\delta\psi_B(\mathbf{x},\tau) \\ + 2\Psi_B(\mathbf{x}',\tau)\,\Psi_B^*(\mathbf{x},\tau)\,\delta\psi_B^*(\mathbf{x}',\tau)\,\delta\psi_B(\mathbf{x},\tau) + 2|\Psi_B(\mathbf{x}',\tau)|^2\,\delta\psi_B^*(\mathbf{x},\tau)\,\delta\psi_B(\mathbf{x},\tau) \Big] \Bigg\}. \end{aligned} \tag{2.17}$$

In the present thesis we restrict ourselves to the Gross-Pitaevskii theory, i.e. we consider only the euclidean action $\mathcal{A}$ up to the zeroth order in the fluctuation fields $\delta\psi_B^*(\mathbf{x},\tau)$, $\delta\psi_B(\mathbf{x},\tau)$:

$$\mathcal{A}[\Psi_B^* + \delta\psi_B^*, \Psi_B + \delta\psi_B, \psi_F^*, \psi_F] = \mathcal{A}^{(0)}(\delta\psi_B^*, \delta\psi_B). \tag{2.18}$$

Thus, the bosonic functional integration in Eq. (2.1), whose integration measure transforms according

$$\mathcal{D}\psi_B^*(\mathbf{x},\tau) = \mathcal{D}\delta\psi_B^*(\mathbf{x},\tau), \qquad \mathcal{D}\psi_B(\mathbf{x},\tau) = \mathcal{D}\delta\psi_B(\mathbf{x},\tau), \tag{2.19}$$

can be dropped. Since the Fermi fields $\psi_F^*(\mathbf{x},\tau)$, $\psi_F(\mathbf{x},\tau)$ occur only quadratically in the euclidean action $\mathcal{A}$ due to the absent fermion-fermion interaction, the fermionic functional integral in Eq. (2.1) can be carried out. In this way we obtain

$$\mathcal{Z}[\Psi_B^*, \Psi_B] = e^{-\mathcal{A}_B[\Psi_B^*,\Psi_B]/\hbar}\,\mathcal{Z}_F[\Psi_B^*, \Psi_B], \tag{2.20}$$

where

$$\mathcal{Z}_F[\Psi_B^*, \Psi_B] = \oint \mathcal{D}\psi_F^* \oint \mathcal{D}\psi_F\, e^{-\left(\mathcal{A}_F[\psi_F^*,\psi_F] + \mathcal{A}_{BF}[\Psi_B^*,\Psi_B,\psi_F^*,\psi_F]\right)/\hbar} \tag{2.21}$$

represents the functional integral over the Fermi fields resulting in a pure functional of the Bose background fields $\Psi_B^*(\mathbf{x},\tau)$, $\Psi_B(\mathbf{x},\tau)$. The euclidean actions depending on the Fermi fields $\psi_F^*(\mathbf{x},\tau)$, $\psi_F(\mathbf{x},\tau)$ are summarized to

$$\mathcal{A}_F[\psi_F^*,\psi_F] + \mathcal{A}_{BF}[\Psi_B^*,\Psi_B,\psi_F^*,\psi_F] = \int_0^{\hbar\beta} d\tau \int d^D x\, \psi_F^*(\mathbf{x},\tau) \left[\hbar\frac{\partial}{\partial\tau} + \hat{H}_F(\mathbf{x},\tau) - \mu_F\right] \psi_F(\mathbf{x},\tau). \tag{2.22}$$

Here $\hat{H}_F(\mathbf{x},\tau)$ denotes the effective one-particle Hamilton operator for fermions

$$\hat{H}_F(\mathbf{x},\tau) = -\frac{\hbar^2}{2m_F}\Delta + V_{\mathrm{eff}}(\mathbf{x},\tau), \tag{2.23}$$

with the effective potential

$$V_{\mathrm{eff}}(\mathbf{x},\tau) = V_F(\mathbf{x}) + \int d^D x'\, V_{BF}^{(\mathrm{int})}(\mathbf{x},\mathbf{x}')\,|\Psi_B(\mathbf{x}',\tau)|^2. \tag{2.24}$$

In the following we evaluate the fermionic functional integral (2.21) within the semiclassical approximation since we are interested only in the lowest-order term in the gradient expansion of the tracelog. Thus, we neglect for the time being the spatio-temporal dependence of the effective potential:

$$V_{\mathrm{eff}}(\mathbf{x},\tau) = V_{\mathrm{eff}}. \tag{2.25}$$

## 2.3 Fermionic Functional Integral

In general, the functional integration in Eq. (2.21) amounts to sum over all fermionic fields which are antiperiodic in the imaginary time according to Eq. (2.2). These fields can be decomposed into one-particle wave functions depending on the space coordinate $\mathbf{x}$ and in a Fourier expansion in the form of Matsubara functions depending on the imaginary time $\tau$:

$$\psi_F^*(\mathbf{x},\tau) = \sum_{\mathbf{n}} \sum_{m=-\infty}^{\infty} c_{\mathbf{n}\,m}^* \, \psi_{\mathbf{n}}^*(\mathbf{x}) \, e^{i\omega_m \tau}, \qquad \psi_F(\mathbf{x},\tau) = \sum_{\mathbf{n}} \sum_{m=-\infty}^{\infty} c_{\mathbf{n}\,m} \, \psi_{\mathbf{n}}(\mathbf{x}) \, e^{-i\omega_m \tau}. \tag{2.26}$$

Here the fermionic Matsubara frequencies $\omega_m$ are half-integer multiples of the Matsubara ground frequency $2\pi/\hbar\beta$:

$$\omega_m = \frac{2\pi}{\hbar\beta}\, m, \qquad\qquad m = \pm\frac{1}{2}, \pm\frac{3}{2}, \pm\frac{5}{2} \ldots \tag{2.27}$$

and the coefficients $c_{\mathbf{n}\,m}^*, c_{\mathbf{n}\,m}$ are complex Grassmann numbers. The one-particle wave functions being periodic in $L_i$

$$\psi_{\mathbf{n}}(\mathbf{x}) = \frac{e^{i\mathbf{k}_{\mathbf{n}}\cdot\mathbf{x}}}{\sqrt{V}}, \qquad\qquad \mathbf{k}_{\mathbf{n}} = \left(\frac{2\pi}{L_1}\, n_1,\, \frac{2\pi}{L_2}\, n_2,\, \ldots,\, \frac{2\pi}{L_D}\, n_D\right), \qquad V = \prod_{i=1}^{D} L_i \tag{2.28}$$

are the eigenfunctions of the Hamilton operator (2.23) with a homogeneous and constant potential (2.25)

$$\hat{H}_F(\mathbf{x},\tau)\, \psi_{\mathbf{n}}(\mathbf{x}) = E_{\mathbf{n}}\, \psi_{\mathbf{n}}(\mathbf{x}), \qquad\qquad E_{\mathbf{n}} = \frac{\hbar^2 {\mathbf{k}_{\mathbf{n}}}^2}{2m_F} + V_{\text{eff}}, \tag{2.29}$$

and they fulfill the orthonormality relation

$$\int d^D x\, \psi_{\mathbf{n}}(\mathbf{x})\, \psi_{\mathbf{n}'}^*(\mathbf{x}) = \delta_{\mathbf{n}\,\mathbf{n}'}, \tag{2.30}$$

as well as the completeness relation

$$\sum_{\mathbf{n}} \psi_{\mathbf{n}}(\mathbf{x})\, \psi_{\mathbf{n}}^*(\mathbf{x}') = \delta(\mathbf{x}-\mathbf{x}'). \tag{2.31}$$

Because of the decomposition in Eq. (2.26), the functional integration can be expressed as a summation over all possible coefficients $c_{\mathbf{n}\,m}^*, c_{\mathbf{n}\,m}$

$$\oint \mathcal{D}\psi_F^* \oint \mathcal{D}\psi_F = \prod_{\mathbf{n}} \prod_{m=-\infty}^{\infty} \int dc_{\mathbf{n}\,m}^* \int dc_{\mathbf{n}\,m}. \tag{2.32}$$

Inserting Eq. (2.26) into Eq. (2.22), we use Eqs. (2.23), (2.25), (2.29), and the orthonormality relation (2.30) of the one-particle wave functions and the corresponding one

$$\frac{1}{\hbar\beta} \int_0^{\hbar\beta} d\tau\, e^{-i\omega_m \tau}\, e^{i\omega_{m'}\tau} = \delta_{m\,m'} \tag{2.33}$$

for the Matsubara functions to obtain

$$\mathcal{A}_F[\psi_F^*, \psi_F] + \mathcal{A}_{BF}[\Psi_B^*, \Psi_B, \psi_F^*, \psi_F] = \sum_{\mathbf{n}} \sum_{m=-\infty}^{\infty} \hbar\beta(-i\hbar\omega_m + E_{\mathbf{n}} - \mu_F) c_{\mathbf{n}\,m}^* c_{\mathbf{n}\,m}. \tag{2.34}$$

Therefore, the functional integral over the fermionic fields in Eq. (2.21) factorizes into ordinary integrals over the Grassmann numbers $c^*_{\mathbf{n}\,m}, c_{\mathbf{n}\,m}$

$$\mathcal{Z}_F[\Psi^*_B, \Psi_B] = \prod_{\mathbf{n}} \prod_{m=-\infty}^{\infty} \int dc^*_{\mathbf{n}\,m} \int dc_{\mathbf{n}\,m}\, e^{-\beta(-i\hbar\omega_m + E_{\mathbf{n}} - \mu_F) c^*_{\mathbf{n}\,m} c_{\mathbf{n}\,m}}. \tag{2.35}$$

Using Eqs. (A.1) and (A.11) in Appendix A, the functional integral over fermionic fields (2.35) results in

$$\mathcal{Z}_F[\Psi^*_B, \Psi_B] = \prod_{\mathbf{n}} \prod_{m=-\infty}^{\infty} \beta(-i\hbar\omega_m + E_{\mathbf{n}} - \mu_F). \tag{2.36}$$

## 2.4 Tracelog

The factors $\lambda_{\mathbf{n}\,m} \equiv \beta(-i\hbar\omega_m + E_{\mathbf{n}} - \mu_F)$ in Eq. (2.36) belong to the eigenvalues of the eigenvalue problem

$$\int_0^{\hbar\beta} d\tau' \int d^D x'\, \hat{O}_F(\mathbf{x}, \tau; \mathbf{x}', \tau')\, \psi_{\mathbf{n}\,m}(\mathbf{x}', \tau') = \frac{\lambda_{\mathbf{n}\,m}}{\hbar\beta}\, \psi_{\mathbf{n}\,m}(\mathbf{x}, \tau) \tag{2.37}$$

with the kernel of the integral equation

$$\hat{O}_F(\mathbf{x}, \tau; \mathbf{x}', \tau') = \frac{1}{\hbar}\, \delta(\mathbf{x} - \mathbf{x}')\, \delta(\tau - \tau') \left[ \hbar \frac{\partial}{\partial \tau'} + \hat{H}_F(\mathbf{x}', \tau') - \mu_F \right], \tag{2.38}$$

which occurs in the euclidean action (2.22):

$$\mathcal{A}_F + \mathcal{A}_{BF} = \hbar \int_0^{\hbar\beta} d\tau \int_0^{\hbar\beta} d\tau' \int d^D x \int d^D x'\, \psi^*_F(\mathbf{x}, \tau)\, \hat{O}_F(\mathbf{x}, \tau; \mathbf{x}', \tau')\, \psi_F(\mathbf{x}', \tau'). \tag{2.39}$$

Because of Eqs. (2.23) and (2.25), the eigenfunctions in Eq. (2.37) are obviously given by

$$\psi_{\mathbf{n}\,m}(\mathbf{x}, \tau) = \psi_{\mathbf{n}}(\mathbf{x})\, e^{-i\omega_m \tau}. \tag{2.40}$$

With respect to these eigenfunctions the kernel (2.38) is diagonal as all nondiagonal elements vanish:

$$\begin{aligned} (\hat{O}_F)_{\mathbf{n}\,m,\,\mathbf{n}'\,m'} &= \int_0^{\hbar\beta} d\tau \int_0^{\hbar\beta} d\tau' \int d^D x \int d^D x'\, \psi^*_{\mathbf{n}\,m}(\mathbf{x}, \tau)\, \hat{O}_F(\mathbf{x}, \tau; \mathbf{x}', \tau')\, \psi_{\mathbf{n}'\,m'}(\mathbf{x}', \tau') \\ &= \delta_{\mathbf{n}\,\mathbf{n}'}\, \delta_{m\,m'}\, \lambda_{\mathbf{n}'\,m'}. \end{aligned} \tag{2.41}$$

Here we used the orthonormality relations (2.30) and (2.33) of the eigenfunctions (2.40). Thus, the diagonal elements represent the eigenvalues of the kernel $\hat{O}_F$. Hence we conclude that the functional integral over fermionic fields (2.36) is the determinant of the kernel

$$\mathcal{Z}_F[\Psi^*_B, \Psi_B] = \prod_{\mathbf{n}} \prod_{m=-\infty}^{\infty} \lambda_{\mathbf{n}\,m} = \det \hat{O}_F. \tag{2.42}$$

Now we define the tracelog of the kernel $\hat{O}_F$ as the trace of its logarithm or, equivalent, as the logarithm of its determinant

$$\mathrm{Tr}\,\ln\hat{O}_F \equiv \sum_{\mathbf{n}}\sum_{m=-\infty}^{\infty}\ln(\lambda_{\mathbf{n}\,m}) = \ln\,\det\hat{O}_F, \tag{2.43}$$

where the kernel in the matrix representation (2.41) is used. With this definition we can express Eq. (2.36) as

$$\mathcal{Z}_F[\Psi_B^*,\Psi_B] = e^{\mathrm{Tr}\ln\hat{O}_F} \tag{2.44}$$

and the grand-canonical partition function (2.20) as

$$\mathcal{Z}[\Psi_B^*,\Psi_B] = e^{-\mathcal{A}_B[\Psi_B^*,\Psi_B]/\hbar+\mathrm{Tr}\ln\hat{O}_F}. \tag{2.45}$$

Thus, the grand-canonical free energy $\mathcal{F}\equiv-(\ln\mathcal{Z})/\beta$ results in

$$\mathcal{F}[\Psi_B^*,\Psi_B] = \frac{1}{\hbar\beta}\,\mathcal{A}_B[\Psi_B^*,\Psi_B] - \frac{1}{\beta}\,\mathrm{Tr}\ln\hat{O}_F. \tag{2.46}$$

Inserting Eq. (2.43), the grand-canonical free energy has the form

$$\mathcal{F}[\Psi_B^*,\Psi_B] = \frac{1}{\hbar\beta}\,\mathcal{A}_B[\Psi_B^*,\Psi_B] - \frac{1}{\beta}\sum_{\mathbf{n}}\sum_{m=-\infty}^{\infty}\ln\left[\beta(-i\hbar\omega_m+E_{\mathbf{n}}-\mu_F)\right]. \tag{2.47}$$

The calculation of the last sum, as shown in detail in Appendices B and C, yields

$$\mathcal{F}[\Psi_B^*,\Psi_B] = \frac{1}{\hbar\beta}\,\mathcal{A}_B[\Psi_B^*,\Psi_B] - \frac{1}{\beta}\sum_{\mathbf{n}}\ln\left[1+e^{-\beta(E_{\mathbf{n}}-\mu_F)}\right]. \tag{2.48}$$

## 2.5 Semiclassical Approximation

In order to evaluate the remaining sum over the quantum numbers $\mathbf{n}$ in the grand-canonical free energy (2.48), we use the energy eigenvalues $E_{\mathbf{n}}$ of the effective one-particle Hamilton operator (2.23) corresponding to the wave functions (2.28). But instead of continuing with a homogeneous and constant potential (2.25) in the effective Hamilton operator, we return to the spatio-temporal dependent effective Hamilton operator (2.23) and apply the semiclassical approximation, also called local density approximation (LDA). Using the one-particle wave function (2.28), Eq. (2.29) can be written as

$$\left[\hat{H}_F(\mathbf{x},\tau)-E_{\mathbf{n}}\right]\frac{e^{i\mathbf{k}_{\mathbf{n}}\cdot\mathbf{x}/\hbar}}{V} = 0. \tag{2.49}$$

As the expression inside the brackets must be zero, the eigenvalues $E_{\mathbf{n}}$ of the effective fermionic Hamilton operator (2.23) depend on the space coordinate $\mathbf{x}$ and the imaginary time $\tau$ as follows:

$$E_{\mathbf{n}}(\mathbf{x},\tau) = \frac{\hbar^2{\mathbf{k}_{\mathbf{n}}}^2}{2m_F} + V_F(\mathbf{x}) + \int d^Dx'\,V_{BF}^{(\mathrm{int})}(\mathbf{x},\mathbf{x}')\,|\Psi_B(\mathbf{x}',\tau)|^2. \tag{2.50}$$

Within the semiclassical approximation the quantum numbers $\mathbf{n}$ are regarded as narrow neighbouring so that the energy values become continuous in momentum $\mathbf{p}=\hbar\mathbf{k}$ and represent the quasi-classical energy spectrum:

$$E_{\mathbf{n}}(\mathbf{x},\tau)\to E(\mathbf{p},\mathbf{x},\tau) = \frac{\mathbf{p}^2}{2m_F} + V_F(\mathbf{x}) + \int d^Dx'\,V_{BF}^{(\mathrm{int})}(\mathbf{x},\mathbf{x}')\,|\Psi_B(\mathbf{x}',\tau)|^2. \tag{2.51}$$

This is justified if the energy difference $\Delta E$ between neighbouring one-particle eigenstates is small in comparison with the thermal energy $k_B T$. Consequently, the sum $\sum_{\mathbf{n}}$ is replaced within the semiclassical approximation by a phase space integral $\int d^D x \int d^D p/(2\pi\hbar)^D$ and an imaginary time integral $\int_0^{\hbar\beta} d\tau/(\hbar\beta)$. Applying this to the grand-canonical free energy (2.48) leads to

$$\mathcal{F}[\Psi_B^*, \Psi_B] = \frac{1}{\hbar\beta}\,\mathcal{A}_B[\Psi_B^*, \Psi_B] - \frac{1}{\hbar\beta^2}\int_0^{\hbar\beta} d\tau \int \frac{d^D x\, d^D p}{(2\pi\hbar)^D}\,\ln\left[1+\exp\left\{-\beta\left(\frac{\mathbf{p}^2}{2m_F} - \tilde{\mu}_F(\mathbf{x},\tau)\right)\right\}\right], \tag{2.52}$$

where we have introduced the local chemical potential for fermions

$$\tilde{\mu}_F(\mathbf{x},\tau) = \mu_F - V_F(\mathbf{x}) - \int d^D x'\, V_{BF}^{(\mathrm{int})}(\mathbf{x},\mathbf{x}')\,|\Psi_B(\mathbf{x}',\tau)|^2, \tag{2.53}$$

giving the kinetic energy of the fermion in the highest energetic state, when it is located at the space point $\mathbf{x}$ at the imaginary time $\tau$. The momentum integral of the logarithm has the general form

$$I = \int \frac{d^D p}{(2\pi\hbar)^D}\, f\left(\frac{\mathbf{p}^2}{2m_F}\right). \tag{2.54}$$

As the function $f(\mathbf{p})$ is spherically symmetric with $p = |\mathbf{p}|$, we use spherical coordinates:

$$I = \frac{O_D}{(2\pi\hbar)^D}\int_0^{\infty} dp\, p^{D-1}\, f\left(\frac{p^2}{2m_F}\right) \tag{2.55}$$

with the area of the $D$-dimensional unit sphere

$$O_D = \frac{2\pi^{D/2}}{\Gamma(D/2)}. \tag{2.56}$$

The substitution $\varepsilon(p) = p^2/2m_F$ leads to

$$I = \frac{1}{\Gamma(D/2)}\left(\frac{m_F}{2\pi\hbar^2}\right)^{D/2}\int_0^{\infty} d\varepsilon\, \varepsilon^{D/2-1}\, f(\varepsilon). \tag{2.57}$$

Applying Eqs. (2.54) and (2.57) to Eq. (2.52) yields

$$\mathcal{F}[\Psi_B^*, \Psi_B] = \frac{1}{\hbar\beta}\,\mathcal{A}_B[\Psi_B^*, \Psi_B] - \frac{D\kappa_D}{2\hbar\beta^2}\int_0^{\hbar\beta} d\tau \int d^D x \int_0^{\infty} d\varepsilon\, \varepsilon^{D/2-1}\,\ln\left[1+e^{-\beta[\varepsilon-\tilde{\mu}_F(\mathbf{x},\tau)]}\right], \tag{2.58}$$

where we have introduced the abbreviation:

$$\kappa_D \equiv \frac{2}{D\,\Gamma(D/2)}\left(\frac{m_F}{2\pi\hbar^2}\right)^{D/2}. \tag{2.59}$$

An integration by parts in the last term of Eq. (2.58), where the boundary terms vanish, leads to

$$\mathcal{F}[\Psi_B^*, \Psi_B] = \frac{1}{\hbar\beta}\,\mathcal{A}_B[\Psi_B^*, \Psi_B] - \frac{\kappa_D}{\hbar\beta}\int_0^{\hbar\beta} d\tau \int d^D x \int_0^{\infty} d\varepsilon\, \frac{\varepsilon^{D/2}}{e^{\beta[\varepsilon-\tilde{\mu}_F(\mathbf{x},\tau)]}+1}. \tag{2.60}$$

## 2.6 Low-Temperature Limit

In order to evaluate the integral over $\varepsilon$ in Eq. (2.60) for low temperatures, we perform the Sommerfeld expansion, which is explained in detail in Appendix D. Within the framework of the Gross-Pitaevskii theory we consider the zero-temperature limit $T \downarrow 0$, where not only all bosonic atoms condense into the lowest energy state, but also the fermion gas becomes quantum degenerate. As mentioned in Chapter 1, a quantum degeneracy of $T/T_F = 0.1$ ($T/T_F = 0.3$) is achieved in the Hamburg (Florence) experiment. Due to the strong attraction between bosons and fermions the local chemical potential (2.53) is inside the overlapping region of bosons and fermions mostly larger than the Fermi energy $\mu_F = E_F = k_B T_F$. Thus, only the zeroth order of the Sommerfeld expansion (D.26) in the smallness parameter $[k_B T/\tilde{\mu}_F(\mathbf{x},\tau)]^2 \approx 0.01\,(0.09) \ll 1$ contributes significantly:

$$\mathcal{F}[\Psi_B^*,\Psi_B] = \frac{1}{\hbar\beta}\int\limits_0^{\hbar\beta} d\tau \int d^D x\, \Psi_B^*(\mathbf{x},\tau)\left[\hbar\frac{\partial}{\partial\tau} - \frac{\hbar^2}{2m_B}\Delta + V_B(\mathbf{x}) - \mu_B \right.$$
$$\left. + \frac{1}{2}\int d^D x'\, V_{BB}^{(\mathrm{int})}(\mathbf{x},\mathbf{x}')\,|\Psi_B(\mathbf{x}',\tau)|^2\right]\Psi_B(\mathbf{x},\tau)$$
$$- \frac{2\kappa_D}{(D+2)\hbar\beta}\int\limits_0^{\hbar\beta} d\tau \int d^D x\,\Theta(\tilde{\mu}_F(\mathbf{x},\tau))\,\tilde{\mu}_F^{D/2+1}(\mathbf{x},\tau). \quad (2.61)$$

Here the Heaviside function takes into account that the integrand in Eq. (2.60) vanishes for $\tilde{\mu}_F(\mathbf{x},\tau) < 0$. This is obvious as the denominator in this integrand becomes infinity (one) with a positive (negative) exponent in the zero-temperature limit $\beta \uparrow \infty$. Thus, it is allowed to replace it by a Heaviside function:

$$\int\limits_0^\infty d\varepsilon\,\frac{\varepsilon^{D/2}}{e^{\beta[\varepsilon-\tilde{\mu}_F(\mathbf{x},\tau)]}+1} = \int\limits_0^\infty d\varepsilon\,\Theta(\tilde{\mu}_F(\mathbf{x},\tau)-\varepsilon)\,\varepsilon^{D/2} = \int\limits_{-\infty}^\infty d\varepsilon\,\Theta(\varepsilon)\,\Theta(\tilde{\mu}_F(\mathbf{x},\tau)-\varepsilon)\,\varepsilon^{D/2}, \quad (2.62)$$

where the first Heaviside function replaces the lower integration limit. Note that an integration by parts, where the boundary terms vanish, yields the above result in a more simple way:

$$\begin{aligned}\int\limits_0^\infty d\varepsilon\,\frac{\varepsilon^{D/2}}{e^{\beta[\varepsilon-\tilde{\mu}_F(\mathbf{x},\tau)]}+1} &= -\frac{2}{D+2}\int\limits_{-\infty}^\infty d\varepsilon\,[\delta(\varepsilon)\,\Theta(\tilde{\mu}_F(\mathbf{x},\tau)-\varepsilon) - \Theta(\varepsilon)\,\delta(\varepsilon-\tilde{\mu}_F(\mathbf{x},\tau))]\,\varepsilon^{D/2+1} \\ &= \frac{2}{D+2}\,\Theta(\tilde{\mu}_F(\mathbf{x},\tau))\,\tilde{\mu}_F^{D/2+1}(\mathbf{x},\tau). \quad (2.63)\end{aligned}$$

## 2.7 Validity of Approximations

One may argue that the zero-temperature limit $T \downarrow 0$ contradicts the validity of the semiclassical approximation as the thermal energy $k_B T$ tends also to zero instead of being much larger than the energy difference $\Delta E$ between neighbouring eigenstates of the Fermi gas. Indeed, the temperature $T$, achieved in the Hamburg (Florence) experiment, is of the order of $0.1\,T_F$ ($0.3\,T_F$). As the density of states $g(\varepsilon)\,d\varepsilon$ gives the number $dn$ of states within the energy interval $d\varepsilon$ at the energy value $\varepsilon$, its inverse

$$d\varepsilon = g(n)^{-1}\,dn \quad (2.64)$$

can be identified with the energy difference $\Delta E$ between neighbouring eigenstates, when we set heuristically $dn = 1$. The fermion number $N_F$ is related to the number $N$ of states in the harmonic trap $V_F(\mathbf{x})$, confining the quantum degenerated Fermi gas, as follows:

$$N_F = \int_0^\infty d\varepsilon \, \frac{g(\varepsilon)}{e^{\beta[\varepsilon - E_F]} + 1} \approx \int_0^{E_F} d\varepsilon \, g(\varepsilon), \tag{2.65}$$

This stems from the fact that, at zero temperature, each one-particle state up to the Fermi energy $E_F$ is occupied with a fermion when we assume, for simplicity, an ideal Fermi gas without interaction with the bosons. The energy difference (E.9) between neighbouring eigenstates of an ideal Fermi gas in a $D$-dimensional trap $V_F(\mathbf{x})$ at the energy level, which is filled up with $N$ fermions reads

$$\Delta E = g(N)^{-1} = \frac{(D!)^{1/D} \, \hbar\tilde{\omega}_F}{D \, N^{1-1/D}}. \tag{2.66}$$

Inserting the number of fermions (E.7) in a $D$-dimensional harmonic oscillator up to the Fermi energy $E_F$ into Eq. (E.9 leads to

$$\Delta E = \frac{1}{DN} \, E_F. \tag{2.67}$$

Thus, we can compare the energy difference (2.67) with the thermal energy $k_B T = 0.1 \, E_F \, (0.3 \, E_F)$ for the Hamburg (Florence) experiment. This shows that the criterion $\Delta E \ll k_B T$ for applying the semiclassical approximation for $D = 3$ is fulfilled for more than $N = 10$ fermions. Hence, as the experiments deals with at least $10^4$ fermions, replacing the sum over all eigenstates with a phase space integral within the semiclassical approximation is justified for almost the entire range of states.

## 2.8 Time-Dependent Gross-Pitaevskii Equation

The grand-canonical free energy $\mathcal{F}$ is obtained as the extremum of the effective action $\Gamma$ with respect to the fields $\Psi_e^*(\mathbf{x}, \tau)$, $\Psi_e(\mathbf{x}, \tau)$:

$$\mathcal{F}[\Psi_B^*, \Psi_B] \equiv \Gamma[\Psi_e^*, \Psi_e]. \tag{2.68}$$

This means that the effective action is a functional of those fields which extremize it according to [47]

$$\left.\frac{\delta\Gamma[\Psi^*, \Psi]}{\delta\Psi^*(\mathbf{x}, \tau)}\right|_{\Psi=\Psi_e}^{\Psi^*=\Psi_e^*} = 0, \qquad \left.\frac{\delta\Gamma[\Psi^*, \Psi]}{\delta\Psi(\mathbf{x}, \tau)}\right|_{\Psi=\Psi_e}^{\Psi^*=\Psi_e^*} = 0. \tag{2.69}$$

Applying Eqs. (2.68) and (2.69) to the grand-canonical free energy (2.61) leads to the Gross-Pitaevskii equation of a trapped ultracold Bose-Fermi mixture with arbitrary boson-boson and boson-fermion interactions and with imaginary time dependence:

$$\begin{aligned}\frac{\delta\mathcal{F}[\Psi_B^*, \Psi_B]}{\delta\Psi_B^*(\mathbf{x}, \tau)} = \Bigg[\hbar\frac{\partial}{\partial\tau} - \frac{\hbar^2}{2m_B}\Delta + V_B(\mathbf{x}) - \mu_B + \int d^D x' \, V_{BB}^{(\mathrm{int})}(\mathbf{x}, \mathbf{x}') \, |\Psi_B(\mathbf{x}', \tau)|^2 \\ + \kappa_D \int d^D x'' \, \Theta(\tilde{\mu}_F(\mathbf{x}'', \tau)) \, V_{BF}^{(\mathrm{int})}(\mathbf{x}, \mathbf{x}'') \, \tilde{\mu}_F^{D/2}(\mathbf{x}'', \tau)\Bigg] \Psi_B(\mathbf{x}, \tau) = 0.\end{aligned} \tag{2.70}$$

This time-dependent nonlinear Schrödinger equation of the condensate wave function $\Psi_B(\mathbf{x},\tau)$ has the form of a partial integrodifferential equation, where the nonlinear terms are due to both interactions. The last term results from the boson-fermion interaction, whereas the other terms have the conventional Gross-Pitaevskii form for a condensate [45,46]. This equation can be transformed back to the real time via a Wick rotation $\tau = it$ to obtain an equation of motion for the condensate wave function:

$$i\hbar\frac{\partial}{\partial t}\,\Psi_B(\mathbf{x},t) = \Bigg[-\frac{\hbar^2}{2m_B}\Delta + V_B(\mathbf{x}) + \int d^D x'\, V_{BB}^{(\mathrm{int})}(\mathbf{x},\mathbf{x}')\,|\Psi_B(\mathbf{x}',t)|^2 + \kappa_D \int d^D x''\,\Theta(\tilde{\mu}_F(\mathbf{x}'',t))\,V_{BF}^{(\mathrm{int})}(\mathbf{x},\mathbf{x}'')\,\tilde{\mu}_F^{D/2}(\mathbf{x}'',t)\Bigg]\,\Psi_B(\mathbf{x},t). \quad (2.71)$$

It allows to study the dynamics of the BEC at zero temperature $T = 0$. Note that the bosonic chemical potential $\mu_B$ has to be omitted since it was introduced in the euclidean action (2.8) in order to describe the thermodynamics in a grand-canonical ensemble with the help of the grand-canonical partition function (2.1). On the other hand the fermionic chemical potential $\mu_F$ is identified with the Fermi energy $E_F$ in the local chemical potential

$$\tilde{\mu}_F(\mathbf{x},t) = E_F - V_F(\mathbf{x}) - \int d^D x'\, V_{BF}^{(\mathrm{int})}(\mathbf{x},\mathbf{x}')\,|\Psi_B(\mathbf{x}',t)|^2. \quad (2.72)$$

However the time-dependent Gross-Pitaevskii equation (2.71) has the disadvantage of an absent independent dynamics of the fermions as their degrees of freedom are already integrated out in Section 2.3, so that the time dependence in their particle density

$$n_F(\mathbf{x},t) = \kappa_D\,\Theta(\tilde{\mu}_F(\mathbf{x},t))\,\tilde{\mu}_F^{D/2}(\mathbf{x},t) \quad (2.73)$$

arises only from the condensate wave function.

## 2.9 Coupled Equations of Motions

In order to include the dynamics of the fermions within a more detailed mean-field description, we go back to the grand-canonical partition function (2.20) and express it in form of the grand-canonical free energy without integrating out the Fermi fields in the fermionic functional integral:

$$\mathcal{F}[\Psi_B^*,\Psi_B] = \frac{1}{\hbar\beta}\,\mathcal{A}_B[\Psi_B^*,\Psi_B] - \frac{1}{\beta}\ln\mathcal{Z}_F[\Psi_B^*,\Psi_B]. \quad (2.74)$$

Extremizing the effective action (2.74) according to Eq. (2.69) yields for the bosonic action the first five terms of the Gross-Pitaevskii equation (2.70) and for the fermionic functional integral (2.21) we obtain

$$\begin{aligned}\frac{\delta\ln\mathcal{Z}_F[\Psi_B^*,\Psi_B]}{\delta\Psi_B^*(\mathbf{x},\tau)} &= \frac{1}{\mathcal{Z}_F[\Psi_B^*,\Psi_B]}\oint\mathcal{D}\psi_F^*\oint\mathcal{D}\psi_F\,e^{-(\mathcal{A}_F[\psi_F^*,\psi_F]+\mathcal{A}_{BF}[\Psi_B^*,\Psi_B,\psi_F^*,\psi_F])/\hbar}\\ &\quad\times\frac{-1}{\hbar}\,\frac{\delta}{\delta\Psi_B^*(\mathbf{x},\tau)}\int_0^{\hbar\beta}d\tau'\int d^D x'\int d^D x''\,V_{BF}^{(\mathrm{int})}(\mathbf{x}',\mathbf{x}'')\,|\Psi_B(\mathbf{x}'',\tau')|^2\,|\psi_F(\mathbf{x}',\tau')|^2\\ &= \frac{1}{\hbar}\int d^D x'\,V_{BF}^{(\mathrm{int})}(\mathbf{x},\mathbf{x}')\,\big\langle\psi_F(\mathbf{x}',\tau)\,\psi_F^*(\mathbf{x}',\tau)\big\rangle\,\Psi_B(\mathbf{x},\tau). \quad (2.75)\end{aligned}$$

Here we used the anticommutation rule (A.2) for the Fermi fields and the definition of the two-point function

$$\langle\psi(\mathbf{x}_1,\tau_1)\,\psi^*(\mathbf{x}_2,\tau_2)\rangle \equiv \frac{1}{\mathcal{Z}}\oint\mathcal{D}\psi^*\oint\mathcal{D}\psi\,\psi(\mathbf{x}_1,\tau_1)\,\psi^*(\mathbf{x}_2,\tau_2)\,e^{-\mathcal{A}[\psi^*,\psi]/\hbar}. \tag{2.76}$$

Thus, the functional differentiation of the effective action (2.74) leads to

$$\left[\hbar\frac{\partial}{\partial\tau}-\frac{\hbar^2}{2m_B}\Delta+V_B(\mathbf{x})-\mu_B+\int d^Dx'\,V_{BB}^{(\mathrm{int})}(\mathbf{x},\mathbf{x}')\,|\Psi_B(\mathbf{x}',\tau)|^2 - \int d^Dx'\,V_{BF}^{(\mathrm{int})}(\mathbf{x},\mathbf{x}')\,\langle\psi_F(\mathbf{x}',\tau)\,\psi_F^*(\mathbf{x}',\tau)\rangle\right]\Psi_B(\mathbf{x},\tau)=0. \tag{2.77}$$

The two-point function of the Fermi fields can be evaluated using the decomposition (2.26) of the Fermi fields and the effective one-particle Hamilton operator (2.23) for fermions with the effective potential (2.24) in the semiclassical approximation according to Eq. (2.25):

$$\langle\psi_F(\mathbf{x}_1,\tau_1)\,\psi_F^*(\mathbf{x}_2,\tau_2)\rangle = \frac{1}{\mathcal{Z}_F}\sum_{\mathbf{p}}\sum_{\mathbf{q}}\sum_{k=-\infty}^{\infty}\sum_{l=-\infty}^{\infty}\psi_{\mathbf{p}}(\mathbf{x}_1)\,\psi_{\mathbf{q}}^*(\mathbf{x}_2)\,e^{-i\omega_k\tau_1}\,e^{i\omega_l\tau_2} \times\left\{\prod_{\mathbf{n}}\prod_{m=-\infty}^{\infty}\int dc_{\mathbf{n}\,m}^*\int dc_{\mathbf{n}\,m}\,[1+\beta(-i\hbar\omega_m+E_{\mathbf{n}}-\mu_F)c_{\mathbf{n}\,m}c_{\mathbf{n}\,m}^*]\right\}c_{\mathbf{p}\,k}\,c_{\mathbf{q}\,l}^*. \tag{2.78}$$

Furthermore, we used the procedure in Section 2.3 and the Taylor expansion (A.10) of the exponential function. Each of the coefficients $c_{\mathbf{p}\,k}$ and $c_{\mathbf{q}\,l}^*$ can be placed within the product over all eigenstates $\mathbf{n}$ and Matsubara modes $m$ to the factors with the same indices. Applying the integration rules (A.8) and (A.9) for Grassmann numbers, one sees that the first term within the bracket contributes only if both coefficients match their indices, whereas the second term contributes only without these coefficients due to Eq. (A.4). Thus, we obtain

$$\langle\psi_F(\mathbf{x}_1,\tau_1)\,\psi_F^*(\mathbf{x}_2,\tau_2)\rangle = \sum_{\mathbf{p}}\sum_{\mathbf{q}}\sum_{k=-\infty}^{\infty}\sum_{l=-\infty}^{\infty}\frac{\delta_{\mathbf{p}\,\mathbf{q}}\,\delta_{k\,l}\,\psi_{\mathbf{p}}(\mathbf{x}_1)\,\psi_{\mathbf{q}}^*(\mathbf{x}_2)\,e^{-i\omega_k\tau_1}\,e^{i\omega_l\tau_2}}{\beta(-i\hbar\omega_k+E_{\mathbf{p}}-\mu_F)} \times\frac{1}{\mathcal{Z}_F}\prod_{\mathbf{n}}\prod_{m=-\infty}^{\infty}\beta(-i\hbar\omega_m+E_{\mathbf{n}}-\mu_F), \tag{2.79}$$

which reduces due Eq. (2.36) to

$$\langle\psi_F(\mathbf{x}_1,\tau_1)\,\psi_F^*(\mathbf{x}_2,\tau_2)\rangle = \sum_{\mathbf{n}}\sum_{m=-\infty}^{\infty}\frac{\psi_{\mathbf{n}}(\mathbf{x}_1)\,\psi_{\mathbf{n}}^*(\mathbf{x}_2)\,e^{-i\omega_m(\tau_1-\tau_2)}}{\beta(-i\hbar\omega_m+E_{\mathbf{n}}-\mu_F)}. \tag{2.80}$$

This two-point function is at the same time a Green function for the fermion fields:

$$G_F(\mathbf{x},\tau;\mathbf{x}',\tau')=\langle\psi_F(\mathbf{x},\tau)\,\psi_F^*(\mathbf{x}',\tau')\rangle, \tag{2.81}$$

obeying the linear inhomogeneous Schrödinger equation for fermions with the delta function in space and the antiperiodic repetitive one (B.11) in imaginary time as the inhomogeneity:

$$\left[\hbar\frac{\partial}{\partial\tau}+\hat{H}_F(\mathbf{x},\tau)-\mu_F\right]G_F(\mathbf{x},\tau;\mathbf{x}',\tau')=\hbar\,\delta(\mathbf{x}-\mathbf{x}')\,\delta^{(a)}(\tau-\tau'). \tag{2.82}$$

Moreover, the kernel (2.38) in Section 2.4 is just the inverse Green function

$$\hat{G}_F^{-1}(\mathbf{x},\tau;\mathbf{x}',\tau') = \hat{O}_F(\mathbf{x},\tau;\mathbf{x}',\tau') = \frac{1}{\hbar}\,\delta(\mathbf{x}-\mathbf{x}')\,\delta(\tau-\tau')\left[\hbar\frac{\partial}{\partial\tau'} + \hat{H}_F(\mathbf{x}',\tau') - \mu_F\right], \tag{2.83}$$

since it acts on the Green function (2.80) as follows

$$\begin{aligned}\int_0^{\hbar\beta} d\tau'' \int d^D x''\, \hat{G}_F^{-1}(\mathbf{x},\tau;\mathbf{x}'',\tau'')\, G_F(\mathbf{x}'',\tau'';\mathbf{x}',\tau') &= \frac{1}{\hbar\beta}\sum_{\mathbf{n}}\sum_{m=-\infty}^{\infty}\psi_{\mathbf{n}}(\mathbf{x})\,\psi_{\mathbf{n}}^*(\mathbf{x}')\,e^{-i\omega_m(\tau-\tau')} \\ &= \delta(\mathbf{x}-\mathbf{x}')\,\delta^{(a)}(\tau-\tau'). \end{aligned}\tag{2.84}$$

Here the completeness relations (2.31) for the one-particle wave functions and (B.9) and (B.11) for the Matsubara functions were used.

A Wick rotation $\tau = it$ and the omission of the chemical potentials in Eqs. (2.77) and (2.82) leads to two coupled equations of motions, namely one for the condensate wave function:

$$\begin{aligned}i\hbar\frac{\partial}{\partial t}\,\Psi_B(\mathbf{x},t) = \Bigg[-\frac{\hbar^2}{2m_B}\Delta + V_B(\mathbf{x}) + \int d^D x'\, V_{BB}^{(\mathrm{int})}(\mathbf{x},\mathbf{x}')\,|\Psi_B(\mathbf{x}',t)|^2 \\ - \int d^D x'\, V_{BF}^{(\mathrm{int})}(\mathbf{x},\mathbf{x}')\,G_F(\mathbf{x}',t;\mathbf{x}',t)\Bigg]\,\Psi_B(\mathbf{x},t),\end{aligned}\tag{2.85}$$

and another one for the fermionic Green function:

$$\begin{aligned}i\hbar\frac{\partial}{\partial t}\,G_F(\mathbf{x},t;\mathbf{x}',t') = \left[-\frac{\hbar^2}{2m_F}\Delta + V_F(\mathbf{x}) + \int d^D x'\, V_{BF}^{(\mathrm{int})}(\mathbf{x},\mathbf{x}')\,|\Psi_B(\mathbf{x}',t)|^2\right] G_F(\mathbf{x},t;\mathbf{x}',t') \\ + i\hbar\,\delta(\mathbf{x}-\mathbf{x}')\,\delta(t-t').\end{aligned}\tag{2.86}$$

This set of coupled equations of motions describes the dynamics in the mixture. Therein the condensate wave function $\Psi_B(\mathbf{x},t)$ in the Gross-Pitaevskii equation (2.85) is modified by the fermionic Green function $G_F(\mathbf{x},t;\mathbf{x},t)$ and, vice versa, the condensate wave function $\Psi_B(\mathbf{x},t)$ influences the fermionic Green function $G_F(\mathbf{x},t;\mathbf{x}',t')$ in the Schrödinger equation (2.86). In Section 2.10 we show that the fermionic Green function $G_F(\mathbf{x},t;\mathbf{x},t)$, which is local in space and time, turns out to be the fermionic particle density $n_F(\mathbf{x},t)$.

## 2.10 Fermionic Green Function

In this section we evaluate the Green function for a Fermi gas interacting with a stationary BEC in a common trap and insert it into the imaginary time dependent Gross-Pitaevskii equation (2.77). To this end the Green function has to obey the inhomogeneous linear Schrödinger equation (2.82) with the time-independent Hamilton operator

$$\hat{H}_F(\mathbf{x}) = -\frac{\hbar^2}{2m_F}\Delta + V_F(\mathbf{x}) + \int d^D x'\, V_{BF}^{(\mathrm{int})}(\mathbf{x},\mathbf{x}')\,|\Psi_B(\mathbf{x}')|^2, \tag{2.87}$$

leading to the eigenvalue problem

$$\hat{H}_F(\mathbf{x})\,\psi_{\mathbf{n}}(\mathbf{x}) = E_{\mathbf{n}}\,\psi_{\mathbf{n}}(\mathbf{x}). \tag{2.88}$$

This eigenvalue problem corresponds to the homogeneous boundary-value problem

$$-\left[p(x)\,y(x)'\right]' + q(x)\,y(x) - \lambda\,y(x) = 0, \qquad x \in [a,b] \tag{2.89}$$

with the Dirichlet boundary condition

$$y(a) = y(b) = 0, \tag{2.90}$$

where $p(x)$, $p'(x)$, and $q(x)$ are real and continuous functions and $p(x) \geq 0$. From the mathematics we know that all eigenvalues $\lambda$ are real numbers and form a monotone series $\lambda_1 < \lambda_2 < \ldots < \lambda_n < \ldots$ so that there is no need to treat the trap potential and interaction potential in the Hamilton operator (2.87) as spatial-independent as in the event of the time-dependent Hamilton operator (2.23).

Now we evaluate the Green function (2.80) without restricting to fermions. The bosonic Green function has to obey a linear inhomogeneous Schrödinger equation and describes therefore bosons interacting only with other species, but not with itself. Indeed it has the same form as in Eq. (2.80), but with Matsubara frequencies as in Eq. (B.1). First we replace the sum over the Matsubara frequencies $\omega_m$ by an integral with the help of the Poisson sum formula (B.8):

$$G(\mathbf{x},\tau;\mathbf{x}',\tau') = \lim_{\eta\downarrow 0}\frac{i}{2\pi}\sum_{\mathbf{n}}\psi_{\mathbf{n}}(\mathbf{x})\,\psi_{\mathbf{n}}^*(\mathbf{x}')\sum_{n=-\infty}^{\infty}(\epsilon)^n\int_{-\infty}^{\infty}d\omega\,\frac{e^{-i\omega[\tau-\tau'+(n-\eta)\hbar\beta]}}{\omega - i(\mu - E_{\mathbf{n}})/\hbar}. \tag{2.91}$$

Here we have introduced, as in Appendix C, the additional factor $\exp\{i\hbar\beta\omega\eta\}$ with $\eta$ as an infinitesimal positive number to achieve the normal-ordering. The integral can be performed with the help of Cauchy's residue theorem where we assume $\mu \geq E_{\mathbf{n}}$ without loss of generality. Indeed the opposite assumption $\mu \leq E_{\mathbf{n}}$ leads also to the same result. For $\tau - \tau' + (n-\eta)\hbar\beta < 0$ the contour of integration can be closed by a semicircle in the upper half of the complex $\omega$-plane without extra contribution where the integrand possess a pole at $\omega = i(\mu_F - E_{\mathbf{n}})$. For $\tau - \tau' + (n-\eta)\hbar\beta > 0$, on the other hand, the contour is closed by a semicircle in the lower half-plane where the integrand has no poles. Both cases are summarized to

$$\begin{aligned} G(\mathbf{x},\tau;\mathbf{x}',\tau') = &-\lim_{\eta\downarrow 0}\sum_{\mathbf{n}}\psi_{\mathbf{n}}(\mathbf{x})\,\psi_{\mathbf{n}}^*(\mathbf{x}') \\ &\times\sum_{n=-\infty}^{\infty}(\epsilon)^n\,\Theta\left(\tau'-\tau-(n-\eta)\hbar\beta\right)\,e^{-(E_{\mathbf{n}}-\mu)[\tau-\tau'+(n-\eta)\hbar\beta]/\hbar}. \end{aligned} \tag{2.92}$$

Now we perform the periodic and antiperiodic repetition, respectively, where the meaning of $\eta$ becomes apparently. For the imaginary time interval $\tau - \tau' \in [0,\hbar\beta)$ the sum over $n$ runs from $-\infty$ to $-1$ whereas the sum for $\tau - \tau' \in [-\hbar\beta, 0)$ runs from $-\infty$ to 0. Thus, using the geometrical series, the result reads

$$\begin{aligned} G(\mathbf{x},\tau;\mathbf{x}',\tau') = &\lim_{\eta\downarrow 0}\sum_{\mathbf{n}}\psi_{\mathbf{n}}(\mathbf{x})\,\psi_{\mathbf{n}}^*(\mathbf{x}')\,e^{-(E_{\mathbf{n}}-\mu)(\tau-\tau'-\eta\hbar\beta)/\hbar} \\ &\times\left[\frac{\Theta\left(\tau-\tau'-\eta\hbar\beta\right)}{1-\epsilon\,e^{-\beta(E_{\mathbf{n}}-\mu)}} + \epsilon\,\frac{\Theta\left(\tau'-\tau+\eta\hbar\beta\right)}{e^{\beta(E_{\mathbf{n}}-\mu)}-\epsilon}\right]. \end{aligned} \tag{2.93}$$

The left term within the brackets represents the retarded solution whereas the right term stands for the advanced solution. The physics behind the Green function means that the retarded (advanced)

solution creates at the space-time point $(\mathbf{x}', \tau')$ $((\mathbf{x}, \tau))$ a particle, which then propagates to the space-time point $(\mathbf{x}, \tau)$ $((\mathbf{x}', \tau'))$, where it is annihilated. In the equal time limit only one of the two mathematical possible limits $\tau' \uparrow \tau$ and $\tau' \downarrow \tau$ can contribute. Due to $\eta > 0$ it turns out to be the last limit which contributes in the Green function (2.93):

$$G(\mathbf{x}, \tau; \mathbf{x}', \tau) = \lim_{\tau' \downarrow \tau} G(\mathbf{x}, \tau; \mathbf{x}', \tau') = \epsilon \sum_{\mathbf{n}} \frac{\psi_{\mathbf{n}}(\mathbf{x})\, \psi_{\mathbf{n}}^*(\mathbf{x}')}{e^{\beta(E_{\mathbf{n}} - \mu)} - \epsilon}. \tag{2.94}$$

The number of particles is related with the grand-canonical free energy $\mathcal{F} = \epsilon \,\mathrm{Tr}\, \ln \hat{O}_F / \beta$ via

$$N = -\frac{\partial \mathcal{F}}{\partial \mu} = \sum_{\mathbf{n}} \frac{1}{e^{\beta(E_{\mathbf{n}} - \mu)} - \epsilon}, \tag{2.95}$$

where we used Eq. (C.17). Because of the normalization condition (2.106) and the orthonormality relation (2.30) for the one-particle wave functions the particle density reads

$$n(\mathbf{x}) = \sum_{\mathbf{n}} \frac{|\psi_{\mathbf{n}}(\mathbf{x})|^2}{e^{\beta(E_{\mathbf{n}} - \mu)} - \epsilon} = \epsilon\, G(\mathbf{x}, \tau; \mathbf{x}, \tau). \tag{2.96}$$

Evaluating the sum over all eigenstates $\mathbf{n}$ requires to know the energy eigenvalues $E_{\mathbf{n}}$ of the effective Hamilton operator (2.87). Because of the yet unknown condensate wave function $\Psi_B(\mathbf{x})$ in the effective Hamilton operator these energy eigenvalues are indetermined. We avoid this difficulty by applying the semiclassical approximation analogous to the procedure in Section 2.5. Due to Eq. (2.49) the quasi-classical energy spectrum reads:

$$E(\mathbf{k}, \mathbf{x}) = \frac{\hbar^2 \mathbf{k}^2}{2m_F} + V_F(\mathbf{x}) + \int d^D x'\, V_{BF}^{(\mathrm{int})}(\mathbf{x}, \mathbf{x}')\, |\Psi_B(\mathbf{x}')|^2. \tag{2.97}$$

Using plane waves for the one-particle wave functions (2.28) and replacing the sum $\sum_{\mathbf{n}}$ in the fermionic particle density (2.96) by the phase space integral $V \int d^D k/(2\pi)^D$ leads to

$$n_F(\mathbf{x}) = \int \frac{d^D k}{(2\pi)^D} \frac{1}{e^{\beta[\hbar^2 \mathbf{k}^2/2m_F - \tilde{\mu}_F(\mathbf{x})]} + 1} \tag{2.98}$$

with the local chemical potential

$$\tilde{\mu}_F(\mathbf{x}) = \mu_F - V_F(\mathbf{x}) - \int d^D x'\, V_{BF}^{(\mathrm{int})}(\mathbf{x}, \mathbf{x}')\, |\Psi_B(\mathbf{x}')|^2. \tag{2.99}$$

With the help of spherical coordinates according to Eqs. (2.54)–(2.56) and the substitution $\varepsilon(k) = \hbar^2 k^2 / 2m_F$ we obtain

$$n_F(\mathbf{x}) = \frac{1}{\Gamma(D/2)} \left(\frac{m_F}{2\pi\hbar^2}\right)^{D/2} \int_0^\infty \frac{d\varepsilon\, \varepsilon^{D/2-1}}{e^{\beta[\varepsilon - \tilde{\mu}_F(\mathbf{x})]} + 1}. \tag{2.100}$$

We apply analogous to the procedure in Section 2.6 the low-temperature limit, where the Sommerfeld expansion (D.26) up to the zeroth order in $1/(\beta\tilde{\mu}(\mathbf{x}))^2$ yields

$$n_F(\mathbf{x}) = \kappa_D\, \Theta\left(\tilde{\mu}_F(\mathbf{x})\right)\, \tilde{\mu}_F^{D/2}(\mathbf{x}) \tag{2.101}$$

with the abbreviation (2.59). Finally, we insert the result for the fermionic particle density (2.101) into the imaginary time dependent Gross-Pitaevskii equation (2.77) with a stationary condensate $\Psi_B(\mathbf{x},\tau) \to \Psi_B(\mathbf{x})$:

$$\left[-\frac{\hbar^2}{2m_B}\Delta + V_B(\mathbf{x}) - \mu_B + \int d^D x'\, V_{BB}^{(\mathrm{int})}(\mathbf{x},\mathbf{x}')\,|\Psi_B(\mathbf{x}')|^2 \right.$$
$$\left. + \kappa_D \int d^D x'\, \Theta\left(\tilde{\mu}_F(\mathbf{x}')\right)\, V_{BF}^{(\mathrm{int})}(\mathbf{x}',\mathbf{x})\,\tilde{\mu}_F^{D/2}(\mathbf{x}')\right]\Psi_B(\mathbf{x}) = 0. \quad (2.102)$$

Now we show that the results for the fermionic particle density (2.101) as well as the Gross-Pitaevskii equation (2.102) can also be derived following a different reasoning.

## 2.11 Stationary Gross-Pitaevskii Equation

Apart from the method with the fermionic Green function in the previous section the stationary Gross-Pitaevskii equation of a trapped ultracold Bose-Fermi mixture with arbitrary boson-boson and boson-fermion interactions can be obtained in two other ways. In the first way we modify the grand-canonical free energy (2.61) so that it becomes time-independent. For that purpose the grand-canonical free energy is derived by the same procedure as for the time-dependent one (2.61) except that the time dependences are dropped and in Section 2.5 the sum $\sum_{\mathbf{n}}$ is replaced by a phase space integral $\int d^D x \int d^D p/(2\pi\hbar)^D$:

$$\mathcal{F}[\Psi_B^*,\Psi_B] = \int d^D x\, \Psi_B^*(\mathbf{x})\left[-\frac{\hbar^2}{2m_B}\Delta + V_B(\mathbf{x}) - \mu_B + \frac{1}{2}\int d^D x'\, V_{BB}^{(\mathrm{int})}(\mathbf{x},\mathbf{x}')\,|\Psi_B(\mathbf{x}')|^2\right]\Psi_B(\mathbf{x})$$
$$- \frac{2}{D+2}\,\kappa_D \int d^D x\, \Theta(\tilde{\mu}_F(\mathbf{x}))\,\tilde{\mu}_F^{D/2+1}(\mathbf{x}), \quad (2.103)$$

Extremizing the grand-canonical free energy (2.103) with respect to $\Psi_B^*(\mathbf{x})$ yields the stationary Gross-Pitaevskii equation:

$$0 = \left[-\frac{\hbar^2}{2m_B}\Delta + V_B(\mathbf{x}) - \mu_B + \int d^D x'\, V_{BB}^{(\mathrm{int})}(\mathbf{x},\mathbf{x}')\,|\Psi_B(\mathbf{x}')|^2 \right.$$
$$\left. + \kappa_D \int d^D x'\, \Theta\left(\tilde{\mu}_F(\mathbf{x}')\right)\, V_{BF}^{(\mathrm{int})}(\mathbf{x},\mathbf{x}')\,\tilde{\mu}_F^{D/2}(\mathbf{x}')\right]\Psi_B(\mathbf{x}). \quad (2.104)$$

This time-independent nonlinear Schrödinger equation with respect to the condensate wave function $\Psi_B(\mathbf{x})$ also follows by omitting the time dependences in the imaginary time-dependent Gross-Pitaevskii equation (2.70) or by inserting the solution for a stationary condensate

$$\Psi_B(\mathbf{x},t) = \Psi_B(\mathbf{x})\, e^{-i\mu_B t/\hbar} \quad (2.105)$$

with $\mu_B$ as the total energy of a boson into the time-dependent Gross-Pitaevskii equation (2.71). The latter possibility justifies the omission of the chemical potential $\mu_B$ at the Wick rotation from the imaginary to the real time in Section 2.8. The number of bosons and fermions are obtained from the free energy (2.61) via the normalization condition

$$N_j = -\frac{\partial \mathcal{F}}{\partial \mu_j} = \int d^D x\, n_j(\mathbf{x}), \qquad j = B, F, \quad (2.106)$$

from which the particle densities of bosons and fermions result in

$$n_B(\mathbf{x}) = |\Psi_B(\mathbf{x})|^2, \tag{2.107}$$

$$n_F(\mathbf{x}) = \kappa_D\, \Theta\left(\tilde{\mu}_F(\mathbf{x})\right)\, \tilde{\mu}_F^{D/2}(\mathbf{x}). \tag{2.108}$$

From Eqs. (2.106) and (2.107) follows that all bosons are condensed, as we would expect it within the Gross-Pitaevskii theory. The particle density of the fermions depends on that of the bosons:

$$n_F(\mathbf{x}) = \kappa_D\, \Theta(\tilde{\mu}_F(\mathbf{x}))\left[\mu_F - V_F(\mathbf{x}) - \int d^D x'\, V_{BF}^{(\mathrm{int})}(\mathbf{x},\mathbf{x}')\, n_B(\mathbf{x}')\right]^{D/2}. \tag{2.109}$$

The condensate wave function $\Psi_B(\mathbf{x})$ is determined by the Gross-Pitaevskii equation (2.104) for chemical potentials $\mu_B$ and $\mu_F$, which have to be fixed by the normalization conditions (2.106) to obtain the desired particle numbers $N_B$ and $N_F$.

# Chapter 3

# Solution of Gross-Pitaevskii Equation

In this chapter we solve at first the stationary Gross-Pitaevskii equation in the Thomas-Fermi approximation in order to calculate the boson and the fermion density distribution for the parameters of the $^{87}$Rb–$^{40}$K experiment in Hamburg and Florence. For a critical number of bosons and fermions the resulting density profiles become complex which indicates the emergence of collapse of the Bose-Fermi mixture. We determine the stability border both within the Thomas-Fermi approximation and, in a separate variational calculation, beyond the Thomas-Fermi approximation. The stability border turns out to depend strongly on the value of the s-wave scattering length between $^{87}$Rb and $^{40}$K. Therefore, comparing our theoretical results with the experimental measurements allows to extract a trustworthy value for this s-wave scattering length.

## 3.1 Homogeneous Bose-Fermi Mixture with Arbitrary Interactions

In a homogeneous mixture the external potentials are absent and therefore the mixture is uniformly distributed. Due to the translational invariance of the system, the condensate wave function $\Psi_B(\mathbf{x})$ is a superposition of $N_B$ plane waves (2.28) in the ground state with vanishing wave number $\mathbf{k} = \mathbf{0}$:

$$\Psi_B(\mathbf{x}) = \sqrt{\frac{N_B}{V}}, \tag{3.1}$$

so that the particle density (2.107) becomes homogeneous. Therefore, the stationary Gross-Pitaevskii equation (2.104) reads

$$\tilde{V}^{(\mathrm{int})}_{BB,\,\mathbf{0}}\, n_B - \mu_B + \tilde{V}^{(\mathrm{int})}_{BF,\,\mathbf{0}}\, \kappa_D\, \Theta\left(\mu_F - \tilde{V}^{(\mathrm{int})}_{BF,\,\mathbf{0}}\, n_B\right) \left[\mu_F - \tilde{V}^{(\mathrm{int})}_{BF,\,\mathbf{0}}\, n_B\right]^{D/2} = 0 \tag{3.2}$$

with the Fourier transform of the interaction potential

$$\tilde{V}^{(\mathrm{int})}_{ij,\,\mathbf{k}} = \int d^D x\, V^{(\mathrm{int})}_{ij}(\mathbf{x}, \mathbf{x}')\, e^{-i\mathbf{k}\cdot(\mathbf{x}-\mathbf{x}')}, \qquad i, j = B, F. \tag{3.3}$$

This equation is fulfilled for arbitrary densities for bosons and fermions, which can be chosen independently from each other, provided that $\mu_F > V^{(\mathrm{int})}_{BF\,\mathbf{0}}\, n_B$ for a nonvanishing density of fermions.

## 3.2 Trapped Bose-Fermi Mixture without Interspecies Interaction

Here we consider a mixture in $D$ dimensions without interspecies interaction, which is confined in a trap described by an arbitrary power-law potential

$$V_i(\mathbf{x}) = \sum_{k=1}^{D} \frac{\hbar\,\omega_{i,k}}{2} \left| \frac{x_k}{L_{i,k}} \right|^{n_k}, \qquad L_{i,k} \equiv \sqrt{\frac{\hbar}{m_i\,\omega_{i,k}}}, \qquad n_k \geq 0, \qquad i = B, F. \tag{3.4}$$

Bose-Einstein condensation in such a power-law potential can be achieved if

$$\frac{D}{2} + \sum_{k=1}^{D} \frac{1}{n_k} > 1, \tag{3.5}$$

from which follows immediately, that for systems with $D > 1$ a BEC is possible at finite temperature $T_\mathrm{c} > 0$ for all potential powers $n_k$ whereas it is for $D = 1$ only achievable for $n_k < 2$. A detailed calculation shows the possibility of a one-dimensional BEC at finite temperature even in a harmonic trap with $n = 2$ [31,48]. If the interaction $V_{BF}^{(\mathrm{int})}(\mathbf{x}, \mathbf{x}')$ vanishes, the stationary Gross-Pitaevskii equation (2.104) is reduced to

$$\left[ -\frac{\hbar^2}{2m_B}\Delta + V_B(\mathbf{x}) - \mu_B + \int d^D x'\, V_{BB}^{(\mathrm{int})}(\mathbf{x}, \mathbf{x}') \left|\Psi_B(\mathbf{x}')\right|^2 \right] \Psi_B(\mathbf{x}) = 0, \tag{3.6}$$

having the conventional form for a pure Bose condensate. The density profile of the bosons is determined by Eqs. (2.107) and (3.6) whereas that of the fermions reads according to Eq. (2.109)

$$n_F(\mathbf{x}) = \kappa_D\, \Theta\left(\mu_F - V_F(\mathbf{x})\right) \left[\mu_F - V_F(\mathbf{x})\right]^{D/2}. \tag{3.7}$$

We see that the density profiles of both components are not influenced by each other and depend only on their intraspecies interaction, so far as it exists, and on the form of the corresponding trap. Hence bosons and fermions coexist independently from each other.

## 3.3 Bose-Fermi Mixture with $\delta$- Interactions in a Harmonic Trap

In this section we refer to the experiments in Hamburg and Florence dealing with a $^{87}$Rb–$^{40}$K boson-fermion mixture. Therefore, we restrict our formulas to three spatial dimensions. In general the trap potential in the experiments is well approximated by a three-dimensional harmonic oscillator

$$V_i(\mathbf{x}) = \frac{m_i}{2} \sum_{k=1}^{3} \omega_{i,k}^2 x_k^2, \qquad i = B, F. \tag{3.8}$$

In most relevant experiments there are either anisotropic harmonic traps with oscillation frequencies $\omega_{i,r} = \omega_{i,1} = \omega_{i,2}$ and $\omega_{i,z} = \omega_{i,3}$ leading to a rotationally symmetric cigar shaped condensate cloud, or isotropic traps are used with $\omega_{i,r} = \omega_{i,k}$, $k = 1, 2, 3$ leading to a spherical condensate cloud. Using cylindrical coordinates $\{r, \phi, z\}$ for the first case, the potential (3.8) takes the form

$$V_i(\mathbf{x}) = \frac{m_i}{2} \left(\omega_{i,r}^2 r^2 + \omega_{i,z}^2 z^2\right), \tag{3.9}$$

whereas it reads in the latter case with the help of spherical coordinates $\{r, \phi, \theta\}$

$$V_i(\mathbf{x}) = \frac{m_i}{2}\, \omega_{i,r}^2 r^2. \tag{3.10}$$

As mentioned in Section 1.2, bosons and fermions at the same space point experience forces of equal size caused by the traps, whose harmonic potentials have equal spring stiffnesses $m_B\,\omega_{B,k}^2 = m_F\,\omega_{F,k}^2$, so that the frequencies for both species are related by $\omega_{F,k} = \sqrt{m_B/m_F}\,\omega_{B,k}$ for $k = r, z$.

In the following we assume that the short-range contact interaction between the atoms is idealized by the Dirac delta function

$$V_{ij}^{(\mathrm{int})}(\mathbf{x}, \mathbf{x}') = g_{ij}\,\delta(\mathbf{x} - \mathbf{x}'), \qquad i, j = B, F, \tag{3.11}$$

where the interaction strength $g_{ij}$ is related to the s- wave scattering length $a_{ij}$ via [47]

$$g_{ij} = 2\pi\hbar^2 a_{ij}\,\frac{m_i + m_j}{m_i\,m_j}. \tag{3.12}$$

With the latter specification the Gross-Pitaevskii equation (2.104) becomes now a local nonlinear partial differential equation:

$$\left[-\frac{\hbar^2}{2m_B}\Delta + V_B(\mathbf{x}) - \mu_B + g_{BB}\,|\Psi_B(\mathbf{x})|^2 + g_{BF}\,\kappa_3\,\Theta(\tilde{\mu}_F(\mathbf{x}))\,\tilde{\mu}_F^{3/2}(\mathbf{x})\right]\Psi_B(\mathbf{x}) = 0 \tag{3.13}$$

with the local chemical potential

$$\tilde{\mu}_F(\mathbf{x}) = \mu_F - V_F(\mathbf{x}) - \,g_{BF}\,|\Psi_B(\mathbf{x})|^2 \tag{3.14}$$

and the value for the abbreviation

$$\kappa_3 = \frac{(2m_F)^{3/2}}{6\pi^2\hbar^3}. \tag{3.15}$$

## 3.4 Density Profiles

### 3.4.1 Thomas-Fermi approximation

Now we assume that the interaction dominates energetically, so that we can use the Thomas-Fermi approximation, where the kinetic term in the Gross-Pitaevskii equation can be neglected, . With this approximation the Gross-Pitaevskii equation (3.13) reduces with the help of Eqs. (2.107) and (2.108) to an algebraic equation with respect to the bosonic particle density $n_B(\mathbf{x})$:

$$V_B(\mathbf{x}) - \mu_B + g_{BB}\,n_B(\mathbf{x}) + g_{BF}\,n_F(\mathbf{x}) = 0. \tag{3.16}$$

The last term in Eqs. (3.16) stands for the fermionic particle density

$$n_F(\mathbf{x}) = \kappa_3\,\Theta\left(\mu_F - V_F(\mathbf{x}) - g_{BF}\,n_B(\mathbf{x})\right)\left[\mu_F - V_F(\mathbf{x}) - g_{BF}\,n_B(\mathbf{x})\right]^{3/2} \tag{3.17}$$

modulating the bosonic density profile $n_B(\mathbf{x})$ and vice versa.

### 3.4.2 Vanishing Boson-Fermion Interaction

Now we discuss the case of vanishing boson-fermion interaction $g_{BF} \to 0$, where we can derive from Eq. (3.16) the well-known particle density of a pure BEC in the Thomas-Fermi approximation

$$n_B^{(0)}(\mathbf{x}) = \frac{\mu_B^{(0)} - V_B(\mathbf{x})}{g_{BB}}, \tag{3.18}$$

provided that $g_{BB} > 0$. Note that the quantities, marked with the upper index (0), represent the respective values for an undisturbed BEC and an undisturbed Fermi gas, respectively, with $g_{BF} \to 0$. In case of an attractive interacting BEC with negative $g_{BB}$ the third term in Eq. (3.16) cannot be balanced in the trap center at $\mathbf{x} = \mathbf{0}$ by the remaining chemical potential $\mu_B^{(0)}$ leading to a collapse of the BEC. As the particle density of bosons (3.18) must be positive, the Thomas-Fermi-radii are obtained from Eqs. (3.8) and (3.18) to

$$R_{B,k}^{(0)} = \sqrt{\frac{2\mu_B^{(0)}}{m_B\,\omega_{B,k}^2}}. \tag{3.19}$$

The chemical potential $\mu_B^{(0)}$ is determined by the number of bosons via the normalization (2.106):

$$N_B = \frac{1}{g_{BB}} \int d^3x\, \Theta\left(1 - \sum_{k=1}^{3} \frac{x_k^2}{(R_{B,k}^{(0)})^2}\right) \left[\mu_B^{(0)} - \frac{m_B}{2} \sum_{k=1}^{3} \omega_{B,k}^2 x_k^2\right]. \tag{3.20}$$

The substitution $x_k = \sqrt{2\mu_B^{(0)}/(m_B\,\omega_{B,k}^2)}\, y_k$ deforms the shape of the condensate cloud from an ellipsoid to an unit sphere:

$$N_B = \left(\frac{2\mu_B^{(0)}}{m_B}\right)^{3/2} \frac{\mu_B^{(0)}}{g_{BB}\,\tilde{\omega}_B^3} \int d^3y\, \Theta(1 - \mathbf{y}^2) \left[1 - \mathbf{y}^2\right]. \tag{3.21}$$

Any physical quantity $A$ with a tilde stands for the geometrical average of its components along the respective axes:

$$\tilde{A} = (A_1 A_2 A_3)^{1/3}. \tag{3.22}$$

Applying spherical coordinates reduces Eq. (3.21) to the elementary integral

$$N_B = \left(\frac{2\mu_B^{(0)}}{m_B}\right)^{3/2} \frac{4\pi\mu_B^{(0)}}{g_{BB}\,\tilde{\omega}_B^3} \int_0^1 dr \left(r^2 - r^4\right), \tag{3.23}$$

which leads to

$$N_B = \left(\frac{2\mu_B^{(0)}}{m_B}\right)^{3/2} \frac{8\pi\mu_B^{(0)}}{15 g_{BB}\,\tilde{\omega}_B^3}. \tag{3.24}$$

Using Eq. (3.12), the chemical potential reads

$$\mu_B^{(0)} = \left(\frac{15 a_{BB} N_B}{\tilde{L}_B}\right)^{2/5} \frac{\hbar\tilde{\omega}_B}{2}, \tag{3.25}$$

where

$$\tilde{L}_B = \sqrt{\frac{\hbar}{m_B\,\tilde{\omega}_B}} \tag{3.26}$$

denotes the geometrical average of the oscillator lengths

$$L_{B,k} = \sqrt{\frac{\hbar}{m_B\,\omega_{B,k}}}. \tag{3.27}$$

With the help of the chemical potential (3.25) the Thomas-Fermi radii (3.19) result in

$$R_{B,k}^{(0)} = \left(\frac{15 a_{BB} N_B}{\tilde{L}_B}\right)^{1/5} \frac{L_{B,k}^2}{\tilde{L}_B}, \tag{3.28}$$

and their geometrical average as a measure for the spatial extension of the BEC cloud follows from

$$\tilde{R}_B^{(0)} = \left(\frac{15 a_{BB} N_B}{\tilde{L}_B}\right)^{1/5} \tilde{L}_B. \tag{3.29}$$

Inserting the chemical potential (3.25) into the bosonic particle density (3.18) and using Eq. (3.12), the density maximum in the trap center results in

$$n_B^{(0)}(\mathbf{0}) = \frac{(15 N_B)^{2/5}}{8\pi a_{BB}^{3/5}\, \tilde{L}_B^{12/5}}. \tag{3.30}$$

In the Thomas-Fermi approximation the BEC needs at least a finite repulsion between the bosons in order to prevent the density from becoming infinity or complex leading to a collapse of the BEC. The particle density (3.17) of fermions, on the other hand, becomes independent of that of bosons:

$$n_F^{(0)}(\mathbf{x}) = \kappa_3\, \Theta\left(\mu_F^{(0)} - V_F(\mathbf{x})\right) \left[\mu_F^{(0)} - V_F(\mathbf{x})\right]^{3/2}. \tag{3.31}$$

The chemical potential $\mu_F^{(0)}$ is determined by the normalization (2.106) yielding with the trap potential (3.9):

$$N_F = \int d^3x\, n_F^{(0)}(\mathbf{x}) = \frac{1}{6}\left(\frac{\mu_F^{(0)}}{\hbar\tilde{\omega}_F}\right)^3, \tag{3.32}$$

which agrees with the number of states (E.7) in a three-dimensional harmonic oscillator up to the energy $E = \mu_F^{(0)}$. The Thomas-Fermi radii of the undisturbed Fermi gas are immediately obtained from the fermionic density (3.31) by setting the latter zero:

$$R_{F,k}^{(0)} = \sqrt{\frac{2\mu_F^{(0)}}{m_F\, \omega_{F,k}^2}}. \tag{3.33}$$

With the chemical potential in Eq. (3.32) the maximum of the fermionic particle density (3.31) reads

$$n_F^{(0)}(\mathbf{0}) = 6^{1/2}\kappa_3 (\hbar\tilde{\omega}_F)^{3/2} N_F^{1/2} = \frac{2 N_F^{1/2}}{3^{1/2}\pi^2\, \tilde{L}_F^3}, \tag{3.34}$$

which increase faster with the particle number than the maximum of the bosonic particle density (3.30) whereas the latter is apart from the oscillator length also determined by $a_{BB}$ as the parameter for the two-particle interaction strength.

### 3.4.3 Discussion of Density Profiles

After reflecting on a undisturbed BEC in a trap, we discuss, for the time being, qualitatively the algebraic equation (3.16) for a BEC coexisting with fermions. The particle density of the BEC in the Thomas-Fermi approximation can be written in the implicit form:

$$n_B(\mathbf{x}) = \frac{1}{g_{BB}} \left(\mu_B - V_B(\mathbf{x}) - g_{BF}\, n_F(\mathbf{x})\right) \tag{3.35}$$

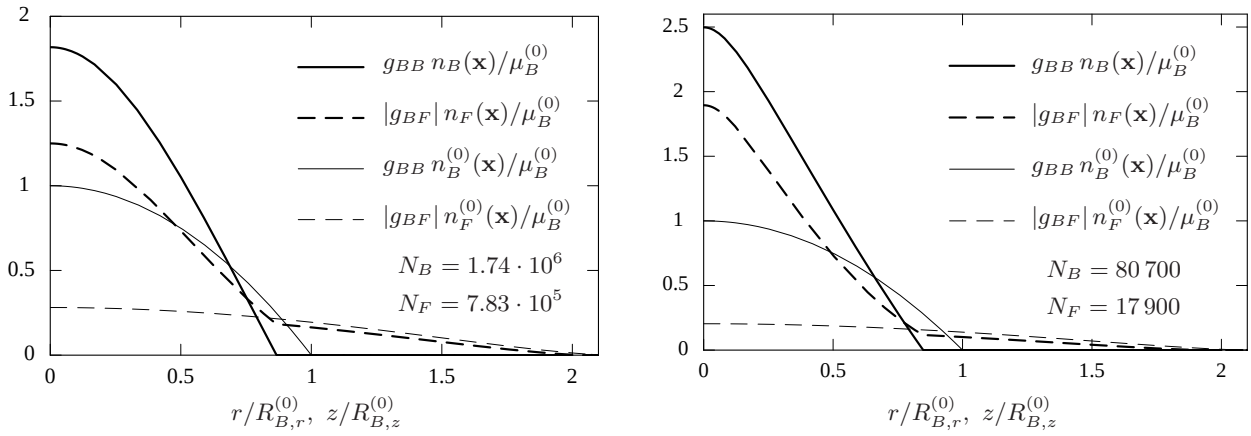


**Figure 3.1:** Comparison of the dimensionless particle densities for bosons and for fermions between a disturbed mixture (thick lines) and an undisturbed BEC and Fermi gas (thin lines). The densities are plotted versus the coordinates $r$ at the plane $z = 0$ and $z$ at the plane $r = 0$, respectively, in units of the Thomas-Fermi radii of the undisturbed BEC. The densities of the disturbed mixture are the solution of Eq. (3.16) whereas those of an undisturbed BEC and Fermi gas are given by Eqs. (3.18) and (3.31), respectively, for an example of typical particle numbers $N_B$, $N_F$ of the Hamburg experiment (left picture) and of the Florence experiment (right picture).

From the fermionic particle density (3.17) we deduce that its maximum occurs in the trap center at $\mathbf{x} = \mathbf{0}$ due to the negative $g_{BF}$. Thus, the BEC possesses its largest density also in the trap center. In other words, the particle densities of both species intensify each other in the overlapping region due to the strong attraction between bosons and fermions. With increasing distance from the trap center both densities (3.17) and (3.35) decrease quickly within their overlap due to the interaction terms with the other species and due to the increasing trap potentials, whereas outside of the overlap only the latter reason is responsible for their decreasing. This behavior is shown in Figure 3.1 for the Hamburg and Florence experiments, respectively. Which of both clouds has the larger extension depends on the particle numbers $N_B$ and $N_F$ and therefore on the chemical potentials $\mu_B$ and $\mu_F$. Usually, the BEC is surrounded with the Fermi gas unless $N_B \gg N_F$. Both chemical potentials as the total energy of a particle of the corresponding species are smaller compared with $\mu_B^{(0)}$ and $\mu_F^{(0)}$ of the undisturbed BEC and Fermi gas, since the particles possess besides the neglected kinetic energy, the potential energy due to the trap and the intraspecies interaction energy now an additional negative interaction energy due to the interaction with the other species. Figure 3.4 shows these energies of a boson in units of $V_B(R_{B,r}, 0) = V_B(0, R_{B,z}) = \mu_B^{(0)}$ for both experiments, where we see that $\mu_B \approx 0.6\, \mu_B^{(0)}$. This reducing of the chemical potentials leads to a decreasing of the Thomas-Fermi radii for both species. For the Fermi gas these radii are immediately obtained from the fermionic density (3.17) by setting $n_B(R_{F,r}, 0) = n_F(R_{F,r}, 0) = 0$:

$$R_{F,k} = \sqrt{\frac{2\mu_F}{m_F\, \omega_{F,k}^2}}, \qquad k = r, z. \tag{3.36}$$

Thus, $R_{F,k} < R_{F,k}^{(0)}$ becomes obvious by comparing the Thomas-Fermi radii (3.33) and (3.36) due to $\mu_F < \mu_F^{(0)}$. Figure 3.1 shows a reduction of the Thomas-Fermi radii of the BEC to $R_{B,k} \approx 0.8\, R_{B,k}^{(0)}$. Hence the attractive interaction between both species leads to an additional confinement of the

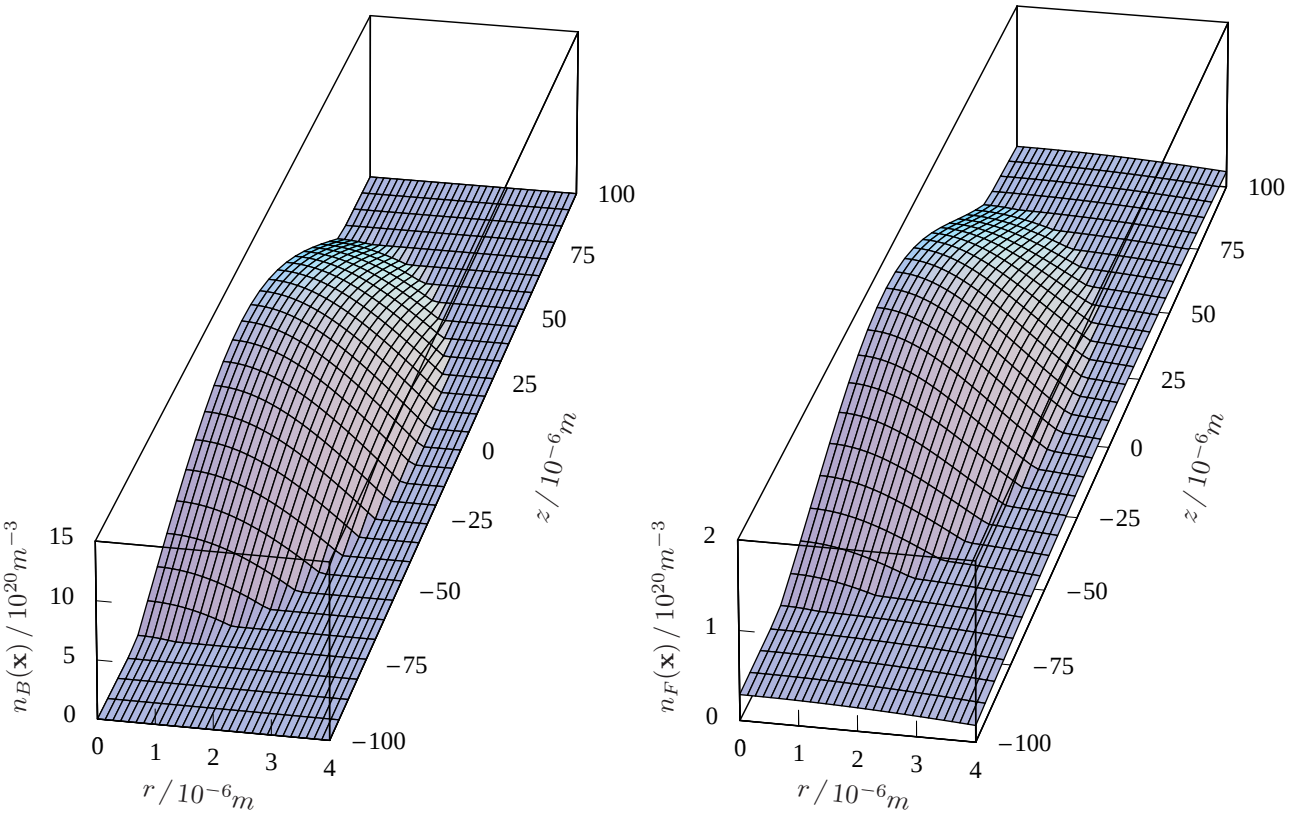


**Figure 3.2:** Spatial particle density distribution for bosons (left picture) and for fermions (3.17) (right picture) of the Hamburg experiment versus the radial coordinate $r$ and the axial coordinate $z$ for the example of particle numbers $N_B$ and $N_F$ as shown in the left picture of Figure 3.1.

BEC and Fermi gas within their overlap. In Figures 3.2 and 3.3 the absolute particle densities $n_B(\mathbf{x})$ and $n_F(\mathbf{x})$ are plotted versus the radial and the axial coordinates. Comparing the radial with the axial extension of the BEC and of the Fermi gas shows the elongated or cigar-shaped form of these clouds. This anisotropy of the shape is determined only by the ratio between the corresponding radial and axial trap frequencies. We compare the density maxima in these figures with the corresponding ones (3.30) and (3.34) of the undisturbed BEC and Fermi gas evaluated with the particle numbers in Figure 3.1 to:

$$\begin{aligned} &\text{Hamburg experiment :} && n_B^{(0)}(\mathbf{0}) = 6.4 \cdot 10^{20}\,\mathrm{m}^{-3}, && n_F^{(0)}(\mathbf{0}) = 0.40 \cdot 10^{20}\,\mathrm{m}^{-3}, \\ &\text{Florence experiment :} && n_B^{(0)}(\mathbf{0}) = 1.9 \cdot 10^{20}\,\mathrm{m}^{-3}, && n_F^{(0)}(\mathbf{0}) = 0.06 \cdot 10^{20}\,\mathrm{m}^{-3}, \end{aligned}$$

and find that in the Hamburg (Florence) experiment the bosonic density maximum is increased by a factor of 1.8 (2.5) whereas the fermionic density maximum is enlarged by 4.4 (9.3) due to the attraction between both species.

### 3.4.4 Solution Method

Now we sketch briefly how we have solved the algebraic equation (3.16) in order to plot the density profiles in Figures 3.1, 3.2, and 3.3. First we bring the fermionic density (3.17) to the other side of the algebraic equation (3.16) and square this equation to obtain a cubic equation with respect to

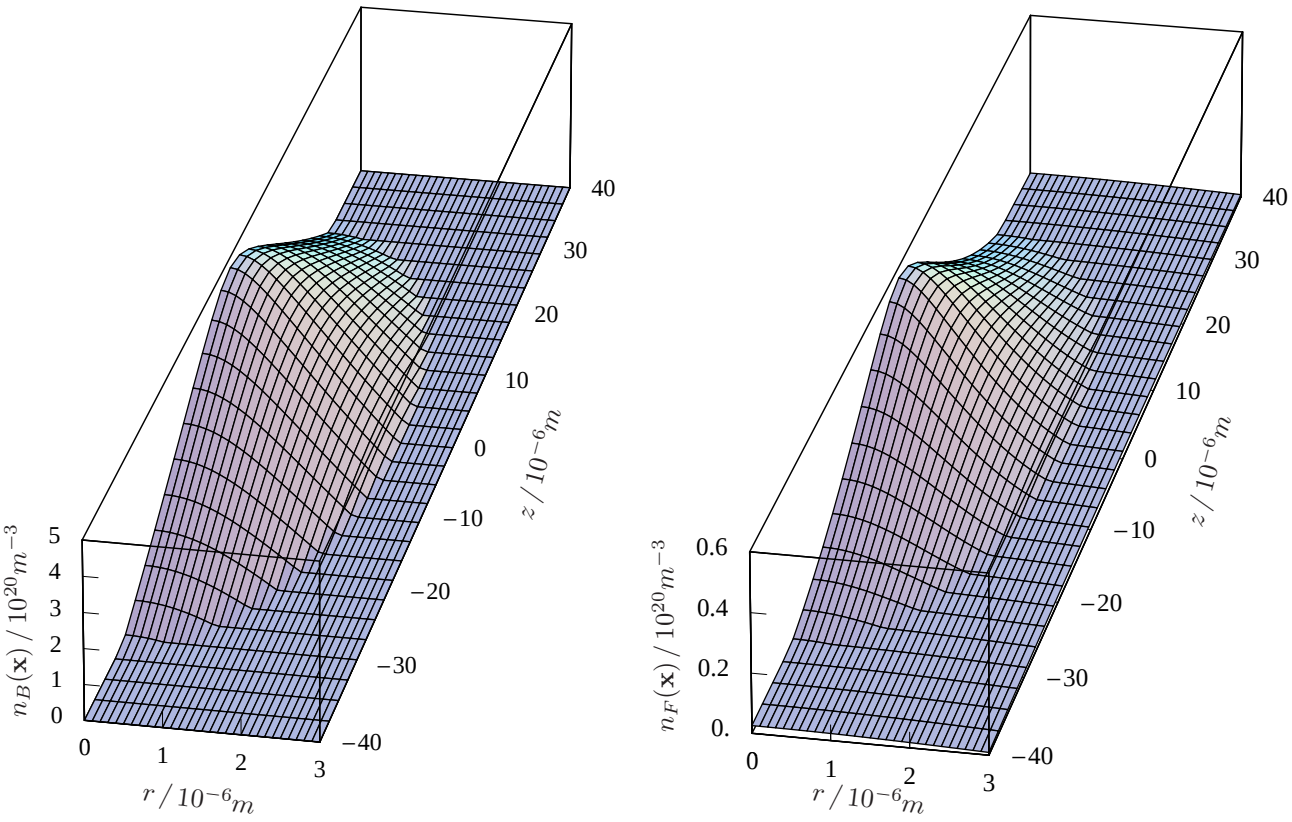


**Figure 3.3:** Spatial particle density distribution for bosons (left picture) and for fermions (3.17) (right picture) of the Florence experiment versus the radial coordinate $r$ and the axial coordinate $z$ for the example of particle numbers $N_B$ and $N_F$ as shown in the right picture of Figure 3.1.

the condensate density $n_B(\mathbf{x})$:

$$n_B^3(\mathbf{x}) + \left[\frac{g_{BB}^2}{\kappa_3^2\, g_{BF}^5} - \frac{3(\mu_F - V_F(\mathbf{x}))}{g_{BF}}\right] n_B^2(\mathbf{x}) + \left[\frac{2 g_{BB}(V_B(\mathbf{x}) - \mu_B)}{\kappa_3^2\, g_{BF}^5} + \frac{3(\mu_F - V_F(\mathbf{x}))^2}{g_{BF}^2}\right] n_B(\mathbf{x}) + \frac{(V_B(\mathbf{x}) - \mu_B)^2}{\kappa_3^2\, g_{BF}^5} - \frac{(\mu_F - V_F(\mathbf{x}))^3}{g_{BF}^3} = 0. \quad (3.37)$$

This cubic equation can be solved exactly with the help of the Cardanian formula [49]. A cubic equation with real coefficients contains always three solutions, where at least one of them is real and the others are complex conjugate. Although all three solutions obey the cubic equation (3.37), only one of the solutions satisfies the algebraic equation (3.16), whereas inserting the two other solutions into the algebraic equation yields the right value but opposite signs on both sides of the algebraic equation

$$V_B(\mathbf{x}) - \mu_B + g_{BB}\, n_B(\mathbf{x}) = -g_{BF}\, \kappa_3 \left[\mu_F - V_F(\mathbf{x}) - g_{BF}\, n_B(\mathbf{x})\right]^{3/2}. \quad (3.38)$$

The reason is that the algebraic equation is the root of the cubic equation, therefore an equation of the order 3/2, which reduces the number of possible solutions. The resulting particle densities for both species for an example of typical particle numbers $N_B$ and $N_F$ are plotted in Figures 3.1, 3.2 and 3.3, using the experimental parameters in Table 1.1. In order to determine the solution outside the BEC, especially the particle density of fermions, we must not forget the origin of the

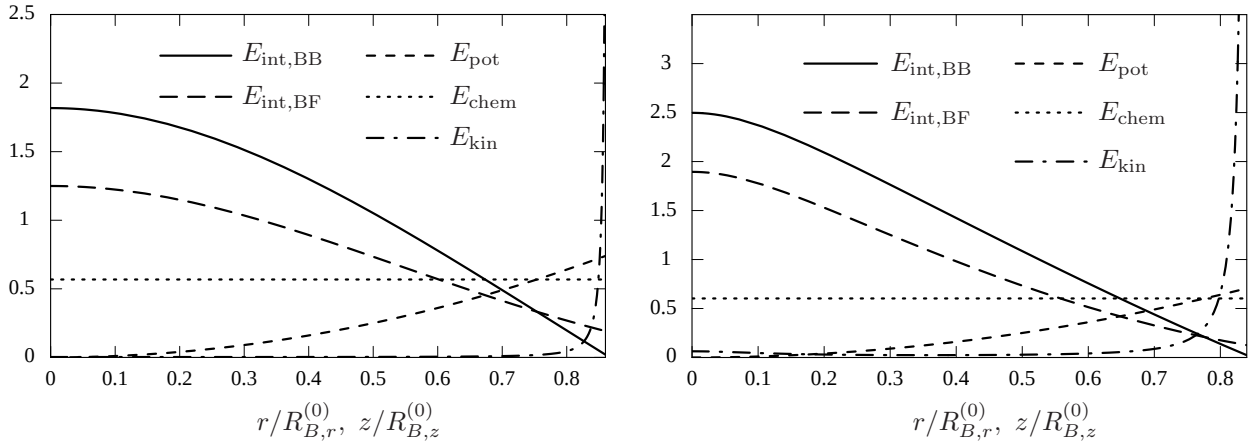


**Figure 3.4:** Comparison of the kinetic energy $E_{\rm kin} = -\hbar^2\Delta\Psi_B(\mathbf{x})/(2m_B\,\Psi_B(\mathbf{x})\,\mu_B^{(0)})$ of a boson, with its remaining energies, namely the intraspecies interaction energy $E_{\rm int,BB} = g_{BB}\,n_B(\mathbf{x})/\mu_B^{(0)}$, the interspecies interaction energy $E_{\rm int,BF} = |g_{BF}|\,n_F(\mathbf{x})/\mu_B^{(0)}$, the potential energy $E_{\rm pot} = V_B(\mathbf{x})/\mu_B^{(0)}$ due to the trap and the chemical potential $E_{\rm chem} = \mu_B/\mu_B^{(0)}$. All energies are related to the value $\mu_B^{(0)}$ of the potential energy at the boundary of the undisturbed BEC cloud and are plotted versus the coordinates $r$ and $z$ within the BEC cloud for the situation in Figure 3.1. The left (right) picture corresponds to the Hamburg (Florence) experiment.

algebraic equation (3.16) from the Gross-Pitaevskii equation (3.13). Although the solution $n_B(\mathbf{x})$ becomes negative outside the BEC, we have to set it equal zero there, as the density must be positive by definition. Thus, the condensate wave function $\Psi_B(\mathbf{x})$ becomes also zero outside the BEC and fulfills the Gross-Pitaevskii equation (3.13) in a trivial way regardless of the expression inside the brackets, which is, apart from the kinetic energy term, the algebraic equation (3.16). Hence the fermionic particle density outside the BEC is described by Eq. (3.17) with $n_B(\mathbf{x}) = 0$ without obeying the algebraic equation (3.16).

### 3.4.5 Validity of Thomas-Fermi approximation

In order to check the validity of the Thomas-Fermi approximation, we have plotted in Figure 3.4 the kinetic energy of a boson

$$E_{\rm kin} = \frac{-\hbar^2\Delta\Psi_B(\mathbf{x})}{2m_B}\,\frac{1}{\Psi_B(\mathbf{x})\mu_B^{(0)}} \tag{3.39}$$

in units of the value $\mu_B^{(0)}$ of the potential energy at the boundary of the undisturbed BEC allowing a direct comparison with the other energies in the algebraic equation (3.16). The kinetic energy is, indeed, negligible in a wide bulk range from the trap center to just before the boundary of the disturbed BEC. Thus, the Thomas-Fermi approximation gives very accurate results except in the outermost 10% of the Thomas-Fermi radii. At the BEC boundary the kinetic energy diverges because the condensate wave function $\Psi_B(\mathbf{x})$ as the square root of the particle density $n_B(\mathbf{x})$ occurs due to the Laplacian derivative in Eq. (3.39) in the denominator, which becomes zero at the BEC boundary. Its is obviously that the proper solution of the Gross-Pitaevskii equation (3.13) matches the one of the algebraic equation (3.16) from the trap center to just before the BEC boundary,

where it tends smoothly to zero improving the sharp bend in the graph of the fermionic particle density there to be smooth.

### 3.4.6 Complex solutions

The solution $n_B(\mathbf{x})$ of the algebraic equation (3.16) doesn't remain always real by varying the particle numbers $N_B$ and $N_F$, i.e. of the corresponding chemical potentials $\mu_B$ and $\mu_F$. We extract the condition for the chemical potentials as the straight line

$$\mu_F = \frac{4g_{BB}^2}{27\kappa_3^2\, g_{BF}^4} + \frac{g_{BF}}{g_{BB}}\,\mu_B, \tag{3.40}$$

which separates the half plane with pairs $(\mu_B, \mu_F)$ leading to a complex solution from that with pairs having a real solution. This can be seen for the Hamburg experiment in part (a) of Figure 3.5. By comparing with the results of Section 3.5, we can allocate the complex solution to a failure of the stability in the mixture with respect to collapse. The parts (b) – (d) in Figure 3.5 demonstrate the change of the density profiles $n_B(\mathbf{x})$ and $n_F(\mathbf{x})$ on the road from stability to instability by increasing the particle numbers with $\Delta N_B \approx 1.8 \cdot 10^5$ and $\Delta N_F \approx 3 \cdot 10^4$ each. The respective pairs $(\mu_B, \mu_F)$ lie on the dashed line, arranged perpendicular to the critical solid line in part (a), so for part (b) just below the critical line, for part (c) on, and for part (d) just above. Part (b) shows a stable configuration, part (c) is on the boundary between stable and unstable where the density gathers at the trap center to a peak, and in part (d) the real part of the densities is chopped off at the trap center and just there an imaginary part of both densities occurs. This imaginary part starts to appear simultaneously for both components at the density maximum at $\mathbf{x} = \mathbf{0}$ and grows in magnitude and in extension out of the trap center with increasing $N_B$ and $N_F$. This behavior was observed in the Hamburg experiment, where the evolution of an overcritical mixture is shown in Figure 3.6. The pictures in this figure were taken during the evaporation of an overcritical mixture, where the density distributions should despite the dynamics in the mixture due to the fast evaporation closely reflect the distribution inside the trap due to the relative short time of flight (TOF) during the expansion of the mixture. Now we describe briefly the phenomenon behind the pictures in Figure 3.6 as stated in Ref. [16]. Picture (a) shows the situation at the phase transition point where the bosons start to condense. The small peak of the BEC in the left picture is surrounded by thermal bosons. The peak on the top of the axial $^{40}$K density profile is ascribed to the interaction with the bosonic component. When the BEC becomes large during the evaporative cooling, the $^{40}$K density profile in picture (b) exhibits a pronounced hole in the trap center, which is ascribed to a strong local loss process due to the interaction with the BEC. The strong depletion of the Fermi cloud in the center, which is accompanied by a rapid particle loss of about two thirds of the $^{40}$K atom number, is caused by a mean-field collapse of the mixture. The strong attraction between bosons and fermions in the overlapping part of the mixture leads to a rapid contraction to such large densities in the trap center, that enormous losses due to three-body Rb-K recombination with each two Rb atoms and a K atom reduces the particle number in this region to an subcritical number. After the sudden collapse the Fermi distribution, which is depleted in the center of the cloud, is refilled from the outside parts of the sample on a time scale $\Delta t \approx 2\pi/\omega_{F,z}$, leading possibly to renewed local collapses, until the mixture becomes subcritical in picture (c). The collapse and the possibly following cascade of decays reveal a comlex dynamic in the mixture.

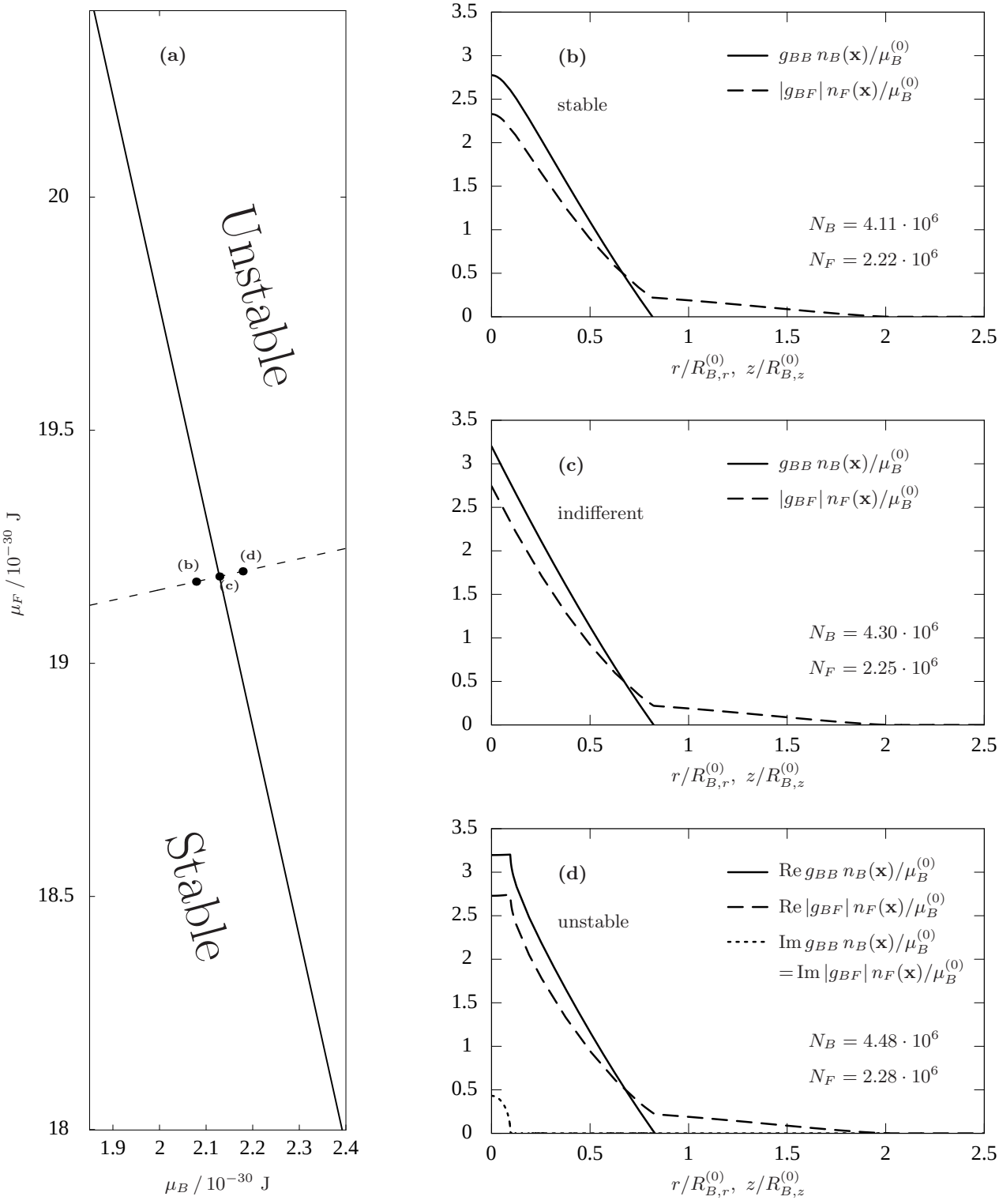


**Figure 3.5:** Phase diagram with respect to the chemical potentials in part (a). The solid line separates the stable phase on the left from the unstable phase on the right. The pictures on the right show a sequence how the bosonic and fermionic particle densities versus the coordinates $r$ at the plane $z = 0$ and $z$ at the plane $r = 0$, respectively, change on the road from stability to instability. The $(\mu_B, \mu_F)$-pairs belonging to parts (b) – (d) are located on the dashed line in part (a) and are equally spaced $\Delta\mu_B = 5 \cdot 10^{-32}$ apart giving rise to particle number differences of about $\Delta N_B \approx 1.8 \cdot 10^5$ and $\Delta N_F \approx 3 \cdot 10^4$.

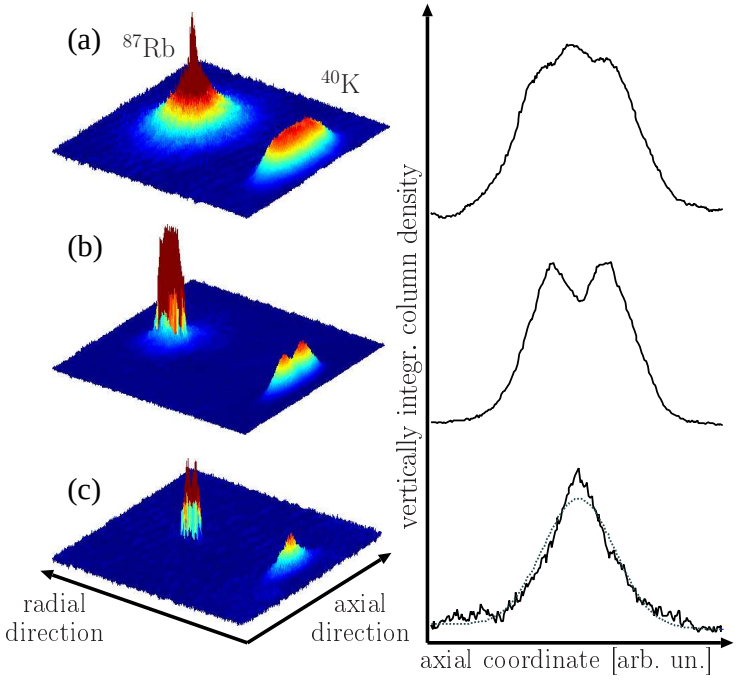


**Figure 3.6:** Typical evolution of an overcritical mixture in the Hamburg experiment [16]. Left hand side: 3D representation of absorption images with false-color coding of the optical density. Right hand side: corresponding $^{40}$K axial line profiles integrated the density along the vertical direction.

## 3.5 Stability

### 3.5.1 Thomas Fermi Approximation

In Subsection 3.4.6 we described in detail the behavior of the particle densities $n_B(\mathbf{x})$ and $n_F(\mathbf{x})$ as the solution of the stationary Gross-Pitaevskii equation within the Thomas-Fermi approximation by varying the particle numbers $N_B$ and $N_F$. We assigned the emergence of a complex density to a loss of the stability against collapse and found a border in form of a line in the $(\mu_B, \mu_F)$-plane, which separates the stable and unstable region as shown in part (a) of Figure 3.5. In order to obtain a stability diagram in the $(N_B, N_F)$-plane, we evaluate the corresponding particle numbers from the chemical potentials by integrating out the respective particle densities according to the normalization condition (2.106). The result is given by the violet line in Figures 3.7 and 3.8. Mixtures with particle number pairs $(N_B, N_F)$ below this line are stable whereas particle number pairs above the line indicate an unstable mixture tending to collapse. The critical particle numbers of both species behave, roughly spoken, inversely proportional to each other in a wide range. Whereas the critical number of bosons $N_{B\mathrm{crit}}$ tends to zero when the number of fermions increases, the critical number of fermions $N_{F\mathrm{crit}}$ remains finite and constant when the number of bosons is enlarged. This situation, where the line in the stability diagram becomes vertical, happens when the BEC cloud becomes sufficient large to surround the Fermi gas.

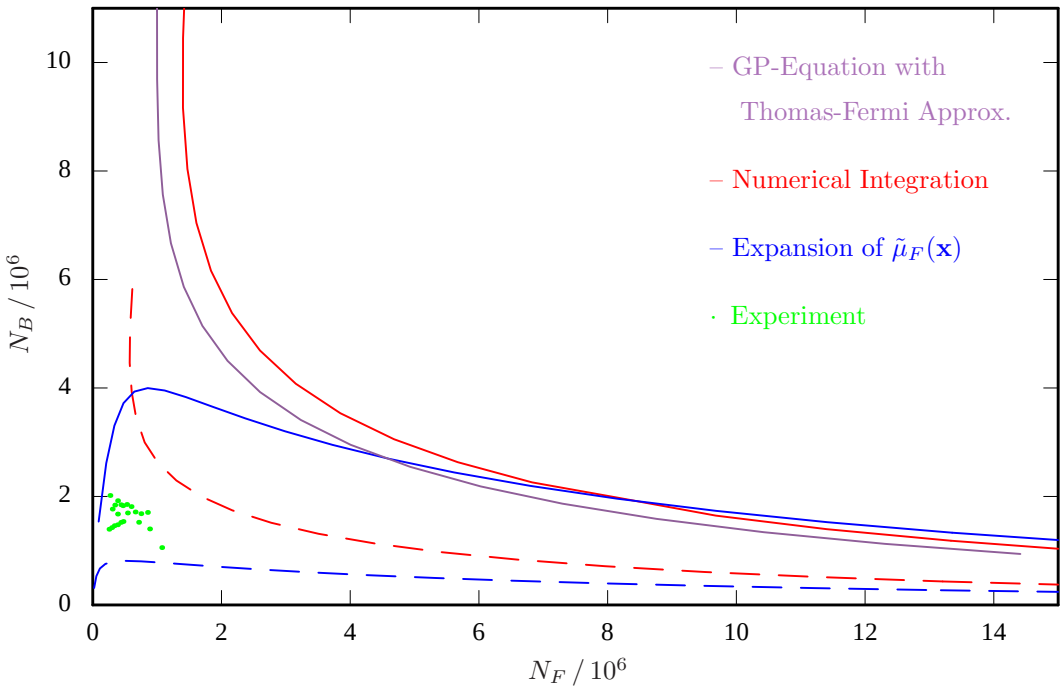


**Figure 3.7:** Stability diagram for the $^{87}$Rb–$^{40}$K mixture of the Hamburg experiment. The particle number pairs $(N_B, N_F)$ below a certain line belong to a stable mixture wheras those above the line indicate an unstable mixture tending to collapse. The dashed lines correspond to the quantum mechanical limit with the ratio $\lambda_{\mathrm{QM}} = \omega_z/\omega_r$ and the solid lines represents the Thomas-Fermi limit with the ratio $\lambda_{\mathrm{TF}} = (\omega_z/\omega_r)^2$. The green points are obtained in the experiment by analyzing decay series in various particle number regimes and are assigned to unstable mixtures [16].

### 3.5.2 Variational Method

Another approach to determine the stability border for a $^{87}$Rb–$^{40}$K mixture is given by extremizing the grand-canonical free energy (2.103) which reads with the delta interaction (3.11):

$$\mathcal{F}[\Psi_B^*, \Psi_B] = \int d^3x \left[ \frac{\hbar^2}{2m_B} |\boldsymbol{\nabla}\Psi_B(\mathbf{x})|^2 + (V_B(\mathbf{x}) - \mu_B)|\Psi_B(\mathbf{x})|^2 + \frac{g_{BB}}{2}|\Psi_B(\mathbf{x})|^4 - \frac{2\kappa}{5}\,\Theta(\tilde{\mu}_F(\mathbf{x}))\,\tilde{\mu}_F^{5/2}(\mathbf{x}) \right], \quad (3.41)$$

where the local chemical potential has the form:

$$\tilde{\mu}_F(\mathbf{x}) = \mu_F - V_F(\mathbf{x}) - g_{BF}\,|\Psi_B(\mathbf{x})|^2. \quad (3.42)$$

But instead of varying the condensate wave function $\Psi_B(\mathbf{x})$, which leads to the Gross-Pitaevskii equation as described in Section 2.11, we use for it the ground-state wave function of a three-dimensional anisotropic harmonic oscillator

$$\Psi_B(\mathbf{x}) = \sqrt{\frac{N_B}{\pi^{3/2}\alpha^3 \tilde{L}_B^3}}\, \exp\left\{ -\sum_{k=1}^{3} \frac{x_k^2}{2\alpha^2 L_{B,k}^2} \right\}, \quad (3.43)$$

as a test function with variational widths $\alpha\, L_{B,k}$. The dimensionless factor $\alpha$ serves as a variational parameter by scaling the oscillator lengths (3.27) to optimize the width of the Gaussian function

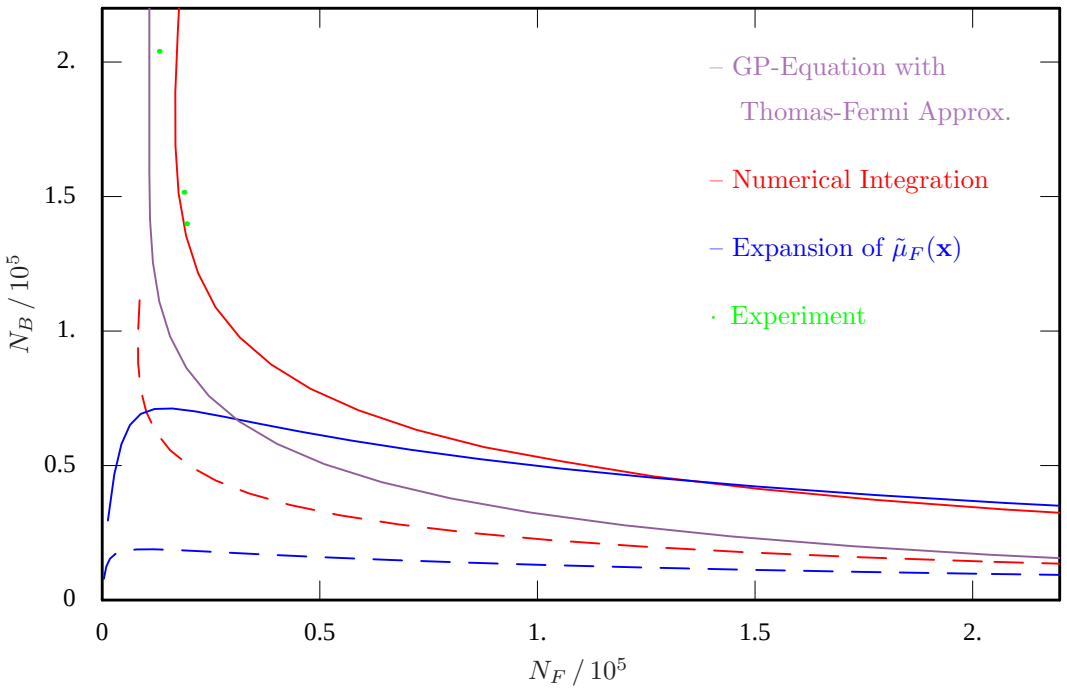


**Figure 3.8:** Stability diagram for the $^{87}$Rb–$^{40}$K mixture of the Florence experiment. The particle number pairs $(N_B, N_F)$ below a certain line belong to a stable mixture whereas those above the line indicate an unstable mixture tending to collapse. The dashed lines correspond to the quantum mechanical limit with the ratio $\lambda_{\mathrm{QM}} = \omega_z/\omega_r$ and the solid lines represents the Thomas-Fermi limit with the ratio $\lambda_{\mathrm{TF}} = (\omega_z/\omega_r)^2$. The green points represent mixtures in the experiment which are found very close to the instability [35].

(3.43) with regard to extremizing the free energy (3.41). The test function is normalized to $N_B$ bosons and obeys for $\alpha = 1$ the Gross-Pitaevskii equation for a trapped noninteracting BEC:

$$\left[-\frac{\hbar^2}{2m_B}\Delta + V_B(\mathbf{x}) - \mu_B\right]\Psi_B(\mathbf{x}) = 0. \tag{3.44}$$

Here we assume that the condensate wave function $\Psi_B(\mathbf{x})$ also in case of intraspecies and interspecies two-particle interactions has qualitative the shape of a Gaussian curve as one can convince of it in Figure 3.1. Using cylindrical coordinates $\{r, \phi, z\}$, the test function (3.43) reads

$$\Psi_B(\mathbf{x}) = \sqrt{\frac{N_B\lambda^{1/2}}{\pi^{3/2}\alpha^3 L_{B,r}^3}}\exp\left\{-\frac{r^2+\lambda z^2}{2\alpha^2 L_{B,r}^2}\right\}, \qquad \lambda = \left(\frac{L_{B,r}}{L_{B,z}}\right)^2 \tag{3.45}$$

Beside the uniform variation of the widths $\alpha L_{B,k}$ by the factor $\alpha$, we have to consider that the ratio $L_{B,z}/L_{B,r}$ also could be changed due to the interactions. In order to include this, we perform the calculation with two ratios $\lambda \equiv (L_{B,r}/L_{B,z})^2$. On the one hand with $\lambda_{\mathrm{QM}} = \omega_z/\omega_r$ which stands for the limit of vanishing interactions $g_{BB} \to 0$ and $g_{BF} \to 0$ and reflects the proper ratio of the oscillator lengths in the quantum-mechanical harmonic oscillator (3.44). On the other hand, we set $\lambda_{\mathrm{TF}} = (\omega_z/\omega_r)^2$, which represents the Thomas-Fermi limit of negligible kinetic energy due to the strong intraspecies and interspecies interaction. Using the Thomas-Fermi radius (3.19), we see that the ratio of the oscillator lengths in $\lambda_{\mathrm{TF}}$ reflects that of the Thomas-Fermi radii:

$$\frac{L_{B,r}}{L_{B,z}} = \frac{R_{B,r}}{R_{B,z}}. \tag{3.46}$$

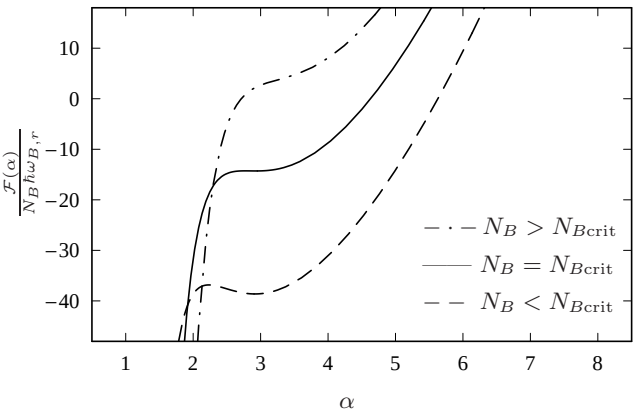


**Figure 3.9:** Grand-canonical free energy $\mathcal{F}(\alpha)/N_B\hbar\omega_{B,r}$ versus the variational parameter $\alpha$ for various boson numbers. A local minimum indicates a metastable state of the mixture.

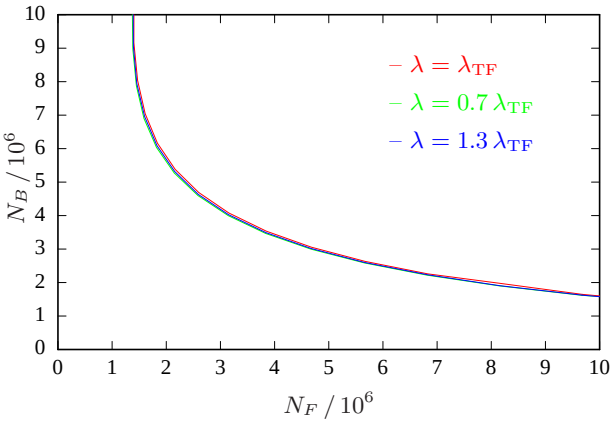


**Figure 3.10:** Comparison of two stability borders which ratio $\lambda$ is 30% smaller and larger, respectively, than $\lambda_{\mathrm{TF}}$ in order to estimate the proper ratio $\lambda$ allowing the largest possible particle number for a stable condensate of the Hamburg experiment.

Inserting the test function (3.45) into the grand canonical free energy (3.41) reduces the latter from the functional $\mathcal{F}[\Psi_B^*, \Psi_B]$ to a function $\mathcal{F}(\alpha)$ with respect to the parameter $\alpha$. As the test function (3.45) is normalized independent of $\mu_B$, the latter plays no longer a role in $\mathcal{F}(\alpha)$ and shifts the free energy only by a constant value. On the other hand, the fermionic chemical potential $\mu_F$ is needed for evaluating the respective fermion number $N_F$ by integrating out the fermionic particle density

$$n_F(\mathbf{x}) = \kappa_3\,\Theta\left(\mu_F - V_F(\mathbf{x}) - g_{BF}\,|\Psi_B(\mathbf{x})|^2\right)\left[\mu_F - V_F(\mathbf{x}) - g_{BF}\,|\psi_B(\mathbf{x})|^2\right]^{3/2} \tag{3.47}$$

according to the normalization (2.106). The dependence of the grand-canonical free energy $\mathcal{F}(\alpha)$ on $\alpha$ for given chemical potentials $\mu_B$, $\mu_F$ is shown in Figure 3.9 for several boson numbers $N_B$. For $N_B < N_{B\mathrm{crit}}$ the free energy $\mathcal{F}(\alpha)$ possesses a local minimum which corresponds to a metastable state of the mixture. The condensate wave function $\Psi_F(\mathbf{x})$ has finite equilibrium widths $\alpha_{\mathrm{eq}} L_{B,k}$ with $\alpha_{\mathrm{eq}}$ as the parameter at the local minimum. When the boson number $N_B > N_{B\mathrm{crit}}$ exceeds the critical value, the local minimum disappears so that the widths tends to zero in order to minimize $\mathcal{F}(\alpha)$. Just this happens when the mixture collapse. Thus, the border between stable and unstable is given by the condition

$$N_B = N_{B\mathrm{crit}} \quad \Leftrightarrow \quad \left.\frac{d\mathcal{F}(\alpha)}{d\alpha}\right|_{\alpha=\alpha_{\mathrm{crit}}} = \left.\frac{d^2\mathcal{F}(\alpha)}{d\alpha^2}\right|_{\alpha=\alpha_{\mathrm{crit}}} = 0, \tag{3.48}$$

where $\mathcal{F}(\alpha)$ has a point of inflexion at $\alpha = \alpha_{\mathrm{crit}}$. The appearance of the local minimum arises from the competition between the positive first three terms of the grand-canonical free energy (3.41) and the negative last term describing the influence of the fermions. We determined the stability border within the variational method in two different ways.

### Numerical Integration

The most accurate possibility is to perform the integration in Eq. (3.41) numerically. We evaluated the critical boson numbers $N_{B\mathrm{crit}}$ for different values of $\mu_F$ in an iterative way until the condition

(3.48) is achieved with sufficient accuracy. The result is the red line in the stability diagrams for the Hamburg and Florence experiment as shown in Figures 3.7 and 3.8, where the resulting particle number pairs $(N_B, N_F)$ are smoothly connected with each other. The red solid line of the Thomas-Fermi limit with the ratio $\lambda_{\mathrm{TF}} = (\omega_z/\omega_r)^2$ lie above, but close to the violet line from the Gross-Pitaevskii equation in the Thomas-Fermi approximation in section 3.5.3. This is expected as both the red solid line and the violet line are evaluated in the Thomas-Fermi limit with the same ratio of the radial and axial extension of the BEC cloud. Furthermore they show the same behavior for very large boson numbers as both lines become vertical so that the fermion number remains constant. In the Florence experiment both lines lie very close to the green points of the experiment where the red line fits them better. This is not surprising as the s-wave scattering length $a_{BF}$ in Table 1.1 is determined with a meanfield analysis in the Florence experiment. The dashed red line lie far below the solid red line and reflects a mixture in the quantum-mechanical limit with the ratio $\lambda_{\mathrm{QM}} = \omega_z/\omega_r$. This line, which is a good approximation for mixtures with vanishing intraspecies and interspecies interactions, is less suitable for the $^{87}$Rb–$^{40}$K mixture as Figure 3.4 reveals that the interaction dominates with respect to the energy. Hence the mixture can be well described in the Thomas-Fermi limit. As the dashed red line doesn't consider the proper ratio $\lambda$ of the oscillator lengths in the test function (3.43) and hence minimize the free energy less optimal for a strong interacting mixture, this line allows much less particle numbers in a stable mixture than the solid red line. In order to estimate the ratio $\lambda$, which yields the stability border with the largest possible numbers for bosons and fermions, we evaluate two lines in the stability diagram for ratios in the neighbourhood of $\lambda_{\mathrm{TF}}$, where one $\lambda$ is 30% smaller and the other one is 30% larger. These lines for $\lambda = 0.7\,\lambda_{\mathrm{TF}}$ and $\lambda = 1.3\,\lambda_{\mathrm{TF}}$ are shown in Figure 3.10. Both lines lie throughout below, but very close to the original one with $\lambda = \lambda_{\mathrm{TF}}$. This indicates that the stability border in the Thomas-Fermi limit is stationary at $\lambda = \lambda_{\mathrm{TF}}$ where it possesses a maximum. Hence, the ratio $\lambda_{\mathrm{TF}}$ turns out to be the proper ratio for the $^{87}$Rb–$^{40}$K mixture allowing the largest possible numbers for bosons and fermions in a stable mixture.

### Expansion of $\tilde{\mu}_F(\mathbf{x})$

Another approach was suggested and performed by Chui et al., where the local chemical potential (3.42 in the grand-canonical free energy (3.41) is expanded up to the third order in $g_{BF}$ in order to get rid off the power in the last term of the free energy [38]. This expansion leads to a Gaussian integral with respect to the test function (3.45):

$$\mathcal{F}[\Psi^*, \Psi] \approx \int d^3x \left[ \frac{\hbar^2}{2m_B} |\boldsymbol{\nabla}\Psi(\mathbf{x})|^2 + V_{\mathrm{eff}}(\mathbf{x})\,|\Psi(\mathbf{x})|^2 + \frac{g_{\mathrm{eff}}}{2}\,|\Psi(\mathbf{x})|^4 + \frac{\kappa g_{BF}^3}{8\mu_F^{1/2}}\,|\Psi(\mathbf{x})|^6 \right], \quad (3.49)$$

where the terms with respect to the power of $|\Psi(\mathbf{x})|$ are summarized in the factors

$$V_{\mathrm{eff}}(\mathrm{x}) = \left[1 - \frac{3}{2}\,\kappa_3\,\mu_F^{1/2} g_{BF}\right] \frac{1}{2}\,m_B \omega_{B,r}^2 (r^2 + \lambda^2 z^2), \quad (3.50)$$

$$g_{\mathrm{eff}} = g_{BB} - \frac{3}{2}\,\kappa_3\,\mu_F^{1/2} g_{BF}^2. \quad (3.51)$$

Here we assume that the radius of the condensate is much less than the radius of the Fermi gas cloud so that the remaining expressions $(\mu_F - V_F(\mathrm{x}))^{n/2}$, arising from the expansion, with $n = 1, 3, 5$ can be expanded in powers of $V_F(\mathrm{x})/\mu_F$ as well. We consider therein only terms which depends

on the parameter $\alpha$. The last term in the free energy (3.49) corresponds to the elastic three-particle collision induced by the interspecies interaction. This term for $g_{BF} < 0$ is responsible for increasing both the bosonic and the fermionic particle density in the trap center in order to minimize the free energy. If the central condensate density $|\Psi(\mathbf{0})|^2$ becomes large enough due to large particle numbers, the positive first three terms in the free energy (3.49) cannot balance the negative last term in order to stabilize the mixture and prevent the collapse. Performing the integration in Eq. (3.49) leads to a algebraic equation with respect to the unknown quantities $\alpha$ and $N_B$:

$$\frac{\mathcal{F}(\alpha)}{N_B \hbar \omega_{B,r}} = \frac{2+\lambda}{4}\frac{1}{\alpha^2} + b\alpha^2 + \frac{c_1 N_B}{\alpha^3} + \frac{c_2 N_B^2}{\alpha^6} \tag{3.52}$$

with the factors

$$\begin{aligned} b &= \frac{3}{4}\left[1 - \frac{3}{2}\,\kappa_3\,\mu_F^{1/2} g_{BF}\right], \\ c_1 &= \frac{1}{2}\left[g_{BB} - \frac{3}{2}\,\kappa_3\,\mu_F^{1/2} g_{BF}^2\right]\frac{\lambda^{1/2}}{(2\pi)^{3/2}\hbar\omega_{B,r}L_{B,r}^3}, \\ c_2 &= \frac{\kappa_3 g_{BF}^3}{8\mu_F^{1/2}}\frac{\lambda}{3^{3/2}\pi^3\hbar\omega_{B,r}L_{B,r}^6}. \end{aligned} \tag{3.53}$$

The condition (3.48) for the stability border provides two equations allowing to determine both unknown quantities for different values of $\mu_F$. The result is shown in Figures 3.7 and 3.8 by the blue line for both limits. The dashed as well as the solid blue line converges with increasing fermion number $N_F$ to the corresponding red line of the numerical integration. But for low $N_F$ or, equivalent, large $N_B$ these blue lines stay below the red lines, where the discrepancy increases with decreasing $N_F$. Moreover for very small $N_F$ the blue lines show the opposite behavior of the red lines as they tends to zero, which seems physical a bit strange. When the radius of the BEC clouds increases with decreasing $N_F$, the above mentioned expansion in powers of $V_F(\mathrm{x})/\mu_F$, which is done up to the zeroth and first order, fails as $V_F(\mathrm{x})$ and $\mu_F$ becomes comparable at the BEC cloud boundary. Thus, more orders of the expansion are needed to obtain more accurate results. Another reason is the strong dependency of the stability border in the stability diagram on the interspecies s-wave scattering wavelength $a_{BF}$ according to the scaling law for the critical numbers of condensate atoms for a fixed ratio between $N_B$ and $N_F$ [35,51]:

$$N_{B\mathrm{crit}} \approx \frac{1}{a_{BF}^{12}}, \qquad \frac{N_B}{N_F} = const. \tag{3.54}$$

The sensitivity of the critical boson number $N_{B\mathrm{crit}}$ with respect to $a_{BF}$ and also to $g_{BF}$ due to Eq. (3.12) doesn't justify a expansion of the local chemical potential $\tilde{\mu}_F(\mathrm{x})$ in the smallness parameter $g_{BF}$

### 3.5.3 New Value of $a_{BF}$

The above described strong dependence of $N_{B\mathrm{crit}}$ on $a_{BF}$, on the other hand, can be used to extract a value for $a_{BF}$ with great accuracy within a meanfield analysis of the stability as performed in this section. Because of the scaling law (3.54) the relative uncertainty of $a_{BF}$ amounts to only a twelfth of the relative uncertainty of the critical boson number $N_{B\mathrm{crit}}$. As the violet and solid red line in

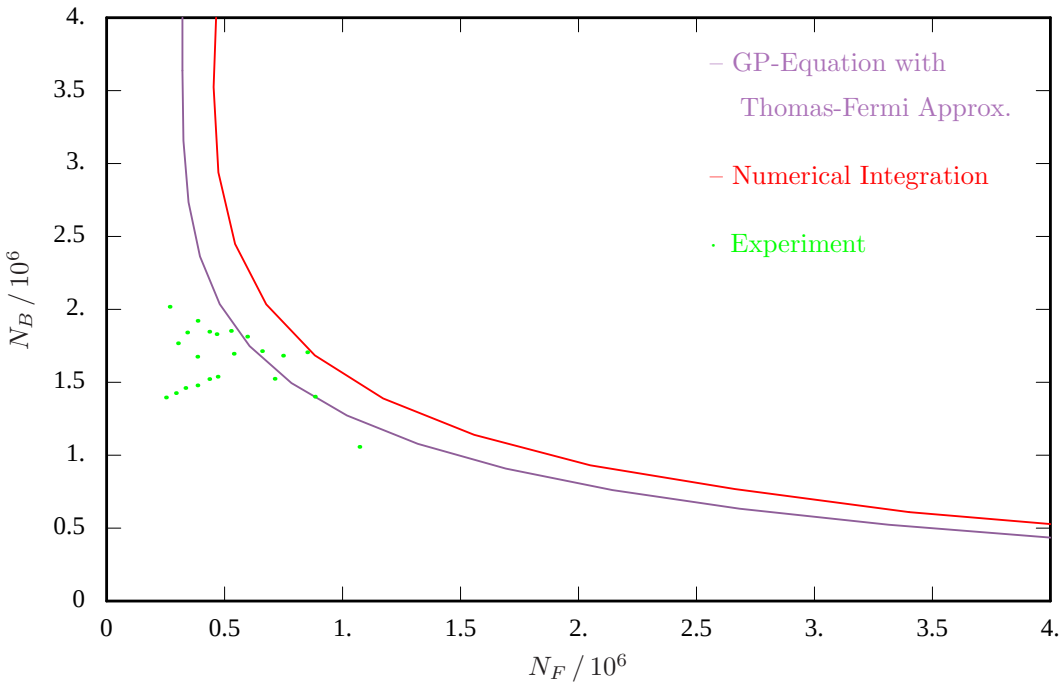


**Figure 3.11:** Stability border for a new value $a_{BF} = 16.2$ nm of the $^{87}$Rb–$^{40}$K mixture in the Hamburg experiment.

Figure 3.8 for the Florence experiment agrees with the green points of the experiments, we restrict here to determine a new value for $a_{BF}$ of the Hamburg experiment without giving an uncertainty for it. For that purpose we plotted the violet and solid red line in Figure 3.11 for a new value of $a_{BF}$ so that the lines lie within the bulk of the green points. The new value $a_{BF} = 16.2$ nm differs by only 8% from the old value $a_{BF} = 15.0$ nm whereas the critical numbers of the green points are by a factor at least of 2 smaller than those of the violet line. The old value was determined by the Sengstock group with the help of Eq. (3.52), but instead of evaluating the respective fermion number $N_F$ by integrating the fermionic density, they used the relation

$$\mu_F = \mu_F^{(0)} - \frac{g_{BF}}{g_{BB}}\,\mu_B^{(0)}, \tag{3.55}$$

where the noninteracting chemical potentials $\mu_B^{(0)}$ and $\mu_F^{(0)}$ are related to the respective particle numbers by Eqs. (3.25) and (3.32). The above relation between disturbed and undisturbed chemical potentials is not correct.

# Chapter 4

# Summary and Outlook

In Chapter 2 we derived the Gross-Pitaevskii equation for the condensate wave function of a Bose-Fermi mixture within the functional integral formalism in a hierarchy of three different approximations . All approximations contain the same conventional terms for a BEC with intraspecies interaction, but differ in the way how the quantum degenerated Fermi gas enters in the Gross-Pitaevskii equation. Most general is the result (2.85) where the dynamics of the condensate function is driven by the fermionic Green function. It obeys the inhomogeneous Schrödinger equation (2.86) and thus depends on the evolution of the condensate wave function. Thus, the complete dynamics of the Bose-Fermi mixture consists of two coupled equations of motions whose solution could not be further analyzed within this thesis. Less general is the Gross-Pitaevskii equation (2.71), (2.73) as it follows from integrating out the fermionic degree of freedom within a semiclassical approximation. Consequently, the fermions have lost their independent dynamics and their time dependence follows the condensate dynamics in a passive way. If we neglect all time dependences, we arrive at the stationary Gross-Pitaevskii equation (2.104). Note that it also follows from the coupled equations of motion (2.85), (2.86) by evaluating the fermionic Green function for a trapped Fermi gas interacting with a stationary BEC in the semiclassical approximation. Further investigation with respect to the dynamics can include the hydrodynamics and the variational method with a time-dependent width of the Gaussian test function in order to obtain macroscopic excitations of the BEC cloud. Furthermore, the influence of the Fermi gas on the superfluidity in the BEC can be investigated.

In Chapter 3 we applied the stationary Gross-Pitaevskii equation in order to determine the density profiles for an ultracold $^{87}$Rb–$^{40}$K boson-fermion mixture realized by the Sengstock group in Hamburg and by the Inguscio group in Florence. For that purpose we neglected the kinetic energy of the condensate corresponding to the Thomas-Fermi approximation, which reduces the Gross-Pitaevskii equation to an algebraic equation. The exact solution of this algebraic equation for typical particle numbers of bosons and fermions shows a strong modification of the density distribution of both species within their overlap compared with the density distribution of a single trapped BEC and a trapped Fermi gas. The strong attraction between bosons and fermions gives rise to an increase of the particle densities within their overlap, accompanied by a shrinkage of the BEC and the Fermi gas cloud. In order to test the validity of the Thomas-Fermi approximation, we have plotted the kinetic energy of a boson together with its potential energy due to the trap, its intraspecies and its interspecies interaction energy, and the chemical potential as the total energy of a boson. This

reveals the Thomas-Fermi approximation to be very good over a wide bulk range of the condensate cloud. The kinetic energy plays a significant role only in the outermost 10% of the BEC cloud.

Furthermore, we found that the particle densities for both species become complex at sufficiently large particle numbers of bosons and fermions. We interpret this as a loss of the stability against collapse. The imaginary part of the density can be regarded as the decay rate of the described species and starts emerging in the trap center, where the densities have their maximum. We extracted a condition in form of a line in the $\mu_B$-$\mu_F$-plane separating the stable and unstable region. The transformation from chemical potentials to particle numbers then leads to a stability diagram in the $N_B$-$N_F$-plane. We have plotted three density profiles for particle number pairs, one just below, another on, and the third just above the critical line in the $N_B$-$N_F$-plane showing the change of the density profiles on the road from stability to instability. This behavior of the density distribution was, indeed, observed in the Hamburg experiment as shown in Figure 3.6.

Beside the stability diagram arising from the complex solution of the Gross-Pitaevskii equation in the Thomas-Fermi approximation we evaluated the stability border within a variational method by extremizing the grand-canonical free energy (3.41) for a $^{87}$Rb–$^{40}$K mixture with a Gaussian test function. It represents the ground-state wave function for a noninteracting BEC. In order to include the influence of the intraspecies and interspecies interaction on the shape of the test function, the radial and axial widths of the test function are scaled by a common variational parameter so that the grand-canonical free energy becomes stationary. Additionally we performed the calculation with two different ratios between the radial and the axial widths. On the one hand in the quantum mechanical limit which stands for a mixture with vanishing interactions. On the other hand in the Thomas-Fermi limit with negligible kinetic energy. The most accurate results are obtained by integrating the grand-canonical free energy numerically. The resulting lines for the Thomas-Fermi limit show the same behavior as the ones of the Gross-Pitaevskii equation. Both lines are located close in the $N_B$-$N_F$-plane. Furthermore, by evaluating two lines with ratios of the radial and axial width besides and in the vicinity of the ratio for the Thomas-Fermi limit, it turns out that the line in the Thomas-Fermi limit yields the largest critical numbers. Thus, this limit reflects the proper ratios of the widths for the $^{87}$Rb–$^{40}$K mixture. This is in accordance with the fact that the density profiles of the mixture are obtained with great accuracy within the Thomas-Fermi approximation. Another approach in order to evaluate the grand-canonical free energy was suggested by Chui et. al by expanding the local chemical potential in the free energy up to the third order in the smallness parameter $g_{BF}$. This approach suffers from low accuracy in the range of small fermion numbers $N_F$. Finally, by comparing the calculated stability borders with the experimental values, we found that the for the Florence experiment the stability border of the Thomas-Fermi limit and of the Gross-Pitaevskii equation is in good agreement with the experimental results. For the Hamburg experiment we found a discrepancy between the calculated lines and the experimental results. We extract a new value of the interspecies s-wave scatterin length to $a_{BF} = 16.2$ nm.

# Appendix A

# Grassmann Numbers

In order to calculate the one-dimensional fermionic Gaussian integrals in Eq. (2.35) for each quantum number $\mathbf{n}$ and each Matsubara mode $m$, we summarize here briefly the main properties of Grassmann numbers [44]. We start with considering an integral over two fermionic variables

$$I_F = \int d\psi^* \int d\psi \, e^{-\psi^* A \psi}, \tag{A.1}$$

where $A$ is a complex number. The fermionic variables $\psi$, $\psi^*$ are Grassmann numbers, so they obey anticommutation relations

$$\left[\psi_i, \psi_j\right]_+ = \left[\psi_i^*, \psi_j\right]_+ = \left[\psi_i, \psi_j^*\right]_+ = 0. \tag{A.2}$$

Here $\psi_1, \ldots, \psi_n$ and $\psi_1^*, \ldots, \psi_n^*$ are two disjoint sets of $n$ Grassmann variables, which are connected by the conjugation operation

$$(\psi_i)^* = \psi_i^*, \quad (\psi_i^*)^* = \psi_i, \quad (\psi_{i_1} \psi_{i_2} \ldots \psi_{i_n})^* = \psi_{i_n}^* \ldots \psi_{i_2}^* \psi_{i_1}^*, \quad (\lambda \psi_i)^* = \lambda^* \psi_i^*, \tag{A.3}$$

with a complex number $\lambda$. From the anticommutation rules (A.2) follows immediately that the square and all higher powers of a Grassmann number vanish:

$$\psi_i^n = 0, \qquad n \geq 2. \tag{A.4}$$

The differentiation rules are analogous to that of complex numbers

$$\frac{\partial}{\partial \psi_i} 1 = 0, \qquad \frac{\partial}{\partial \psi_i} \psi_j = \delta_{ij}, \tag{A.5}$$

except that the order of differentiation plays a role:

$$\frac{\partial}{\partial \psi_i}(\psi_j \, \psi_k) = \delta_{ij} \, \psi_k - \delta_{ik} \, \psi_j = -\frac{\partial}{\partial \psi_i}(\psi_k \, \psi_j). \tag{A.6}$$

The integration over Grassmann variables differs from the ordinary one, as it can neither be defined via a Riemannian sum nor via the inversion of the differentation since there exists no graphical interpretation of an area below a curve and no integration limits. In order to define an integration over Grassmann variables, one proceeds axiomatically and demands linearity and translation invariance. We consider the integral of the function $f(\psi) = f_1 + f_2 \, \psi$, where linearity and translation

invariance lead to

$$\begin{aligned}\int d\psi\,[f_1 + f_2\,\psi] &= \int d\psi\, f(\psi) \equiv \int d\psi\, f\,(\psi+\eta) = \int d\psi\,[f_1 + f_2\,(\psi+\eta)] \\ &= \int d\psi\,[f_1 + f_2\,\psi] + \left(\int d\psi\, 1\right) f_2\,\eta. \end{aligned} \tag{A.7}$$

Thus, we read off the integration rule

$$\int d\psi\, 1 = 0. \tag{A.8}$$

This rule is completed by choosing an arbitrary normalization

$$\int d\psi_i\,\psi_j = \delta_{ij}. \tag{A.9}$$

Thus, we see that differentiation and integration amount to the same operations in the space of Grassmann numbers.

With these rules we are able to calculate the integral (A.1). Since quadratic and higher terms of the same Grassmann variable vanish, the Taylor series of the integrand in Eq. (A.1) breaks down after the first order

$$e^{-\psi^* A\psi} = 1 + A\psi\,\psi^*. \tag{A.10}$$

Starting with the inner integral and applying the rules (A.8) and (A.9), we obtain

$$I_F = \int d\psi^* \int d\psi\,(1 + A\psi\,\psi^*) = \int d\psi^*\, A\psi^* = A. \tag{A.11}$$

# Appendix B

# Poisson Sum Formula

In the following we derive the Poisson sum formula, which is useful for evaluating Matsubara series for bosons and fermions, respectively [43]. It follows from the fact, that the comb function

$$C(x) = \sum_{m=-\infty}^{\infty} \delta(x-m), \qquad m = \begin{cases} 0, \pm 1, \pm 2 \dots & \text{bosons,} \\ \pm\frac{1}{2}, \pm\frac{3}{2}, \pm\frac{5}{2} \dots & \text{fermions} \end{cases} \tag{B.1}$$

has the property to be periodic:

$$C(x+k) = C(x), \qquad k = 0, \pm 1, \pm 2, \dots . \tag{B.2}$$

Therefore, the comb function can be Fourier expanded

$$C(x) = \sum_{n=-\infty}^{\infty} C_n \, e^{-i2\pi n x}. \tag{B.3}$$

The Fourier coefficients are obtained by integration over one period:

$$C_n = \int_{a-1/2}^{a+1/2} dx \, C(x) \, e^{-i2\pi n x} = \epsilon^n, \qquad a = \begin{cases} 0 & \text{bosons,} \\ 1/2 & \text{fermions,} \end{cases} \tag{B.4}$$

where $\epsilon = \pm 1$ holds for bosons and fermions, respectively. Inserting Eq. (B.4) into Eq. (B.3) leads to the distribution identity

$$\sum_{m=-\infty}^{\infty} \delta(x-m) = \sum_{n=-\infty}^{\infty} \epsilon^n \, e^{-i2\pi n x}. \tag{B.5}$$

Multiplying with a function $f(x)$ and integrating over the whole $x$-axis yields the desired Poisson sum formula

$$\sum_{m=-\infty}^{\infty} f(m) = \sum_{n=-\infty}^{\infty} \epsilon^n \int_{-\infty}^{\infty} dx \, f(x) \, e^{-i2\pi n x}. \tag{B.6}$$

In order to make this formula more applicable for Matsubara series with Matsubara frequencies

$$\omega_m = \frac{2\pi}{\hbar\beta}\, m \tag{B.7}$$

with $m$ corresponding to Eq. (B.1), we specialize to a function $f(m) = F(\omega_m)$:

$$\sum_{m=-\infty}^{\infty} F(\omega_m) = \frac{\hbar\beta}{2\pi} \sum_{n=-\infty}^{\infty} \epsilon^n \int_{-\infty}^{\infty} d\omega\, F(\omega)\, e^{-in\hbar\beta\omega}. \tag{B.8}$$

As a particular useful example we derive the completeness relation of the Matsubara functions $e^{-i\omega_m\tau}$. Using Eq. (B.6), we obtain

$$\frac{1}{\hbar\beta} \sum_{m=-\infty}^{\infty} e^{-i\omega_m\tau}\, e^{i\omega_m\tau'} = \frac{1}{\hbar\beta} \sum_{m=-\infty}^{\infty} e^{-i2\pi m(\tau-\tau')/\hbar\beta} = \sum_{n=-\infty}^{\infty} \epsilon^n\, \delta(\tau - \tau' + n\hbar\beta). \tag{B.9}$$

The right expression in Eq. (B.9) is also called the periodic repetitive delta function for bosons:

$$\delta^{(p)}(\tau - \tau') = \sum_{n=-\infty}^{\infty} \delta(\tau - \tau' + n\hbar\beta) \tag{B.10}$$

and the antiperiodic repetitive delta function for fermions:

$$\delta^{(a)}(\tau - \tau') = \sum_{n=-\infty}^{\infty} (-1)^n\, \delta(\tau - \tau' + n\hbar\beta). \tag{B.11}$$

Thus, the Matsubara functions represent a basis in the space of the $\hbar\beta$–periodic functions and $\hbar\beta$–antiperiodic functions, respectively. This justifies the Fourier expansion (2.26) of the Grassmann fields with fermionic Matsubara frequencies (2.27).

# Appendix C

# Tracelog Calculation

Here we evaluate the Matsubara sum of the tracelog $\mathrm{Tr}\ln\hat{O}$, which reads for bosons and fermions

$$\mathrm{Tr}\,\ln\hat{O} = \sum_{\mathbf{n}}\sum_{m=-\infty}^{\infty}\ln\left[\beta(-i\hbar\omega_m + E_{\mathbf{n}} - \mu)\right], \tag{C.1}$$

respectively, with the Matsubara frequencies (B.7) and $m$ corresponding to Eq. (B.1). At first, we replace the sum over the Masubara frequencies by an integral with the help of the Poisson sum formula (B.8). Setting $F(\omega_m) = \ln\left[\beta(-i\hbar\omega_m + E_{\mathbf{n}} - \mu)\right]$, the Poisson sum formula (B.8) leads to

$$\mathrm{Tr}\,\ln\hat{O} = \lim_{\eta\downarrow 0}\frac{\hbar\beta}{2\pi}\sum_{\mathbf{n}}\sum_{n=-\infty}^{\infty}\epsilon^n\int_{-\infty}^{\infty}d\omega\,\ln\left[\beta(-i\hbar\omega_m + E_{\mathbf{n}} - \mu)\right]\,e^{-i\hbar\beta(n-\eta)\omega}. \tag{C.2}$$

Here the additional factor $\exp\{i\hbar\beta\omega\eta\}$ with $\eta$ as an infinitesimal positive number is introduced to achieve the normal-ordering. In this way we avoid a divergent contribution which doesn't play any role within the nonrelativistic many-body theory. The logarithm in the integral can be replaced with the help of the Schwinger trick:

$$\ln a = -\frac{\partial}{\partial x}\frac{1}{a^x}\bigg|_{x=0} = -\frac{\partial}{\partial x}\left\{\frac{1}{\Gamma(x)}\int_0^\infty d\lambda\,\lambda^{x-1}\,e^{-\lambda a}\right\}\bigg|_{x=0}. \tag{C.3}$$

Applying Eq. (C.3) to Eq. (C.2) yields

$$\mathrm{Tr}\,\ln\hat{O} = -\lim_{\eta\downarrow 0}\frac{\hbar\beta}{2\pi}\sum_{\mathbf{n}}\sum_{n=-\infty}^{\infty}\epsilon^n\,\frac{\partial}{\partial x}\left\{\frac{1}{\Gamma(x)}\int_0^\infty d\lambda\,\lambda^{x-1}\,e^{-\lambda\beta(E_{\mathbf{n}}-\mu)}\int_{-\infty}^{\infty}d\omega\,e^{i\hbar\beta(\lambda-n+\eta)\omega}\right\}\bigg|_{x=0}. \tag{C.4}$$

The integral over $\omega$ can be directly performed:

$$\int_{-\infty}^{\infty}d\omega\,e^{i\hbar\beta(\lambda-n+\eta)\omega} = \frac{2\pi}{\hbar\beta}\,\delta(\lambda - n + \eta). \tag{C.5}$$

Inserting this into Eq. (C.4) leads to

$$\mathrm{Tr}\,\ln\hat{O} = -\lim_{\eta\downarrow 0}\sum_{\mathbf{n}}\sum_{n=-\infty}^{\infty}\epsilon^n\,\frac{\partial}{\partial x}\left\{\frac{1}{\Gamma(x)}\int_0^\infty d\lambda\,\lambda^{x-1}\,e^{-\lambda\beta(E_{\mathbf{n}}-\mu)}\,\delta(\lambda - n + \eta)\right\}\bigg|_{x=0}. \tag{C.6}$$

As the integration is restricted to the positive $\lambda$-axis, only the terms with positive summation index $n$ contribute:

$$\mathrm{Tr}\,\ln\hat{O} = -\lim_{\eta\downarrow 0}\sum_{\mathbf{n}}\sum_{n=1}^{\infty}\epsilon^n\,\frac{\partial}{\partial x}\left\{\frac{1}{\Gamma(x)}\,(n-\eta)^{x-1}\,e^{-(n-\eta)\beta(E_{\mathbf{n}}-\mu)}\right\}\Bigg|_{x=0}. \tag{C.7}$$

Performing the limit $\eta\downarrow 0$ yields

$$\mathrm{Tr}\,\ln\hat{O} = -\sum_{\mathbf{n}}\sum_{n=1}^{\infty}\epsilon^n\,\frac{\partial}{\partial x}\left\{\frac{1}{\Gamma(x)}\,n^{x-1}\,e^{-n\beta(E_{\mathbf{n}}-\mu)}\right\}\Bigg|_{x=0}. \tag{C.8}$$

In order to determine the derivative with respect to $x$ in Eq. (C.8), we use the identity

$$\Gamma(x) = \frac{1}{x}\,\Gamma(x+1), \tag{C.9}$$

and perform the Taylor expansion

$$\Gamma(x) = \frac{1}{x}\,\left[\Gamma(1) + \Gamma'(1)\,x + \ldots\right], \tag{C.10}$$

in order to yield for small $x$

$$\frac{1}{\Gamma(x)} = \frac{x}{1+\Gamma'(1)\,x} = x - \Gamma'(1)\,x^2 + \Gamma'(1)^2\,x^3 - \ldots\,. \tag{C.11}$$

Finally, multiplying with a regular function $f(x)$, which is expanded around $x=0$, yields

$$\begin{aligned}\frac{1}{\Gamma(x)}\,f(x) &= \left[x - \Gamma'(1)\,x^2 + \Gamma'(1)^2\,x^3 - \ldots\right]\left[f(0) + f'(0)\,x + \frac{f''(0)}{2}\,x^2 + \ldots\right]\\ &= f(0)\,x + \left[f'(0) - \Gamma'(1)f(0)\right]\,x^2 + \ldots,\end{aligned} \tag{C.12}$$

so that the derivative with respect to $x$ at $x=0$ results in

$$\frac{\partial}{\partial x}\left\{\frac{1}{\Gamma(x)}\,f(x)\right\}\Bigg|_{x=0} = f(0). \tag{C.13}$$

Applying Eq. (C.13) to Eq. (C.8), we obtain

$$\mathrm{Tr}\,\ln\hat{O} = -\sum_{\mathbf{n}}\sum_{n=1}^{\infty}\frac{\epsilon^n}{n}\,e^{-n\beta(E_{\mathbf{n}}-\mu)}. \tag{C.14}$$

With the help of the Taylor series

$$\ln(1-\epsilon\,z) = -\sum_{n=1}^{\infty}\frac{\epsilon^n z^n}{n}, \qquad\qquad |z|<1, \tag{C.15}$$

we replace the sum over $n$ as follows

$$\mathrm{Tr}\,\ln\hat{O} = \sum_{\mathbf{n}}\ln\left[1-\epsilon\,e^{-\beta(E_{\mathbf{n}}-\mu)}\right]. \tag{C.16}$$

Thus, the result of the tracelog reads

$$\mathrm{Tr}\,\ln\hat{O} = \begin{cases}\displaystyle\sum_{\mathbf{n}}\ln\left[1-e^{-\beta(E_{\mathbf{n}}-\mu)}\right] & \text{bosons,}\\[2ex] \displaystyle\sum_{\mathbf{n}}\ln\left[1+e^{-\beta(E_{\mathbf{n}}-\mu)}\right] & \text{fermions.}\end{cases} \tag{C.17}$$

# Appendix D

# Sommerfeld Expansion

In this appendix we follow [50] and evaluate the Sommerfeld expansion, which is applied in the low-temperature limit $k_B T \ll \mu$ to integrals of the form

$$I(T) = \int_{-\infty}^{\infty} dE\, g(E)\, f(E,T), \tag{D.1}$$

where the function $f(E,T)$ is the Fermi-Dirac distribution

$$f(E,T) = \frac{1}{e^{(E-\mu)/k_B T} + 1} \tag{D.2}$$

with the Fermi energy $\mu$. The other function $g(E)$ can be expanded arround $E = \mu$ and has the properties

$$\lim_{E\to-\infty} g(E) = 0, \qquad \lim_{E\to\infty} g(E) \propto E^{\alpha}. \tag{D.3}$$

We consider the function

$$G(E) = \int_{-\infty}^{E} dE'\, g(E'), \tag{D.4}$$

which has the properties

$$g(E) = \frac{dG(E)}{dE}, \qquad \lim_{E\to-\infty} G(E) = 0, \qquad \lim_{E\to\infty} G(E) \propto E^{\alpha+1}. \tag{D.5}$$

We perform an integration by parts in Eq. (D.1):

$$I(T) = G(E)\, f(E,T)\Big|_{-\infty}^{\infty} - \int_{-\infty}^{\infty} dE\, G(E)\, \frac{df(E,T)}{dE}, \tag{D.6}$$

where the boundary terms vanish due to (D.2) and (D.5). In the low-temperature limit $k_B T \ll \mu$ the Fermi-Dirac distribution $f(E,T)$ differs only slightly from the Heaviside function $\Theta(\mu - E)$, so that its derivative $df(E,T)/dE$ represents approximately the delta function $-\delta(E-\mu)$. Thus, it's useful to expand $G(E)$ in a Taylor series around $E = \mu$:

$$G(E) = G(\mu) + \sum_{n=1}^{\infty} \frac{(E-\mu)^n}{n!}\, \frac{d^n G(E')}{dE'^n}\bigg|_{E'=\mu}, \tag{D.7}$$

which reduces due to (D.4) and (D.5) to

$$G(E) = \int_{-\infty}^{\mu} dE'\, g(E') + \sum_{n=1}^{\infty} \frac{(E-\mu)^n}{n!} \left.\frac{d^{n-1}g(E')}{dE'^{n-1}}\right|_{E'=\mu}. \tag{D.8}$$

Inserting Eq. (D.7) into Eq. (D.6) yields

$$\begin{aligned} I(T) &= -\int_{-\infty}^{\mu} dE'\, g(E') \int_{-\infty}^{\infty} dE\, \frac{df(E,T)}{dE} \\ &\quad - \sum_{n=1}^{\infty} \frac{1}{n!} \left.\frac{d^{n-1}g(E')}{dE'^{n-1}}\right|_{E'=\mu} \int_{-\infty}^{\infty} dE\, (E-\mu)^n \frac{df(E,T)}{dE}. \end{aligned} \tag{D.9}$$

Since

$$\frac{df(E,T)}{dE} = -\frac{1}{k_B T} \frac{e^{(E-\mu)/k_B T}}{\left[e^{(E-\mu)/k_B T}+1\right]^2} = -\frac{1}{k_B T} \frac{1}{\left[e^{(E-\mu)/2k_B T}+e^{-(E-\mu)/2k_B T}\right]^2} \tag{D.10}$$

is an even function with respect to $E=\mu$, all odd powers $n$ in Eq. (D.9) vanish while integrating. Using this and the observation

$$\int_{-\infty}^{\infty} dE \frac{df(E,T)}{dE} = \lim_{E\to\infty} f(E,T) - \lim_{E\to-\infty} f(E,T) = -1, \tag{D.11}$$

Eq. (D.9) reads

$$I(T) = \int_{-\infty}^{\mu} dE'\, g(E') + \sum_{n=1}^{\infty} a_n\, (k_B T)^{2n} \left.\frac{d^{2n-1}g(E')}{dE'^{2n-1}}\right|_{E'=\mu}. \tag{D.12}$$

With the substitution $x(E) = (E-\mu)/k_B T$ in the last integral in Eq. (D.9) the coefficients $a_n$ are calculated as follows:

$$a_n = -\frac{1}{(2n)!} \int_{-\infty}^{\infty} dx\, x^{2n} \frac{d}{dx} \frac{1}{e^x+1}. \tag{D.13}$$

As both factors of the integrand are even with respect to $x=0$ due Eq. (D.10), we restrict the integration to the positive $x$-axis. Moreover, an integration by parts leads to

$$a_n = \frac{2}{(2n-1)!} \int_{0}^{\infty} dx\, \frac{x^{2n-1}\, e^{-x}}{1+e^{-x}}. \tag{D.14}$$

Expanding the denominator in a geometrical series and performing the integration yield the series representation

$$a_n = \frac{2}{(2n-1)!} \sum_{k=0}^{\infty} (-1)^k \frac{(2n-1)!}{(k+1)^{2n}} = 2 \sum_{k=1}^{\infty} (-1)^{k-1} \frac{1}{k^{2n}}. \tag{D.15}$$

We decompose the alternating series

$$a_n = 2\left\{\frac{1}{1^{2n}} - \frac{1}{2^{2n}} + \frac{1}{3^{2n}} - \frac{1}{4^{2n}} + \dots\right\} \tag{D.16}$$

into two nonalternating series

$$a_n = 2\left\{\left[\frac{1}{1^{2n}} + \frac{1}{2^{2n}} + \frac{1}{3^{2n}} + \frac{1}{4^{2n}} + \dots\right] - \frac{2}{2^{2n}}\left[\frac{1}{1^{2n}} + \frac{1}{2^{2n}} + \dots\right]\right\}. \tag{D.17}$$

Summarizing these series results in

$$a_n = 2\left\{1 - \frac{1}{2^{2n-1}}\right\}\zeta(2n), \tag{D.18}$$

where the Riemann zeta function is defined as

$$\zeta(z) \equiv \sum_{k=1}^{\infty} \frac{1}{k^z}. \tag{D.19}$$

For the first even numbers it has the values

$$\zeta(2) = \frac{\pi^2}{6}, \qquad \zeta(4) = \frac{\pi^4}{90}, \qquad \zeta(6) = \frac{\pi^6}{945}, \dots . \tag{D.20}$$

Thus, the Sommerfeld expansion (D.12) reads

$$I(T) = \int_{-\infty}^{\mu} dE'\, g(E') + 2\sum_{n=1}^{\infty}(k_B T)^{2n}\left\{1 - \frac{1}{2^{2n-1}}\right\}\zeta(2n)\left.\frac{d^{2n-1}g(E')}{dE'^{2n-1}}\right|_{E'=\mu}. \tag{D.21}$$

Let us specialize the function $g(E)$ to an arbitrary power $\nu$:

$$g(E) = \Theta(E)\, E^{\nu-1}, \tag{D.22}$$

which fulfills the properties (D.3). Then its derivatives reads for $\mu > 0$

$$\left.\frac{d}{dE}\, g(E)\right|_{E=\mu} = (\nu-1)\,\mu^{\nu-2}, \qquad \left.\frac{d^n}{dE^n}\, g(E)\right|_{E=\mu} = \left\{\prod_{k=1}^{n}(\nu-k)\right\}\mu^{\nu-n-1}. \tag{D.23}$$

Furthermore, we obtain

$$\int_{-\infty}^{\mu} dE'\, g(E') = \frac{\mu^\nu}{\nu}. \tag{D.24}$$

Applying Eqs. (D.22), (D.23), and (D.24) to Eq. (D.21) leads to the special Sommerfeld expansion

$$\int_0^{\infty} dE\, \frac{E^{\nu-1}}{e^{(E-\mu)/k_B T}+1} = \frac{\mu^\nu}{\nu}\left\{1 + 2\sum_{n=1}^{\infty}\left(\frac{k_B T}{\mu}\right)^{2n}\left[1 - \frac{1}{2^{2n-1}}\right]\left[\prod_{k=0}^{2n-1}(\nu-k)\right]\zeta(2n)\right\}. \tag{D.25}$$

Its first three terms read explicitly

$$\begin{aligned}\int_0^{\infty} dE\, \frac{E^{\nu-1}}{e^{(E-\mu)/k_B T}+1} \quad &= \quad \frac{\mu^\nu}{\nu} + \frac{\pi^2}{6}(\nu-1)\,\mu^\nu\left(\frac{k_B T}{\mu}\right)^2 \\ &\quad + \frac{7\pi^4}{360}(\nu-1)(\nu-2)(\nu-3)\,\mu^\nu\left(\frac{k_B T}{\mu}\right)^4 + \dots .\end{aligned} \tag{D.26}$$

Thus, the Sommerfeld expansion represents a low-temperature expansion of the Integral (D.1).

# Appendix E

# Density of States in a Harmonic Oscillator

The density of states $g(\varepsilon)$ is defined as the number $dn = g(\varepsilon)\, d\varepsilon$ of states within the energy interval $d\varepsilon$ at the energy value $\varepsilon$. Hence it can be calculated as the differentiation of the states number

$$N = \int_0^E d\varepsilon\, g(\varepsilon) \tag{E.1}$$

with respect to the energy $E$:

$$g(E) = \frac{dN}{dE}. \tag{E.2}$$

The energy of a $D$-dimensional harmonic oscillator is given by

$$\varepsilon = \hbar \sum_{i=1}^{D} \omega_i \left( n_i + \frac{1}{2} \right), \qquad n_i = 0, 1, 2, \ldots, \tag{E.3}$$

where $n_i$ is the occupation number of the one-dimensional oscillator along the $i$-axis. For $D > 1$ the energy values (E.3) are degenerate as the same energy can be obtained with different sets of occupation numbers $\{n_1, n_2, \ldots, n_D\}$. Thus, to obtain the number $N$ of all possible states up to the energy $E$, we have to count the number of $\hbar\omega_i$ spaced points in the Volume of the orthogonal coordinate system, which is spanned by $D$ positive axes $\varepsilon_i = \hbar\, \omega_i\, x_i$ and bounded by the $(D-1)$-dimensional plane hypersurface

$$E - \hbar \sum_{i=1}^{D} \omega_i\, x_i = 0, \tag{E.4}$$

where $x_i$ is a continuous variable. As we consider harmonic oscillators with a very large number of states, the number $N$ of all points below $E$ can be obtained by dividing the above described $D$-dimensional volume by the product of $D$ distances $\Delta\varepsilon_i = \hbar\omega_i$ between the points. This Volume can be evaluated with a $D$-dimensional integral, which can be constructed for that purpose successively as a product of $D$ one-dimensional integrals. Starting with $D = 1$, we integrate from zero to $E$ and divide by the distance $\Delta\varepsilon_1 = \hbar\omega_1$. For $D = 2$ we calculate the area of the isosceles triangle in

the first quadrant, which is bounded by the line $\varepsilon_2 = E - \varepsilon_1$, so that we only need to multiply the first $\varepsilon_1$-integral with a second one with the obove line as a variable upper integration limit. And for $D = 3$ we calculate the volume of the tetrahedron in the first octant, which is bounded by the plane $\varepsilon_3 = E - \varepsilon_1 - \varepsilon_2$, so that we multiply the two integrals in case of $D = 2$ with a third one with the obove plane as a variable upper integration limit and so on. Thus, by iteration the number of states is evaluated as follows:

$$N = \frac{1}{\hbar^D \tilde{\omega}^D} \int_0^E d\varepsilon_1 \int_0^{E-\varepsilon_1} d\varepsilon_2 \ldots \int_0^{E-\sum_{i=1}^{D-2}\varepsilon_i} d\varepsilon_{D-1} \int_0^{E-\sum_{i=1}^{D-1}\varepsilon_i} d\varepsilon_D, \tag{E.5}$$

where $\tilde{\omega} = (\omega_1 \omega_2 \ldots \omega_D)^{1/D}$ denotes the geometrical average of the $D$ oscillator frequencies. Starting with the innermost integral, we obtain

$$N = \frac{1}{\hbar^D \tilde{\omega}^D} \int_0^E d\varepsilon_1 \int_0^{E-\varepsilon_1} d\varepsilon_2 \ldots \int_0^{E-\sum_{i=1}^{D-2}\varepsilon_i} d\varepsilon_{D-1} \left[E - \varepsilon_1 - \ldots - \varepsilon_{D-2} - \varepsilon_{D-1}\right]. \tag{E.6}$$

From now on the evaluation of each of the following integrals increases the exponent of the integrand by one and divides the integrand by the new exponent, where the upper integration limit yields zero and the lower one returns the expression inside the brackets without the latter variable. Thus, performing the remaining integrations results in

$$N = \frac{1}{D!} \left(\frac{E}{\hbar\tilde{\omega}}\right)^D. \tag{E.7}$$

Applying Eq. (E.2) yields for the density of states in a $D$-dimensional harmonic oscillator:

$$g(E) = \frac{E^{D-1}}{(D-1)!\,(\hbar\tilde{\omega})^D}. \tag{E.8}$$

Its inverse

$$g^{-1}(E) = \frac{(D-1)!\,(\hbar\tilde{\omega})^D}{E^{D-1}}, \qquad g^{-1}(N) = \frac{(D!)^{1/D}\,\hbar\tilde{\omega}}{D\,N^{1-1/D}} \tag{E.9}$$

gives the energy difference $dE$ between neighbouring states at the energy level $E$, which is filled up with $N$ states.

# Acknowledgement

This thesis could be written only with the help of several people. I would like to thank Professor Dr. Hagen Kleinert for giving the opportunity to prepare this thesis under his supervision. He froth over with ideas to almost all problems in physics and no other can convoy better in the lectures that physics is a fascinating field.

I'm especially grateful to Priv. Doz. Axel Pelster for his committed and personal support from the beginning of the thesis. He gave me the crucial impulses without them this thesis could not be written.

I thanks Konstantin Glaum for many explanations and valuable critics. To discuss with him about physics is very amusing.

I owe my parents a debt of gratitude for supporting me during the study and life.

# List of Figures

# List of Tables

# Bibliography


[1] A. Einstein, *Quantentheorie des einatomigen idealen Gases*, Sitzungsb. Kgl. Preuss. Akad. Wiss., 261 (1924)

[2] A. Einstein, *Quantentheorie des einatomigen idealen Gases. Zweite Abhandlung*, Sitzungsb. Kgl. Preuss. Akad. Wiss., 3 (1925)

[3] S.N. Bose, *Plancks Gesetz und Lichtquantenhypothese*, Zeitschrift für Physik **26**, 178 (1924)

[4] P.E. Sokol, *Bose-Einstein Condensation in Liquid Helium* in A. Griffin, D.W. Snoke, and S. Stringari (Editors), *Bose-Einstein Condensation*, p. 51 (Cambridge University Press, Cambridge, 1995)

[5] J.P Wolfe, J.L. Lin, and D.W. Snoke, *Bose-Einstein Condensation of a Nearly Ideal Gas: Excitons in $Cu_2O$* in A. Griffin, D.W. Snoke, and S. Stringari (Editors), *Bose-Einstein Condensation*, p. 281 (Cambridge University Press, Cambridge, 1995)

[6] M.H. Anderson, J.R. Ensher, M.R. Matthews, C.E. Wiemann, and E.A. Cornell, *Observation of Bose-Einstein Condensation in a Dilute Atomic Vapor*, Science **269**, 198 (1995)

[7] C.C. Bradley, C.A. Sackett, J.J. Tollett, and R.G. Hulet, *Evidence of Bose-Einstein Condensation in an Atomic Gas with Attractive Interactions*, Phys. Rev. Lett. **75**, 1687 (1995)

[8] K.B. Davis, M.-O. Mewes, M.R. Andrews, N.J. van Druten, D. S. Durfee, D. M. Kurn, and W. Ketterle, *Bose-Einstein Condensation in a Gas of Sodium Atoms*, Phys. Rev. Lett. **75**, 3969 (1995)

[9] A. Griesmaier, J. Werner, S. Hensler, J. Stuhler, and T. Pfau, *Bose-Einstein Condensation of Chromium*, Phys. Rev. Lett. **94**, 160401 (2005)

[10] G. Modugno, G. Ferrari, G. Roati, R.J. Brecha, A. Simoni, and M. Inguscio, *Bose-Einstein Condensation of Potassium Atoms by Sympathetic Cooling*, Science **294**, 1320 (2001)

[11] A.G. Truscott, K.E. Strecker, W.I. McAlexander, G.B. Partridge, and R.G. Hulet, *Observation of Fermi Pressure in a Gas of Trapped Atoms*, Science **291**, 2570 (2001)

[12] F. Schreck, L. Khaykovich, K.L. Corwin, G. Ferrari, T. Bourdel, J. Cubizolles, and C. Salomon, *Quasipure Bose-Einstein Condensate Immersed in a Fermi Sea*, Phys. Rev. Lett. **87**, 080403 (2001)

[13] Z. Hadzibabic, C.A. Stan, K. Dieckmann, S. Gupta, M.W. Zwierlein, A. Görlitz, and W. Ketterle, *Two-Species Mixture of Quantum Degenerate Bose and Fermi Gases*, Phys. Rev. Lett. **88**, 160401 (2002)

[14] G. Roati, F. Riboli, G. Modugno, and M. Inguscio, *Fermi-Bose Quantum Degenerate $^{40}K$-$^{87}Rb$ Mixture with Attractive Interaction*, Phys. Rev. Lett. **89**, 150403 (2002)

[15] B. DeMarco and D.S. Jin, *Onset of Fermi Degeneracy in a Trapped Atomic Gas*, Science **285**, 1703 (1999)

[16] C. Ospelkaus, S. Ospelkaus, K. Sengstock, and K. Bongs, *Interaction-driven Dynamics of $^{40}K$-$^{87}Rb$ Fermion-Boson Gas Mixtures in the Large-Particle-Number Limit*, Phys. Rev. Lett. **96**, 020401 (2006)

[17] N. Yokoshi and S. Kurihara, *Effects of Fermion-Boson Interaction in Neutral Atomic Systems*, Phys. Rev. B **68**, 064501 (2003)

[18] P. Capuzzi and E. S. Hernández, *Phase Separation and Response of $^3He$-$^4He$ Mixtures within a Magnetic Trap*, Phys. Rev. A **66**, 035602 (2002)

[19] G. Modugno, G. Roati, F. Riboli, F. Ferlaino, R.J. Brecha, and M. Inguscio, *Collapse of a Degenerate Fermi Gas*, Science **297**, 2240 (2002)

[20] C.A. Regal, M. Greiner, and D.S. Jin, *Observation of Resonance Condensation of Fermionic Atom Pairs*, Phys. Rev. Lett. **92**, 040403 (2004)

[21] M.W. Zwierlein, A. Schirotzek, C.H. Schunck, and W. Ketterle, *Fermionic Superfluidity with Imbalanced Spin Populations*, Science **311**, 492 (2006)

[22] R.A. Duine and H.T.C. Stoof, *Dynamics of a Bose-Einstein Condensate near a Feshbach Resonance*, Phys. Rev. A **68**, 013602 (2003)

[23] L. Viverit, *Boson-Induced s-Wave Pairing in Dilute Boson-Fermion Mixtures*, Phys. Rev. A **66**, 023605 (2002)

[24] M.J. Bijlsma, B.A. Heringa, and H.T.C. Stoof, *Phonon Exchange in Dilute Fermi-Bose Mixtures: Tailoring the Fermi-Fermi Interaction*, Phys. Rev. A **61**, 053601 (2000)

[25] D.B.M. Dickerscheid, D. van Oosten, E.J. Tillema, and H.T.C. Stoof, *Quantum Phases in a Resonantly Interacting Boson-Fermion Mixture*, Phys. Rev. Lett. **94**, 230404 (2005)

[26] M. Greiner, O. Mandel, T. Esslinger, Th.W. Hänsch, and I. Bloch, *Quantum Phase Transition from a Superfluid to a Mott Insulator in a Gas of Ultracold Atoms*, Nature **415**, 39 (2002)

[27] A. Albus, F. Illuminati, and J. Eisert, *Mixtures of Bosonic and Fermionic Atoms in Optical Lattices*, Phys. Rev. A **68**, 023606 (2003)

[28] M. Lewenstein, L. Santos, M.A. Baranov, and H. Fehrmann, *Atomic Bose-Fermi Mixtures in an Optical Lattice*, Phys. Rev. Lett. **92**, 050401 (2004)

[29] S. Ospelkaus, C. Ospelkaus, O. Wille, M. Succo, P. Ernst, K. Sengstock, and K. Bongs, *Localization of Bosonic Atoms by Fermionic Impurities in a 3d Optical Lattice*, cond-mat/0604179

[30] W. Ketterle, *Experimental Studies of Bose-Einstein Condensation*, Physics Today, December 1999

[31] F. Dalfovo, S. Giorgini, L.P. Pitaevskii, and S. Stringari, *Theory of Bose-Einstein Condensation in Trapped Gases*, Rev. Mod. Phys. **71**, 463 (1999)

[32] D.A. Butts and D.S. Rokhsar, *Trapped Fermi Gases*, Phys. Rev. A **55**, 4346 (1997)

[33] C.J. Pethick and H. Smith, *Bose-Einstein Condensation in Dilute Gases* (Cambridge University Press, Cambridge, 2002)

[34] G. Ferrari, M. Inguscio, W. Jastrzebski, G. Modugno, and G. Roati, *Collisional Properties of Ultracold K-Rb Mixtures*, Phys. Rev. Lett. **89**, 053202 (2002)

[35] M. Modugno, F. Ferlaino, F. Riboli, G. Roati, G. Modugno, and M. Inguscio, *Mean-Field Analysis of the Stability of a K-Rb Fermi-Bose Mixture*, Phys. Rev. A **68**, 043626 (2003)

[36] S. Inouye, J. Goldwin, M.L. Olsen, C. Ticknor, J.L. Bohn, and D. S. Jin, *Observation of Heteronuclear Feshbach Resonances in a Mixture of Bosons and Fermions*, Phys. Rev. Lett. **93**, 183201 (2004)

[37] J. Goldwin, S. Inouye, M.L. Olsen, B. Newman, B.D. DePaola, and D.S. Jin, *Measurement of the Interaction Strength in a Bose-Fermi Mixture with* $^{87}Rb$ *and* $^{40}K$, Phys. Rev. A **70**, 021601 (2004)

[38] S.T. Chui, V.N. Ryzhov, and E.E. Tareyeva, *Stability of Bose System in Bose-Fermi Mixture with Attraction between Bosons and Fermions*, JETP Lett. **80**, 274 (2004)

[39] F. Ferlaino, C. D'Errico, G. Roati, M. Zaccanti, M. Inguscio, and G. Modugno, *Feshbach Spectroscopy of a K-Rb Atomic Mixture*, Phys. Rev. A **73**, 040702 (2006)

[40] B. De Witt, *Dynamical Theory of Groups and Fields* (Gordon and Breach, New York, 1965)

[41] R. Jackiw, *Functional Evaluation of the Effective Potential*, Phys. Rev. D **9**, 1686 (1974)

[42] H. Kleinert and V. Schulte-Frohlinde, *Critical Properties of* $\phi^4$*-Theories* (World Scientific, Singapore, 2001)

[43] H. Kleinert, *Path Integrals in Quantum Mechanics, Statistics, Polymer Physics, and Financial Markets*, Fourth Edition (World Scientific, Singapore, 2006); Internet: `http://www.physik.fu-berlin.de/~kleinert/kleiner_re.html`

[44] W. Greiner und J. Reinhardt, *Feldquantisierung*, Buchreihe Theoretische Physik, Band 7A (Verlag Harri Deutsch, Frankfurt, 1993)

[45] L.P. Pitaevskii, *Vortex Lines in an Imperfect Bose Gas*, Zh. Eksp. Teor. Fiz. **40**, 646 (1961) [Sov. Phys. JETP **13**, 451 (1961)]

[46] E.P. Gross, *Structure of a Quantized Vortex in Boson Systems*, Nuovo Cimento **20**, 454 (1961)

[47] A. Pelster, *Lecture Notes on Bose-Einstein Condensation* (in German), University Duisburg-Essen; `http://www.theo-phys.uni-essen.de/tp/ags/pelster_dir/SS04/skript.pdf`

[48] V. Bagnato, D.E. Pritchard, and D. Kleppner, *Bose-Einstein Condensation in an External Potential*, Phys. Rev. A **35**, 4354 (1987)

[49] W. Greiner, *Mechanik Teil 2*, Buchreihe Theoretische Physik, Band 2, 5. Auflage (Verlag Harri Deutsch, Frankfurt, 1989)

[50] N.W. Ashcroft and N.D. Mermin, *Solide State Physics*, International Edition (Saunders College, Philadelphia, 1976)

[51] K. Molmer, *Bose Condensates and Fermi Gases at Zero Temperature*, Phys. Rev. Lett. **80**, 1804 (1998)